

NASA CR-144843

SJT

RSCR 76-1

Characteristics of Magnetospheric Radio Noise Spectra

(NASA-CR-144843) CHARACTERISTICS OF MAGNETOSPHERIC RADIO NOISE SPECTRA Final Report, Dec. 1974 - Dec. 1975 (Radio Sciences Co., Lowell, Mass.) 83 p HC A05/MF A01	N77-17326  Unclas CSCI 20N G3/32 16292
---	---

John R. Herman

Radio Sciences Company  
665 Andover Street  
Lowell, Massachusetts 01852

January 22, 1976



Prepared for

National Aeronautics and Space Administration  
Goddard Space Flight Center  
Greenbelt, Maryland 20771

Characteristics of Magnetospheric Radio Noise Spectra

John R. Herman  
Radio Sciences Company  
665 Andover Street  
Lowell, Massachusetts 01852

January 22, 1976

Final Report  
December 1974 - December 1975

Contract No. NAS5-20807

Prepared for  
GODDARD SPACE FLIGHT CENTER  
Greenbelt, Maryland 20771

TECHNICAL REPORT STANDARD TITLE PAGE

1 Report No		2 Government Accession No		3 Recipient's Catalog No.	
4 Title and Subtitle Characteristics of Magnetospheric Radio Noise Spectra				5 Report Date January 22, 1976	
				6 Performing Organization Code	
7 Author(s) John R. Herman				8 Performing Organization Report No RSCR 76-1	
9 Performing Organization Name and Address Radio Sciences Company 665 Andover Street Lowell, Massachusetts 01852				10. Work Unit No	
				11 Contract or Grant No. NAS5-20807	
12. Sponsoring Agency Name and Address Nat'l Aeronautics & Space Administration Goddard Space Flight Center Radio Astronomy Branch				13. Type of Report and Period Covered Final Dec. 1974 - Dec. 1975	
				14 Sponsoring Agency Code	
15 Supplementary Notes					
16 Abstract Magnetospheric radio noise spectra (30 kHz to 10 MHz) taken by IMP-6 and RAE-2 exhibit time-varying characteristics which are related to spacecraft position and magnetospheric processes. In the mid-frequency range (100-1000 kHz) intense noise peaks rise a factor of 100 or more above background; 80% of the peak frequencies are within the band 125 kHz to 600 kHz, and the peak occurs most often (18% of the time) at 280 kHz. Bandwidths of the peaks range from about 100 kHz to more than 500 kHz; most often the lower cutoff is at about 100 kHz and the upper at 380 kHz for a total bandwidth of 280 kHz. This intense mid-frequency noise has been detected at radial distances from 1.3 Re to 60 Re on all sides of the Earth (i.e., all local times) during magnetically quiet as well as disturbed periods. Maximum occurrence of the mid-frequency noise is in the evening to midnight hours where splash-type energetic particle precipitation takes place. "Magnetospheric lightning", characterized by transient electric current surges of a few to a few tens of microseconds travelling over distances typically 50 to 250 m, can be invoked to explain the spectral shape of the observed spectra.					
17. Key Words (Selected by Author(s)) Magnetosphere, topside radio noise, electromagnetic spectra, magnetospheric emissions, electrostatic waves, auroral kilometric radiation				18. Distribution Statement	
19 Security Classif. (of this report) Unclassified		20 Security Classif. (of this page) Unclassified		21. No of Pages 84	22 Price*

\*For sale by the Clearinghouse for Federal Scientific and Technical Information, Springfield, Virginia 22151.

## ABSTRACT

Magnetospheric radio noise spectra (30 kHz to 10 MHz) taken by IMP-6 and RAE-2 exhibit time-varying characteristics which are related to spacecraft position and magnetospheric processes. In the mid-frequency range (100-1000 kHz) intense noise peaks rise a factor of 100 or more above background; 80% of the peak frequencies are within the band 125 kHz to 600 kHz, and the peak occurs most often (18% of the time) at 280 kHz. Bandwidths of the peaks range from about 100 kHz to more than 500 kHz; most often the lower cutoff is at about 100 kHz and the upper at 380 kHz for a total bandwidth of 280 kHz. This intense mid-frequency noise has been detected at radial distances from 1.3 Re to 60 Re on all sides of the Earth (i.e., all local times) during magnetically quiet as well as disturbed periods. Maximum occurrence of the mid-frequency noise is in the evening to midnight hours where splash-type energetic particle precipitation takes place. "Magnetospheric lightning", characterized by transient electric current surges of a few to a few tens of microseconds travelling over distances typically 50 to 250 m, can be invoked to explain the spectral shape of the observed spectra. The spectral peak frequency is related to the lightning channel length and the bandwidth is dictated by the lightning current duration.

#### ACKNOWLEDGEMENTS

I thank Dr. R.G. Stone of Goddard Space Flight Center for his constant interest and encouragement throughout the course of the work. Thanks go also to H.A. Jemison and C.T. Herman of Radio Sciences Co., who helped considerably with the data reduction and analysis. Mr. Jemison executed the figures and Mrs. N. Jemison typed the manuscript for the final report. Mr. J.D. Chang and Mr. P. Bankhead of Washington Data Processing, Inc. produced special computer runs to expedite the analysis.

## TABLE OF CONTENTS

Abstract	
List of Illustrations	
1. Introduction	1
2. Representative Spectra	3
3. Statistics of Terrestrial Kilometric Radiation	29
3.1 Parameters Used	29
3.2 Preliminary Analysis	29
3.3 Computer Analysis	34
3.3.1 Peak Brightness vs Peak Frequency	35
3.3.2 Diurnal Distribution of Peak Frequency	40
3.3.3 Relationships with Bandwidth	43
3.3.4 Summary of Spectral Characteristics	48
4. Noise Sources and Generation Mechanisms	52
4.1 Noise Source Regions	52
4.2 Generation Mechanisms	58
4.3 Magnetospheric Lightning	62
5. Summary and Conclusions	70
6. References	73

## LIST OF ILLUSTRATIONS

- Fig. 1. Spectral distribution of intense radio noise in the magnetosphere (after Stone, 1973). p.3.
- Fig. 2. Sample IMP-6 spectrum with the spacecraft on the evening side (20.4 LMT) close to Earth (4.6 Re) during quiet planetary magnetic conditions ( $K_p = 1^-$ ). p. 5.
- Fig. 3. Sample IMP-6 spectrum taken at approximately same position (21.2 LMT, 5.8 Re) as in previous figure, but with  $K_p = 8^+$ . p. 6.
- Fig. 4. IMP-6 spectrum in postmidnight sector (03.6 LMT) near apogee (31.3 Re) during a strong geomagnetic disturbance ( $K_p = 7^+$ ). p. 7.
- Fig. 5. IMP-6 spectrum in postmidnight sector (03.1 LMT) near apogee (29.6 Re) during a moderate geomagnetic disturbance ( $K_p = 5^-$ ). p. 8.
- Fig. 6. Sample spectra derived from data taken by the lunar-orbiting RAE-2. p. 10.
- Fig. 7. IMP-6 orbits projected to ecliptic plane to show relative spacecraft positions (A,B,C,D) corresponding to spectra illustrated in Figs. 8-11. p. 12, 13.
- Fig. 8. IMP-6 noise spectrum taken on the predawn side (03.6 LMT) corresponding to position A of Fig. 7. p. 14, 15.
- Fig. 9. IMP-6 noise spectrum taken in position B of Fig. 7. p. 16.
- Fig. 10. IMP-6 noise spectrum taken at position C of Fig. 7. p. 17.
- Fig. 11. IMP-6 noise spectrum taken in the noon sector at position D of Fig. 7. p. 18.
- Fig. 12. IMP-6 spectral peak frequencies over a 24-hr period during a major geomagnetic disturbance (Aug. 5, 1972). p. 20.
- Fig. 13. IMP-6 spectral peak frequencies over the Aug. 6, 1972, 24-hr period. p. 21.
- Fig. 14. IMP-6 spectral peak frequencies for a 24-hr period (Nov. 1, 1971) of moderate substorm activity. p. 22.
- Fig. 15. IMP-6 spectral peak frequencies during a 24-hr period with no auroral substorms (Jan. 5, 1972). p. 23.

LIST OF ILLUSTRATIONS (CONT)

- Fig. 16. IMP-6 ten-minute average spectral peaks for two 1-hr periods on Aug. 5, 1972 (top) and Aug. 6, 1972 (bottom). p. 25.
- Fig. 17. Statistical distribution of TKR peak frequencies based on ~700 IMP-6 data points. p. 31.
- Fig. 18. Upper ( $f_u$ ) and lower ( $f_l$ ) cutoff-frequency statistical distribution of TKR enhancements. p. 32.
- Fig. 19. Peak brightness as a function of peak frequency derived from ~700 IMP-6 data points. p. 32.
- Fig. 20. Peak brightness as a function of peak frequency for the 18-22 LMT time block. p. 36.
- Fig. 21. Same as Fig. 20 but for 06-10 LMT time block. p. 37.
- Fig. 22. Peak brightness as a function of peak frequency for quiet magnetic conditions. p. 38.
- Fig. 23. Same as Fig. 22 but for  $2 \leq K_p \leq 5^-$ . p. 39.
- Fig. 24. Same as Fig. 22 but for  $K_p \geq 5$ . p. 39.
- Fig. 25. Composite distribution of IMP-6 spectral peak brightnesses as a function of local time. p. 41.
- Fig. 26. Diurnal distribution of relative occurrence - frequency of TKR peaks. p. 42.
- Fig. 27. Distribution of peak frequencies of TKR noise as a function of local time. p. 44.
- Fig. 28. Diurnal distribution of IMP-6 spectral peak bandwidths. p. 45.
- Fig. 29. Peak brightness as a function of IMP-6 spectral peak (3-dB) bandwidth for the 18-22 LMT time block. p. 46.
- Fig. 30. Same as Fig. 29 but for 06-10 LMT time block. p. 47.
- Fig. 31. Peak frequency (ordinate) as a function of 3-dB bandwidth in the 02-06 LMT time block. p. 49.
- Fig. 32. Same as Fig. 31 but for 14-18 LMT time block. p. 50.
- Fig. 33. Distribution of 200 kHz whistler-mode noise observed by Alouette 2. p. 53.
- Fig. 34. Idealized representation of auroral particle precipitation. p. 55.
- Fig. 35. Direction finding measurements on IMP-6 for 110 kHz noise. p. 56.

LIST OF ILLUSTRATIONS (CONT)

- Fig. 36. (A) Representative TKR spectra.  
(B) Contours of relative occurrence probability of TKR noise.  
p. 57.
- Fig. 37. Direction-finding measurements of TKR source regions by RAE-2 occultation techniques. p. 59.
- Fig. 38. Distribution of radial distances to TKR sources determined by RAE-2 occultations. p. 60.
- Fig. 39. Normalized IMP-6 TKR spectrum from Fig. 9 compared to theoretical spectrum generated by magnetospheric lightning with two streamer channels. p. 66.
- Fig. 40. Normalized TKR spectrum from Fig. 3 compared to theoretical spectrum generated by magnetospheric lightning with two streamer channels. p. 67.

## 1. INTRODUCTION

Radio noise generated above the ionosphere has come to be recognized as an important manifestation of magnetospheric dynamics. Its discovery (Ellis, 1957) and early study of some of its characteristics (Jorgensen, 1966) were made with ground-based observation techniques, and numerous rocket and satellite measurements in subsequent years have shown it to be a complex, multifaceted phenomenon which is intimately related to dynamic processes in the magnetosphere.

The radio emissions constituting this noise have been identified as either electromagnetic waves (Dunckel, et al, 1970) or electrostatic waves (Kennel, et al, 1970), depending upon the relative positions of the observing satellite and suspected region of noise generation. In many cases no unambiguous determination could be made of which type of wave was being observed. The observed waves may also be non-propagating plasma resonances (Bauer and Stone, 1968), or propagating in various modes according to their radio frequency and the region of space in which they are observed. Propagation modes deduced from measurements of presumably electromagnetic waves include free-space, whistler, and ducted modes. Noise in the magnetosphere has been observed on frequencies ranging from a few Hertz (Hz) representing mostly magnetic fluctuations to several megahertz (MHz) representing electrostatic and electromagnetic radiation.

Source regions of the radio noise have been broadly defined by Herman (1974), based upon the fundamental fact that radiation will be produced by accelerating electrons wherever they may be found. On this basis, the regions include the trapped radiation belts (Frankel, 1973), the night-side auroral oval (Barrington, et al, 1971), the dayside polar cusp (James, 1973), the magnetotail and the plasma sheath. Simultaneous measurements of precipitating electrons and noise emissions by Gurnett and Frank (1972) and Hoffman and Laaspere (1972) support the suggested model of source regions.

Several generation mechanisms within these source regions have been proposed, including the cerenkov process (Ellis, 1957; Taylor and Shawhan, 1974); gyrosynchrotron radiation (Frankel, 1973); excitation of

odd harmonics of the gyrofrequency (Kennel, et al, 1970; Fredericks, 1971) among others.

To organize and clarify these multi-faceted aspects of magnetospheric radio noise, it is helpful to consider the spectral characteristics (the frequency dependence) of the emissions, and their variations with time and observing location. A number of satellite experiments have measured magnetospheric noise in various parts of the radio spectrum from a few Hertz to several megahertz, but the widest frequency range of simultaneous measurements has been provided by the Radio Astronomy Branch at Goddard Space Flight Center from experiments on the IMP-6 and RAE-2 satellites under the direction of R.G. Stone. Noise spectra from these two satellites are therefore utilized in this report in an attempt to show how the spectral characteristics change with time, satellite location, and magnetospheric conditions.

Representative spectra taken at various times are discussed in section 2, where it will be seen that significant enhancements of noise intensity appear in different parts of the spectrum. The most striking of these intensity peaks appears in many spectra on frequencies near 300 kHz. Occurrence statistics of the peaks are investigated in section 3.

Source regions and generation mechanisms of the noise and their effects on spectral characteristics, are treated in section 4.

## 2. REPRESENTATIVE SPECTRA

A composite spectrum illustrating the major features of interest in this report is given in Fig. 1. Apart from the galactic background noise, the spectrum has two major components attributable to magnetospheric sources. The mid-frequency peak near 250 kHz is highly variable with time; the peak amplitude varies by a factor of 100 in brightness, and the peak frequency ranges from about 150 kHz to 500 kHz. The statistics of these variations are treated in the next section. This component is referred to as "terrestrial kilometric radiation," or TKR, after Kaiser and Alexander (1975).

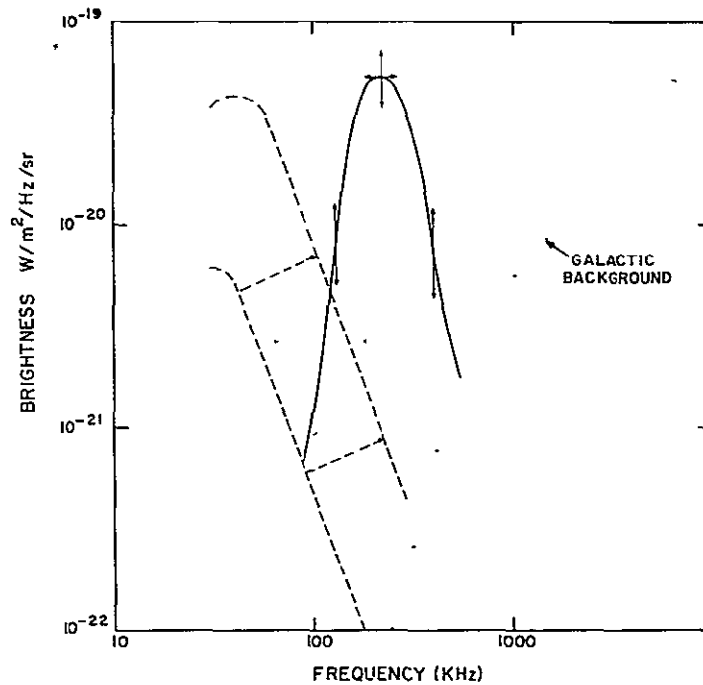


Fig. 1. Spectral distribution of intense radio noise in the magnetosphere (after Stone, 1973). The quasi-continuous component at and below 100 kHz (dashed line) varies up and down in frequency and brightness but maintains relatively steady spectral index of  $-2.8$ . The peak near 300 kHz is terrestrial kilometric radiation (TKR).

A broadband component overlaps the TKR peak and extends downward in frequency to about 25 kHz. It varies in amplitude with time but the spectral index remains approximately constant at -2.8. As will become evident below, subsidiary peaks akin to the TKR peak sometimes are superimposed on this quasi-continuous background component.

The detailed shape and average intensity of the noise spectra often depart considerably from this illustrative spectrum (Fig. 1), depending upon spacecraft position, particle precipitation, and magnetic storm or substorm activity. A series of hourly-averaged spectra taken by the IMP-6 spacecraft under various conditions will serve to demonstrate these changes.

The 1-hr average spectrum in Fig. 2 was made with IMP-6 on Earth's evening side (20.4 LMT) at a radial distance of 4.6 Re, during quiet geomagnetic conditions. The time of measurement places IMP-6 outside the plasmapause. The TKR peak is evident at about 300 kHz, but the lower frequency quasi-continuous background reaches a comparable intensity at about 60 kHz. A subsidiary peak is superimposed on this background at about 140 kHz. The intensity of this spectrum does not exceed  $10^{-19} \text{ Wm}^{-2} \text{ Hz}^{-1}$  at any frequency. (A contribution from galactic background noise in the band 1-3 MHz can be seen, and at and above 5 MHz there is some evidence of high frequency (HF) noise or interference penetrating through the ionosphere from the ground. In this report no analysis will be given to these two contributors.)

Another spectrum taken at roughly the same spacecraft position (5.8 Re, 21.2 LMT) during a magnetic storm ( $K_p = 8^+$ ) is given in Fig. 3 for comparison. Note that here the TKR peak brightness is nearly two orders of magnitude higher than that in Fig. 2, and its peak frequency at 400 kHz is higher than that in the quiet-time spectrum (Fig. 2). Also in Fig. 3, a lower frequency peak appears at about 40 kHz with an intensity approximately a factor of six greater than the 60 kHz peak appearing in Fig. 2. The largest peak in Fig. 3 occurs at about 3 MHz; this is probably not due to terrestrial interference, but it may be related to the strong 2-4 MHz emissions observed at much lower altitudes by James, et al (1974).

Two spectra taken on a single pass with IMP-6 near apogee ( $\sim 30 \text{ Re}$ ) on the morning side ( $\sim 0300 \text{ LT}$ ) during a magnetic disturbance ( $K_p \geq 5^-$ )

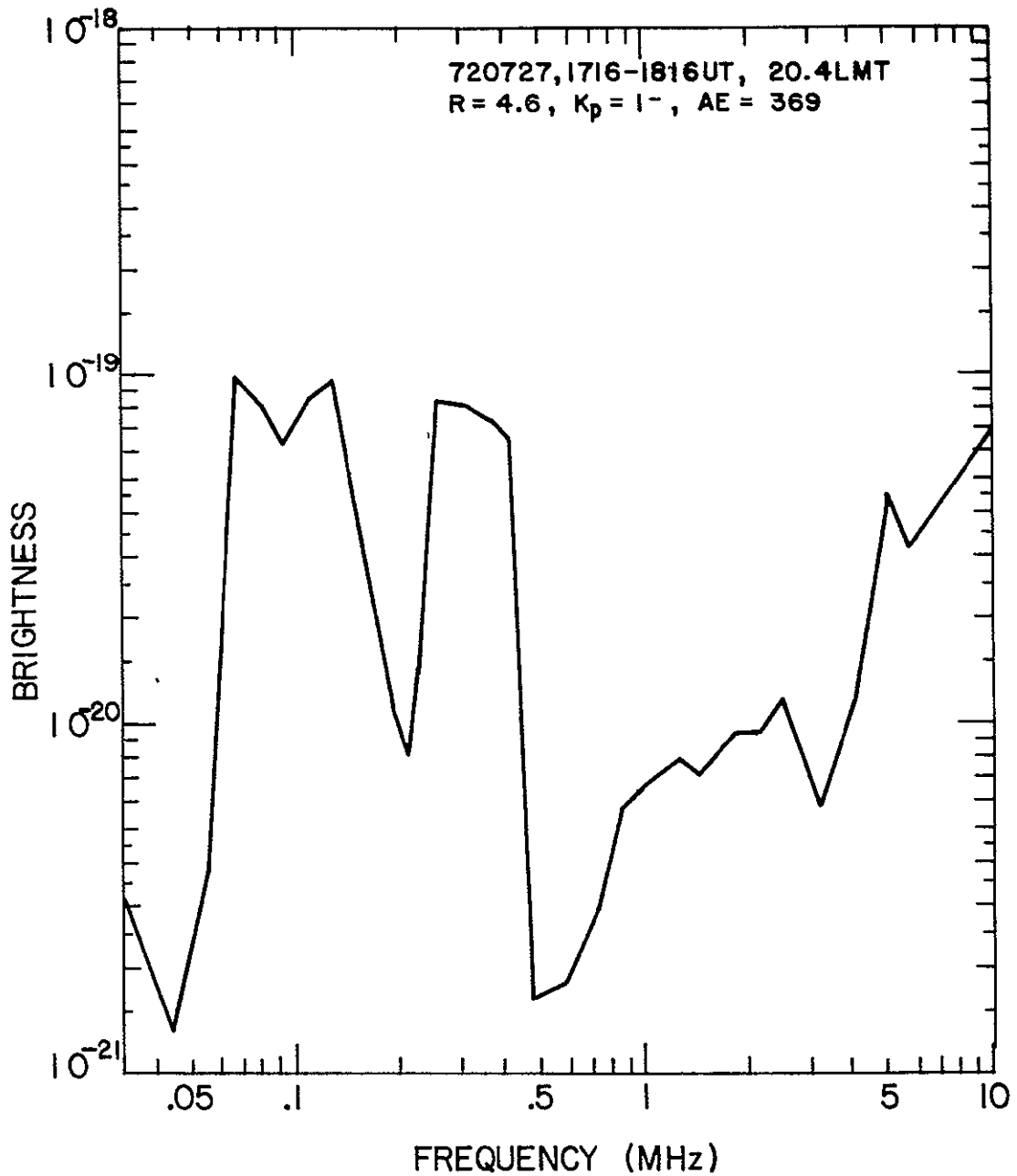


Fig. 2. Sample IMP-6 spectrum with the spacecraft on the evening side (20.4 LMT) close to Earth (4.6 Re) during quiet planetary magnetic conditions ( $K_p = 1^-$ ).

are shown in Figs. 4 and 5 to illustrate time variations in spectral character. At the earlier universal time (Fig. 4) the 1-hour average TKR

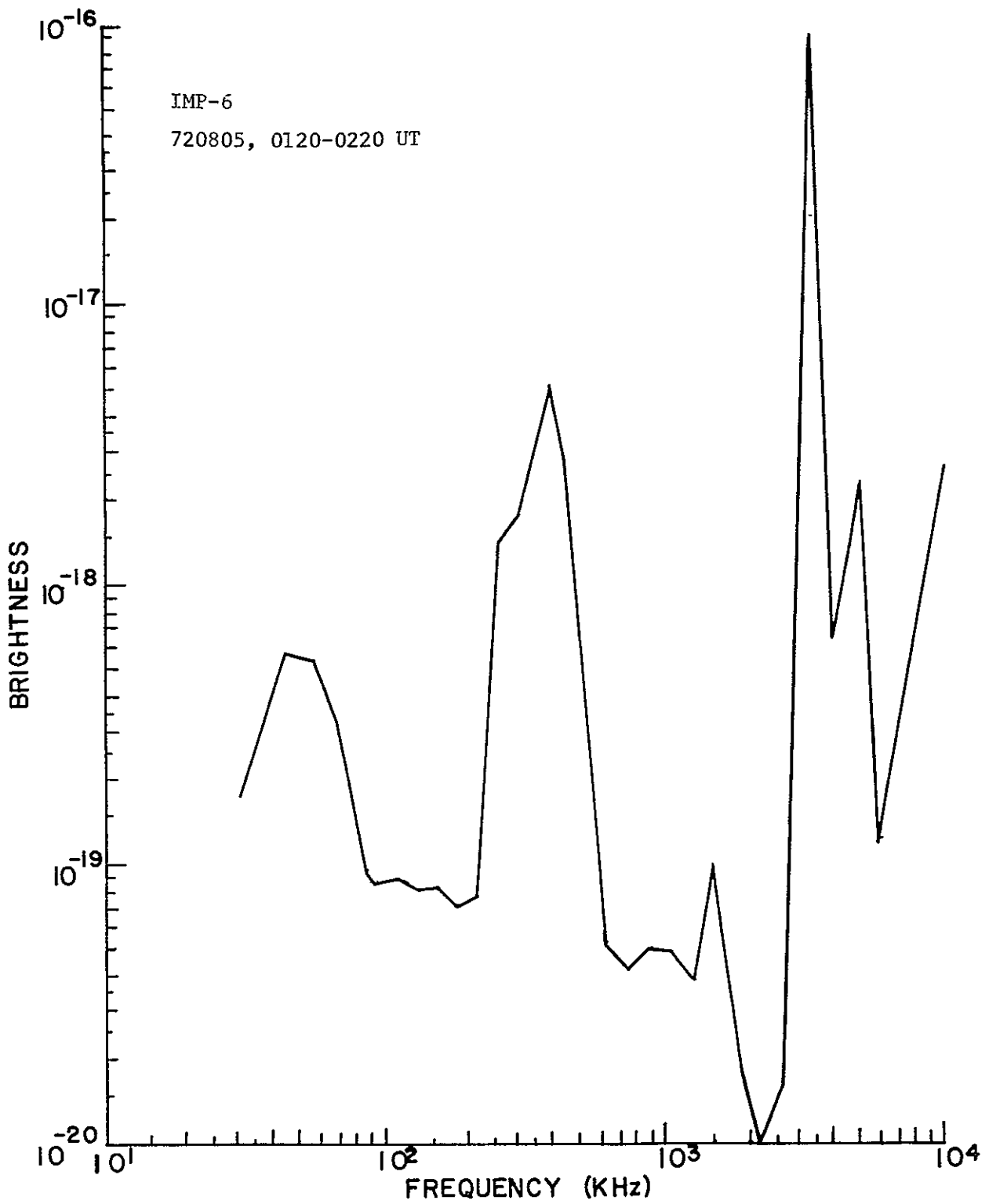


Fig. 3. Sample IMP-6 spectrum taken at approximately same position (21.2 LMT, 5.8 Re) as in previous figure, but with  $K_p = 8^+$ .

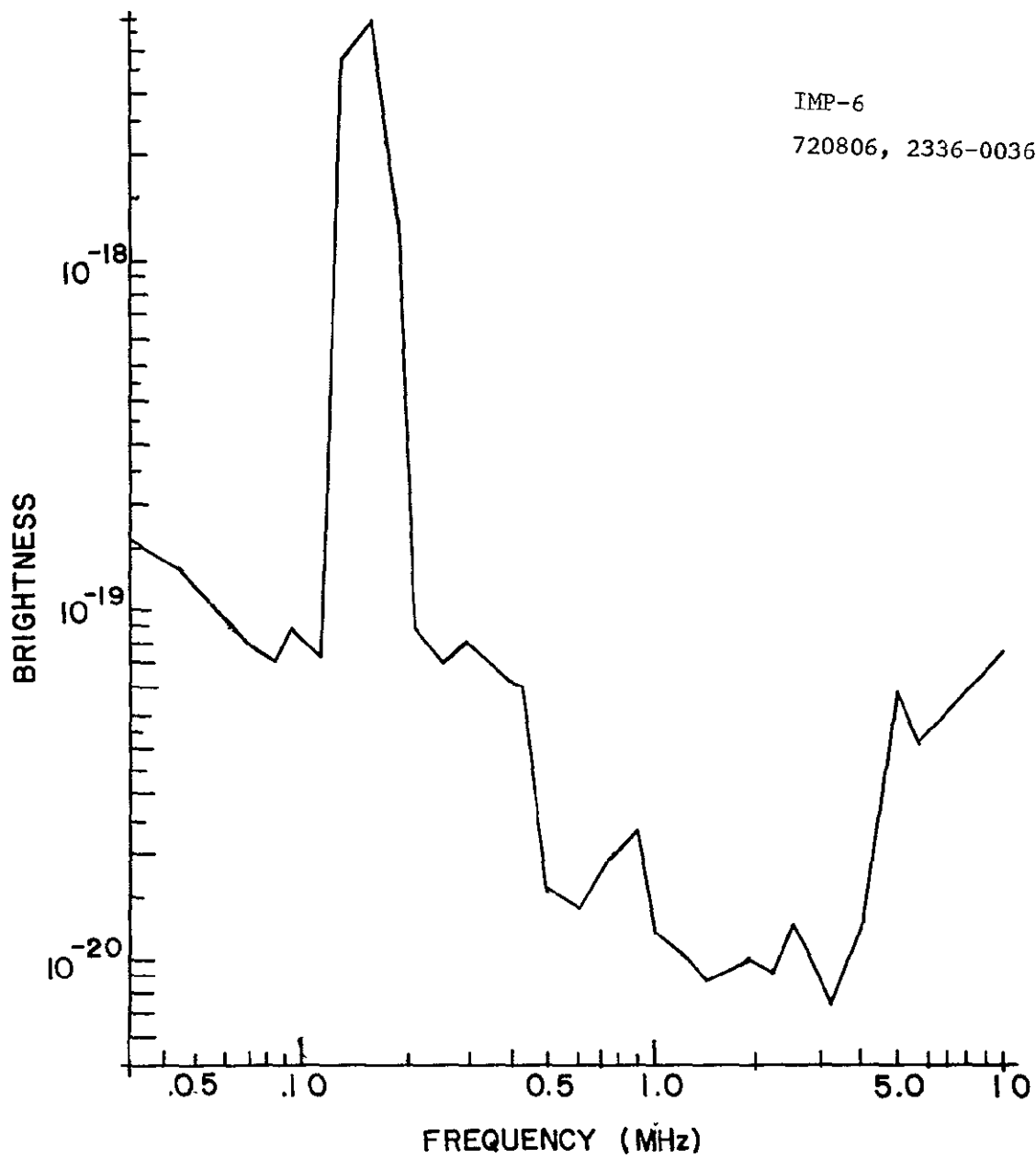


Fig. 4. IMP-6 spectrum in postmidnight sector (03.6 LMT) near apogee (31.1 Re) during a strong geomagnetic disturbance ( $K_p = 7^+$ ).

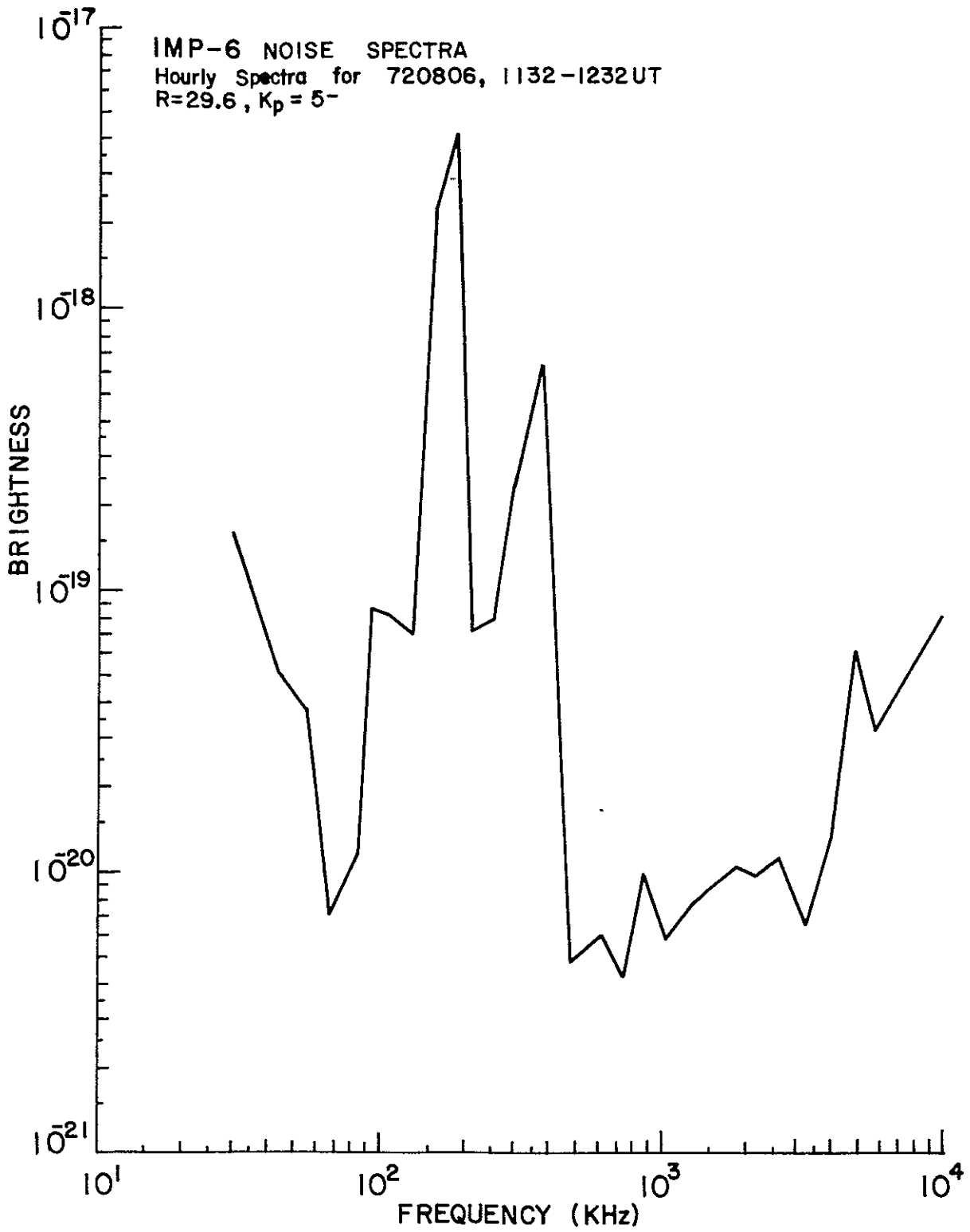


Fig. 5. IMP-6 spectrum in postmidnight sector (03.1 LMT) near apogee (29.6 Re) during a moderate geomagnetic disturbance ( $K_p = 5^-$ ).

has a single large peak at about 150 kHz; above about 3 MHz ground breakthrough of noise from below the ionosphere increases in intensity with increasing frequency. Twelve hours later (Fig. 5) the spacecraft is still in nearly the same place with respect to the sun and the earth, but now the TKR exhibits two peaks at about 180 kHz and 370 kHz. The character of ground breakthrough noise above 3 MHz has not changed much. In the frequency range of about 40 to 100 kHz, the noise intensity is greater for  $K_p = 7^+$  (Fig. 4) than it is for  $K_p = 5^-$  (Fig. 5).

To gain a different perspective, sample relative spectra derived from RAE-2 calibration-temperature data are presented in Fig. 6. These were taken with the lunar-orbiting spacecraft located in the magnetotail near local midnight (full moon) at two times when the earth-moon-spacecraft-antenna geometry was nearly identical. The variable of interest is the  $K_p$  index, being  $2^+$  for one spectrum and  $5^+$  for the other. Even though the observing location is at a distance of 60  $R_e$ , nearly twice the distance of IMP-6 apogee, a pronounced TKR peak is evident at about 475 kHz when  $K_p = 2^+$ . Two days later with a magnetic index of  $5^+$ , the whole spectrum is shifted upward in magnitude by 20-30 dB, and the spacecraft radiometers are saturated in the TKR range of 250-425 kHz. The disturbed-day spectrum is also saturated below 70 kHz. To compare these two spectra with the IMP-6 spectra in the earlier figures, use can be made of the relation

$$b = \frac{2 kT}{\lambda^2}$$

where  $b$  is brightness ( $\text{Wm}^{-2} \text{Hz}^{-1}$ ),  $k$  is Boltzmann's constant ( $1.38 \times 10^{-23} \text{J } ^\circ\text{K}^{-1}$ ),  $T$  is the noise temperature ( $^\circ\text{K}$ ), and  $\lambda$  is the observing wavelength (m).

From this relation, it can be seen that the RAE-2 TKR peak centered on 300 kHz with  $K_p = 5^+$  saturates at about  $3 \times 10^{-18} \text{Wm}^{-2} \text{Hz}^{-1}$  and is thus comparable in magnitude to the IMP-6 spectral peaks in Figs. 3, 4 and 5. For the lower  $K_p$  in Fig. 6, the peak temperature corresponds to a brightness of about  $10^{-20} \text{Wm}^{-2} \text{Hz}^{-1}$ , compared to about  $10^{-19}$  observed by IMP-6

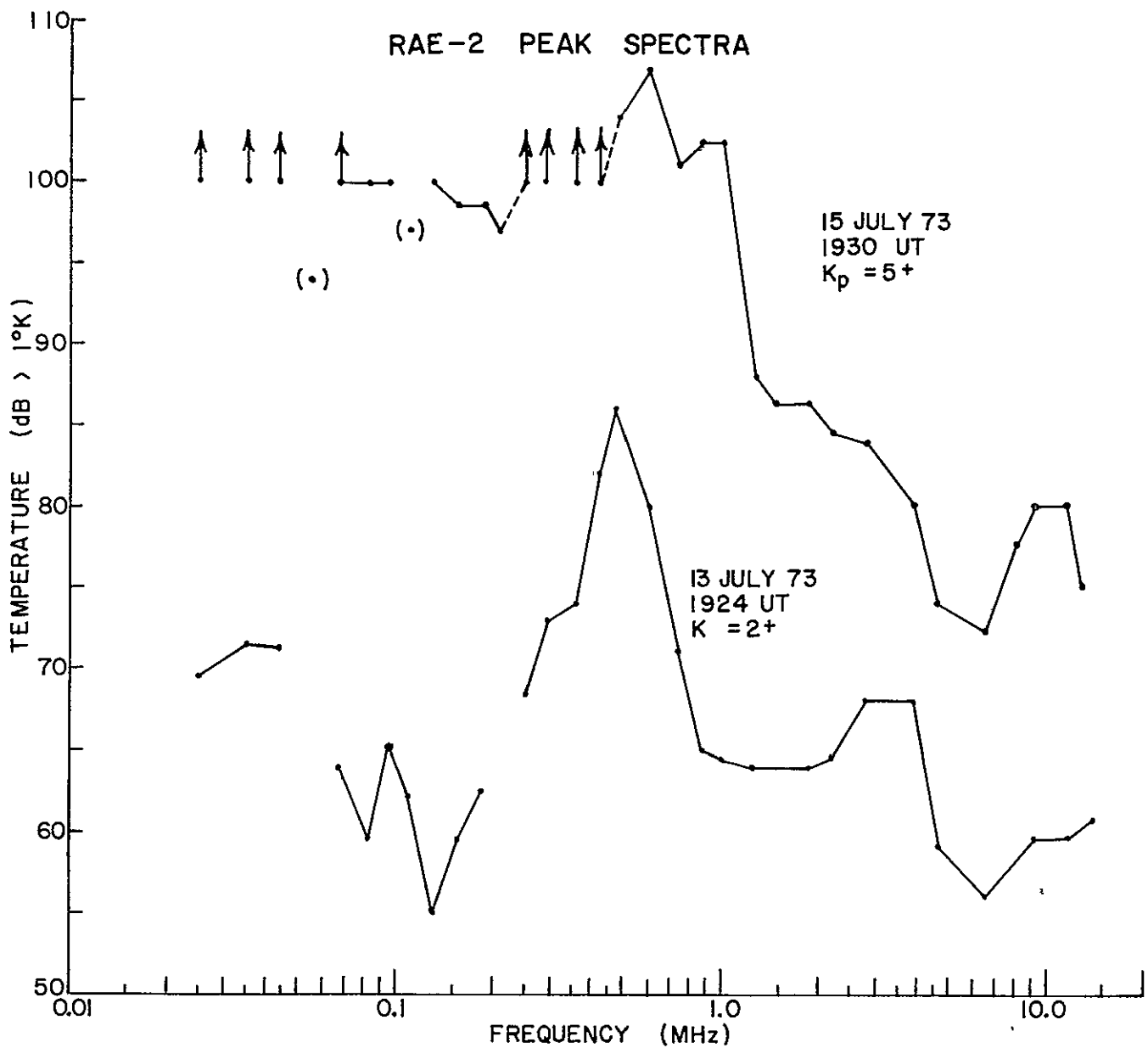


Fig. 6. Sample spectra derived from data taken by the lunar-orbiting RAE-2 at two times when the spacecraft faced Earth on the midnight side under quiet conditions (July 13) and 13 orbits later under moderately disturbed conditions (July 15).

in Fig. 2.

Principal features of the spectra in Figs. 2-6 are illustrative of several general characteristics of magnetospheric noise spectra. That is,

the high intensity peak occurring at frequencies in the approximate range of 150-450 kHz is observed on the evening and night sides of Earth at radial distances from 4.5 Re to 60 Re at all Kp levels. There is some indication that the intensity is higher during magnetically disturbed periods compared to quiet periods, but as will become evident below, a high Kp level is not a requisite for intense noise peaks.

The next series of spectra presented here serve to illustrate changing characteristics as a function of local time with IMP-6 at apogee and  $K_p \leq 2^+$ . Fig. 7 shows the position of the spacecraft relative to the sun and magnetospheric orientation. Position B, near local midnight, has IMP-6 immersed in the magnetotail, while A, C, and D, for morning, evening, and mid-day positions, places IMP-6 outside the magnetosphere.

On the postmidnight side in orbit A, the spectrum (Fig. 8) has a peak brightness of about  $2 \times 10^{-18} \text{ Wm}^{-2} \text{ Hz}^{-1}$  near 200 kHz, discounting the high intensity spike at 3 MHz. In the tail (Fig. 9), the TKR peak at about 300 kHz is a factor of 10 higher and somewhat broader than the enhancement in Fig. 8. On the evening side (Fig. 10), the peak brightness of  $\sim 2 \times 10^{-17}$  is comparable to that in the midnight sector but its width is more narrow. The spectrum taken in the noon sector (Fig. 11) has a TKR peak of about  $10^{-19} \text{ Wm}^{-2} \text{ Hz}^{-1}$  centered near 200 kHz, with a sharp spike a factor of 10 higher at 130 kHz.

In all four cases (Figs. 8-11), the noise below 100 kHz has a tendency to decrease with increasing frequency, cosmic noise background peaking near 3 MHz is always evident, and ground-breakthrough noise increases with increasing frequency above 3 MHz.

The dayside spectrum from orbit D (Fig. 11) in the frequency band 100-500 kHz is similar to spectra derived from ISIS-1 data by James (1973) at times when the spacecraft was in the dayside auroral oval (polar cusp) at altitudes of 2000-3000 km (i.e., radial distances of  $\sim 1.3-1.5 \text{ Re}$ ). The spectral shape at both 31.2 Re (Fig. 11) and at 1.5 Re (James, 1973, not shown) is marked by a peak near 200 kHz and rather sharp upper and lower cut-offs at about 300 kHz and 100 kHz, respectively.

To see how the spectra vary over the course of a 24-hr period, let us consider only peak enhancements. In Fig. 3, for example, an average "baseline" - or background - level can be established which is gradually

Fig. 7. IMP-6 orbits projected to ecliptic plane to show relative spacecraft positions (A,B,C,D) corresponding to spectra illustrated in Figs. 8-11.

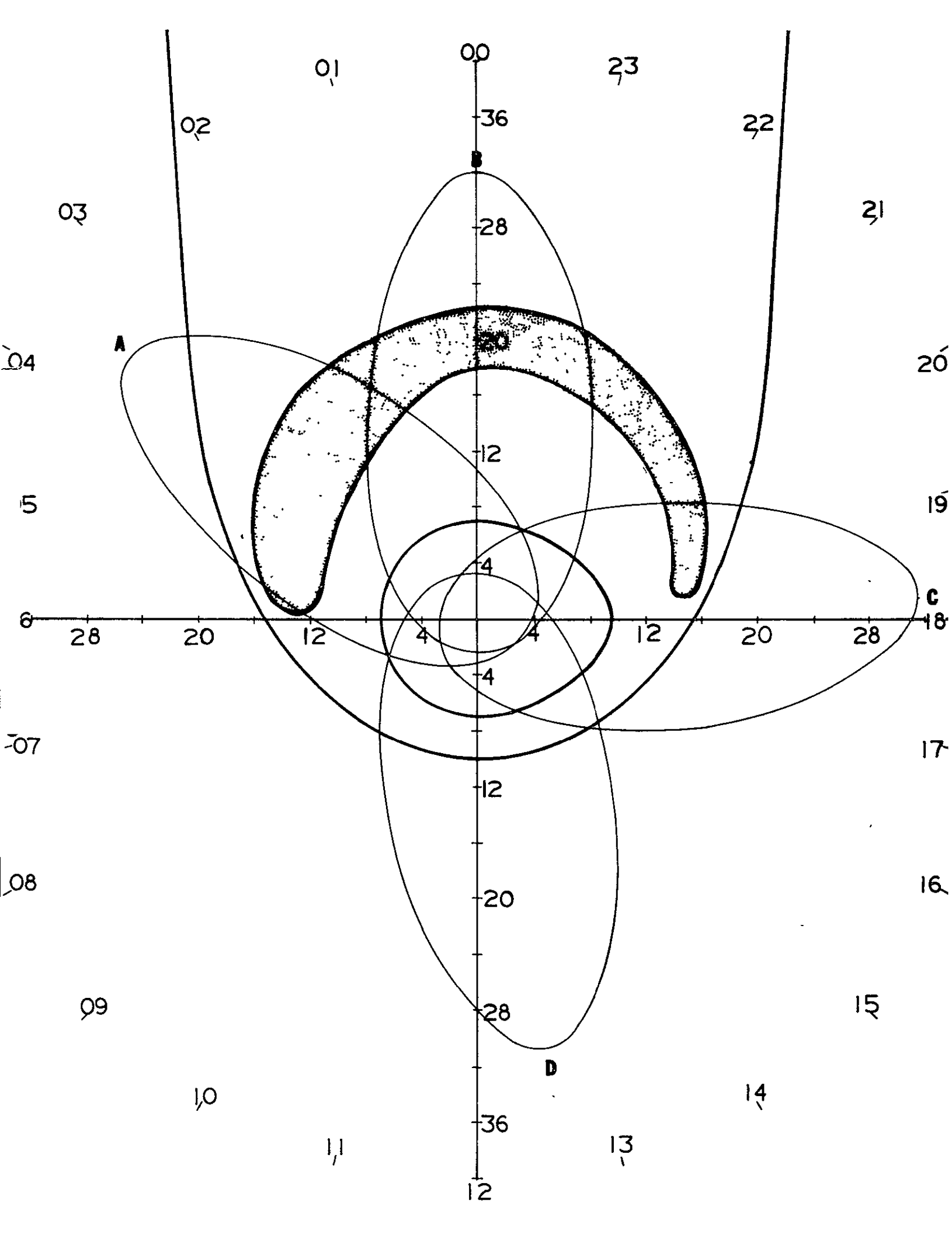
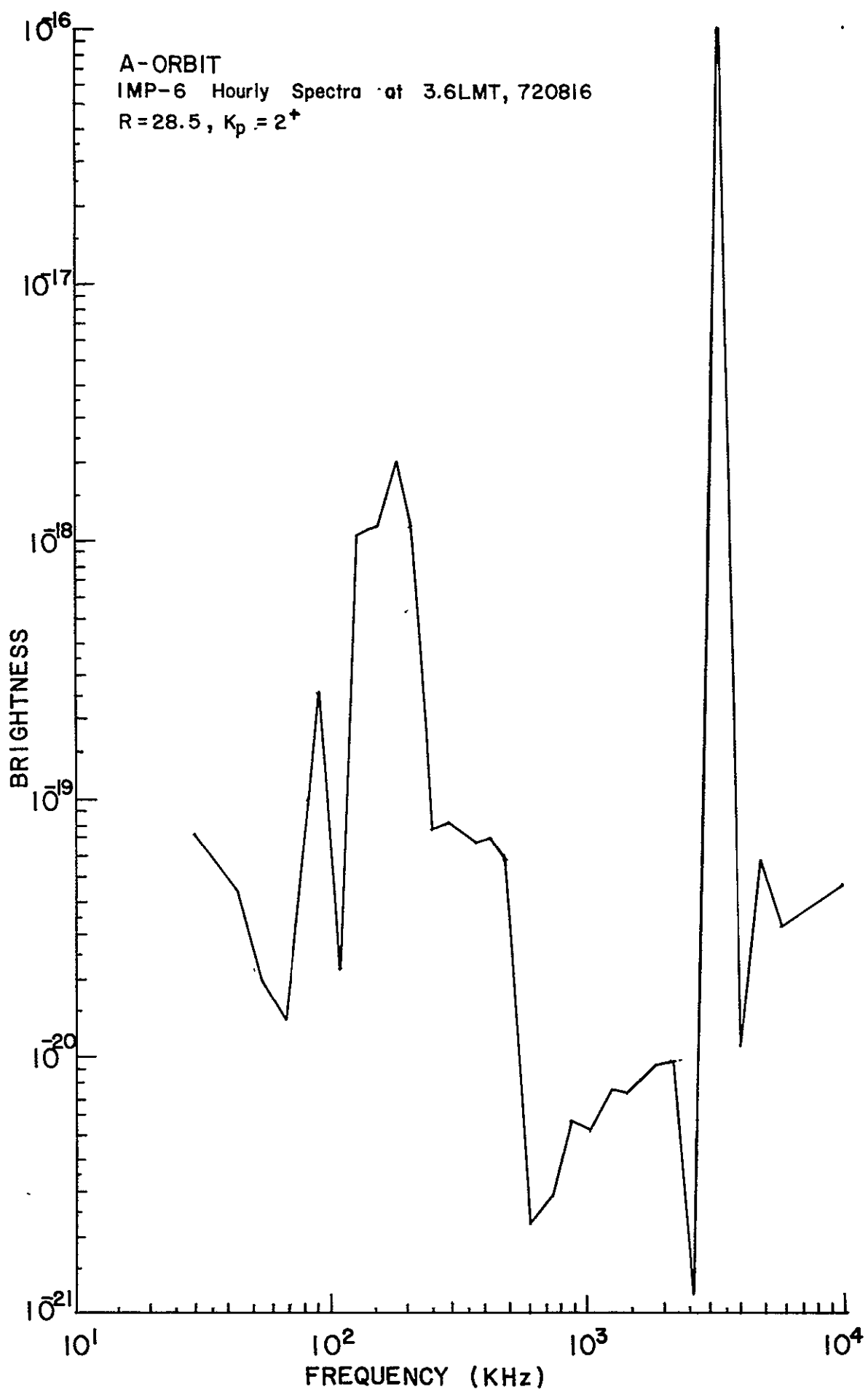


Fig. 8. IMP-6 noise spectrum taken on the predawn side (03.6 LMT) corresponding to position A of Fig. 7.



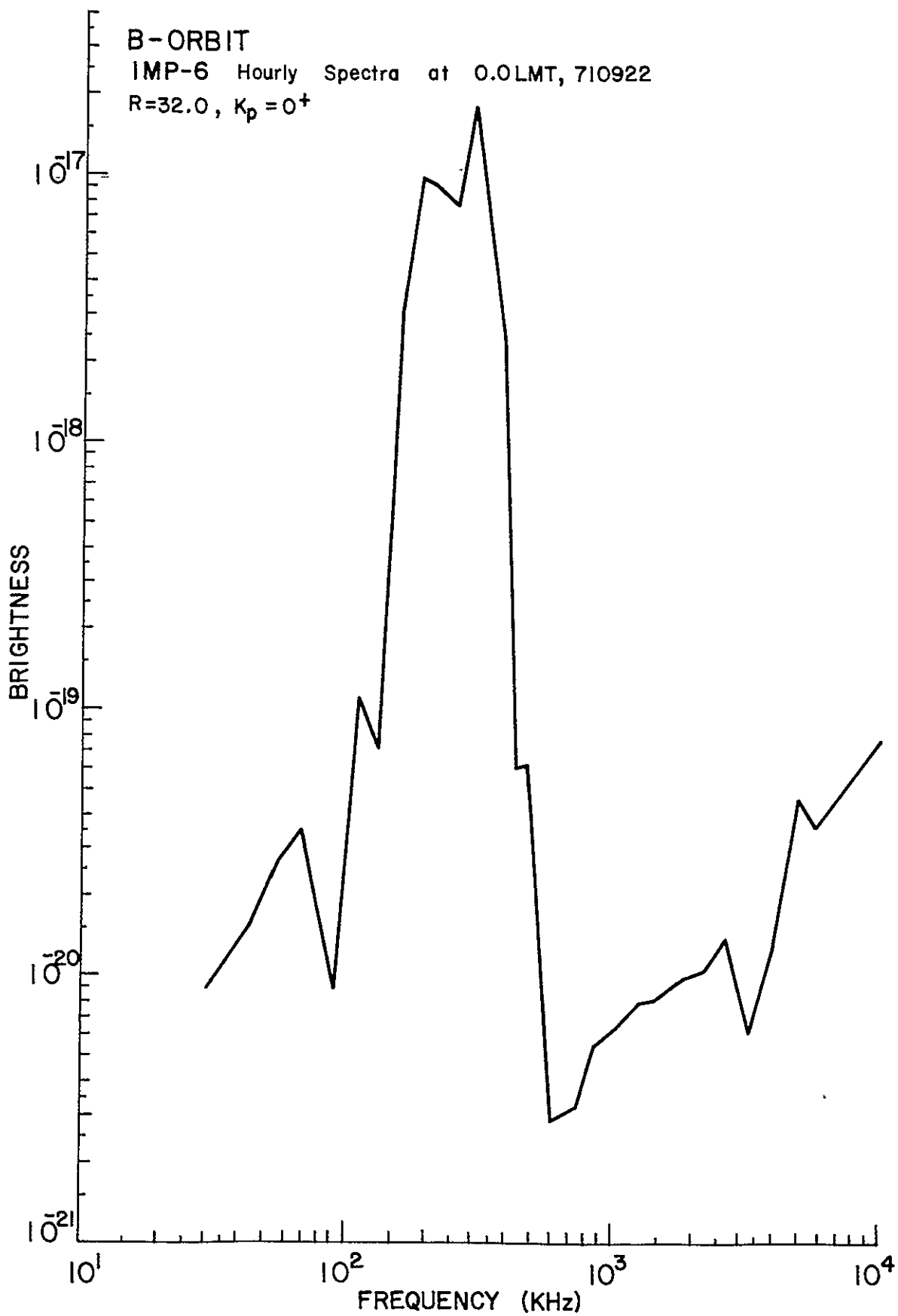


Fig. 9. IMP-6 noise spectrum taken in position B of Fig. 7.

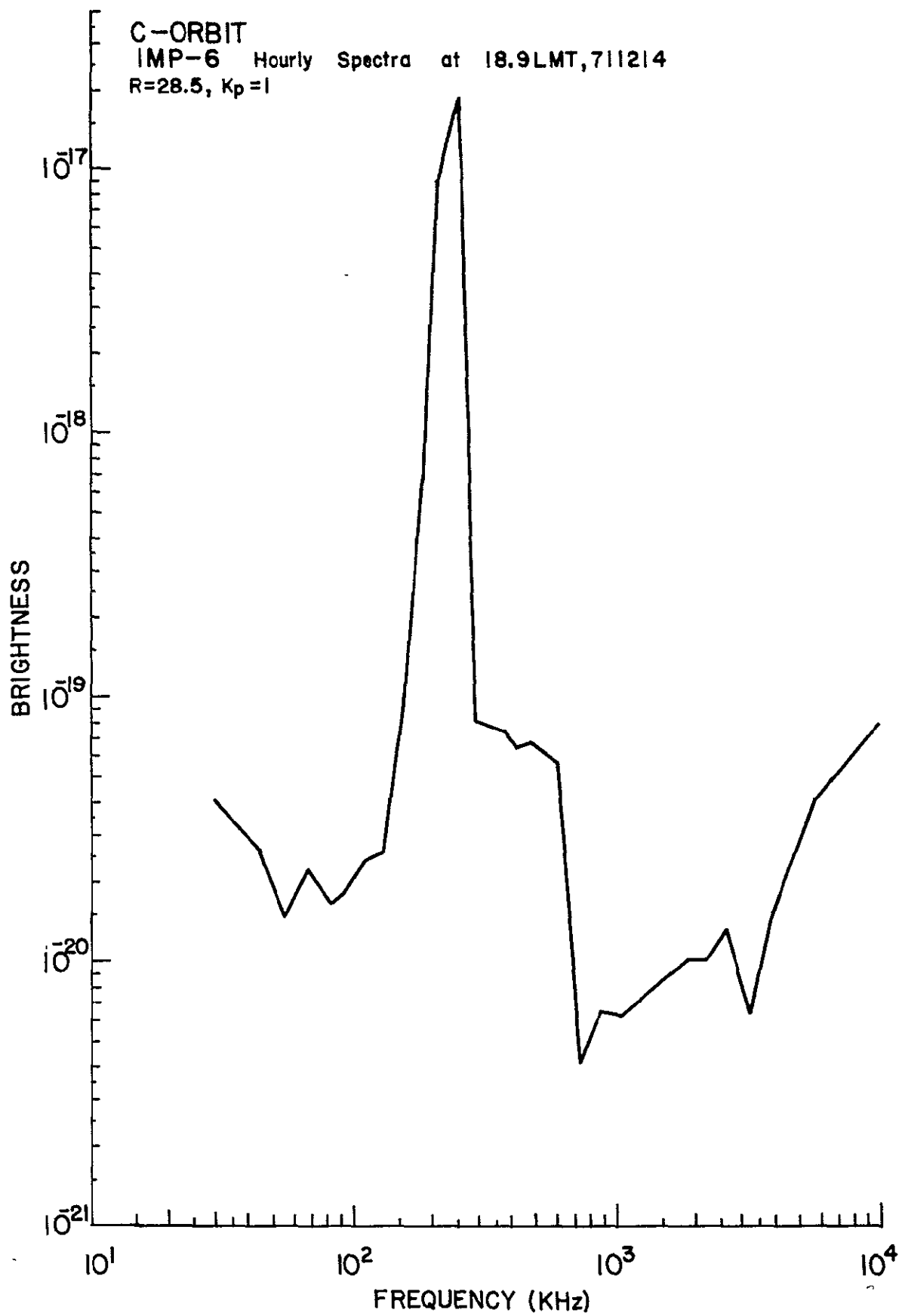


Fig. 10. IMP-6 noise spectrum taken at position C of Fig. 7.

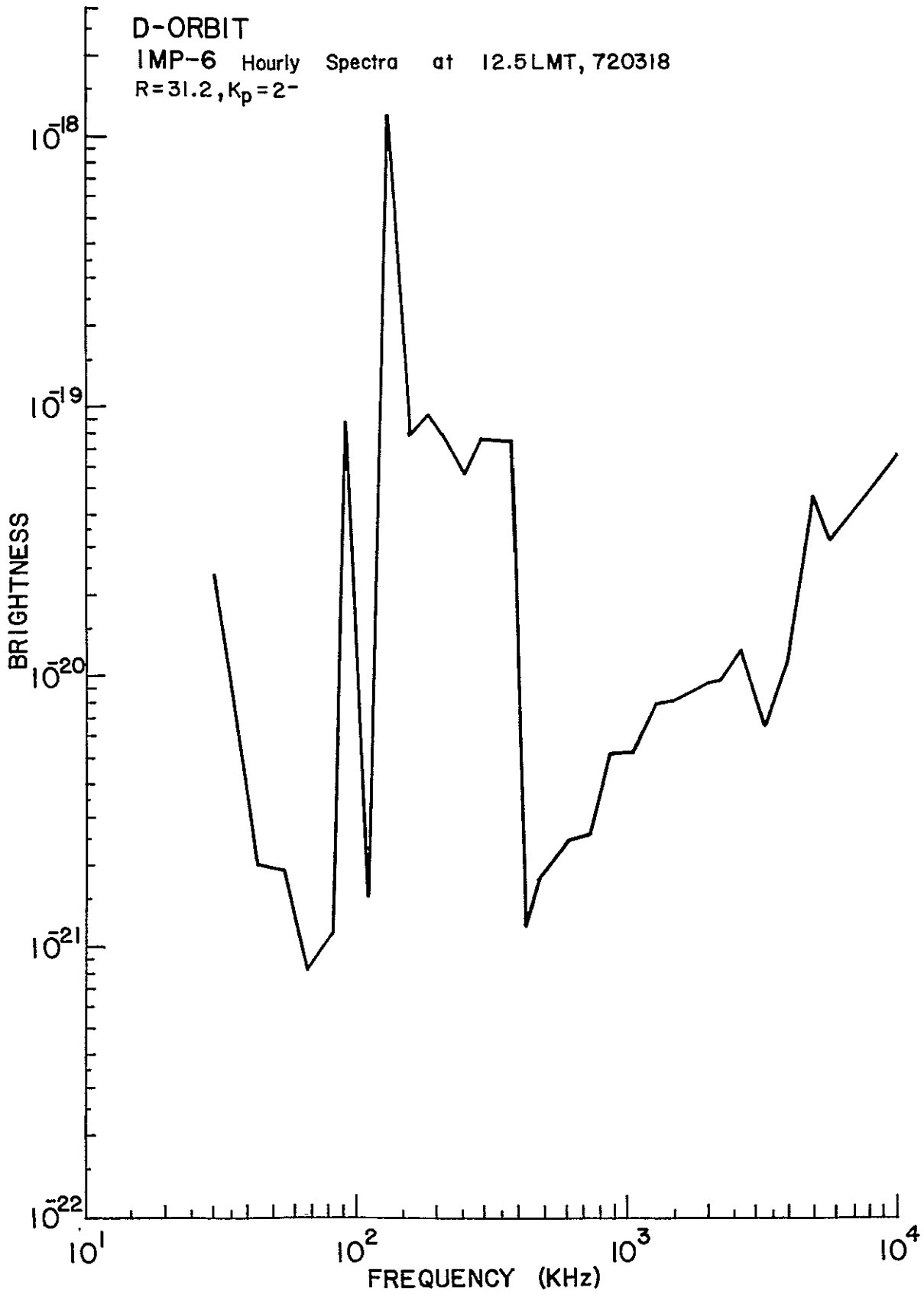


Fig. 11. IMP-6 noise spectrum taken in the noon sector at position D of Fig. 7.

decreasing from  $2 \times 10^{-19} W_m^{-2} \text{ Hz}^{-1}$  at 25 kHz to  $2 \times 10^{-20}$  at 1 MHz and then increasing through  $10^{-19}$  at 5 MHz. The magnitude of the peaks found at the frequencies of 44-55 kHz, 375-425 kHz, 1450-kHz, 3250-kHz, and 4900-kHz in Fig. 3 are expressed as the decibel (dB) increase above the established baseline. Successive hourly-averaged spectra are treated in the same way. The results for August 5, 1972, are shown in Fig. 12.

August 5, 1972 was a highly disturbed day; the Kp 3-hourly index ranged from  $6^-$  to  $9^-$ , and the AE hourly index, as indicated in Fig. 12, was as high as 1165. Multiple spectral peaks from the IMP-6 data occurred in all 1-hr average spectra. The most intense ones in Fig. 12 range from 185 to 737 kHz in the TKR band, and appear on 4.9 MHz for most of the 24 hours. The very strong peak at 3250 kHz (see also Fig. 3) persists for four hours early in the day, and appears again in the 2600 kHz channel in the hourly spectrum centered at 20 UT (Fig. 12). During the period covered by Fig. 12, IMP-6 was on an outward bound orbit on the night side, starting at a radial distance of 5.8 Re and reaching 25.4 Re by 24 UT. In this plot there appears to be no pattern for a systematic variation in peak frequency or peak magnitude as a function of magnetic index AE or radial distance. The following day, August 6, 1972 was also magnetically disturbed, with Kp ranging from  $3^+$  to  $7^+$ . The radio frequency and magnitude of spectral peaks derived as before are shown in Fig. 13. During this day IMP-6 progressed from a radial distance of 25.9 Re to 31.2 Re and moved in local time from 02.7 hours to 03.5 hours. In general the peak intensities do not rise as far out of the background level as they did on the previous day. It should be noted, however, that an intense peak appears at 3250 kHz for 3 hours early in the universal day, during a time when IMP-6 was at a radial distance of 26-27 Re. Its magnitude is comparable to the peak on the same frequency occurring on the previous day at distances of 6-9 Re (Fig. 12).

On both days, the AE index as noted in Figs. 12 and 13 is variable but quite high, ranging from 332 to 1186, and TKR peaks persist at all AE levels in this range. Days selected for moderate (AE 88 to 828) and minimum (AE 19 to 194) substorm activity are shown in Figs. 14 and 15, respectively, where it can be seen that TKR peaks occur even during magnetically

720805

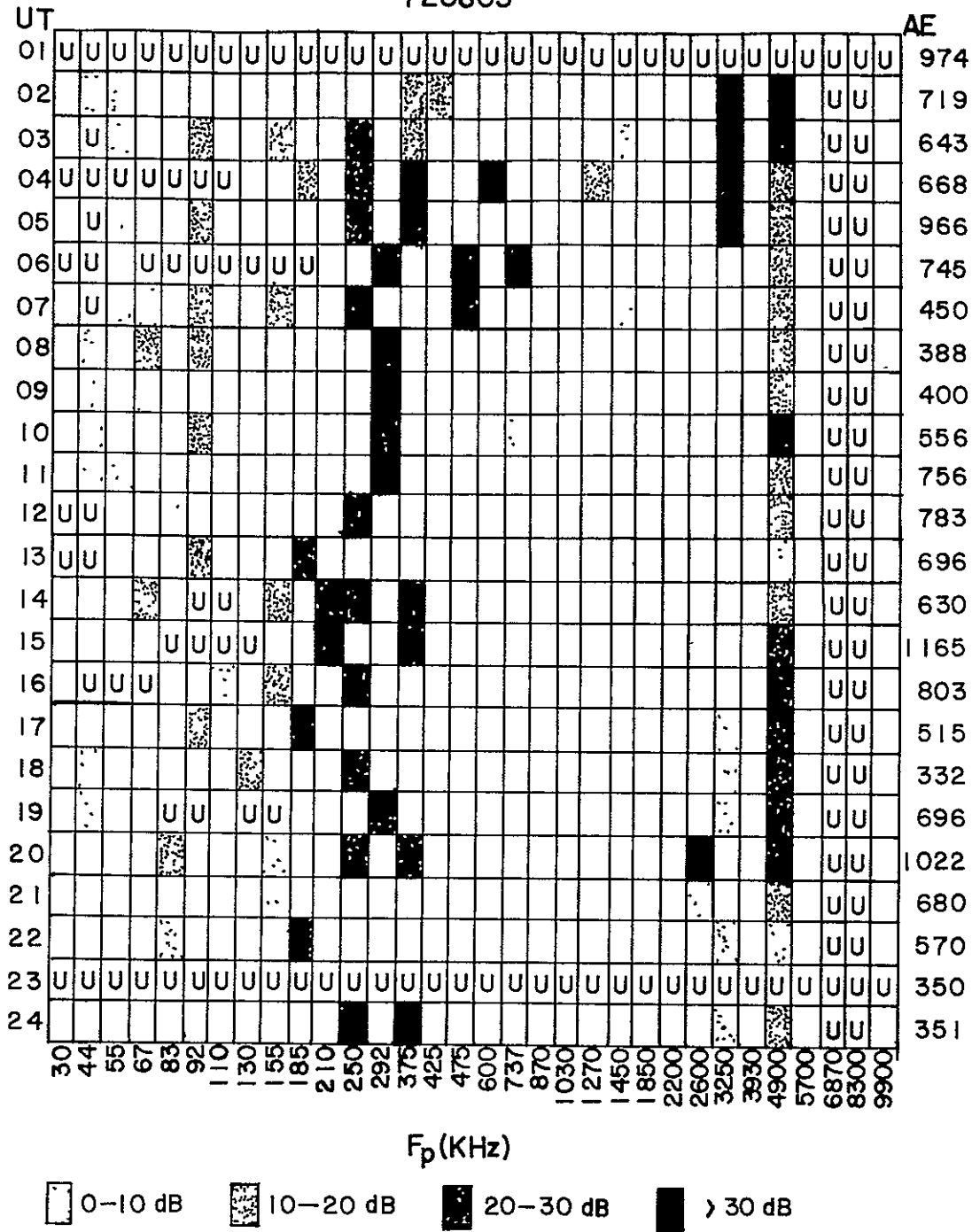


Fig. 12. IMP-6 spectral peak frequencies over a 24-hr period during a major geomagnetic disturbance (Aug. 5, 1972). The AE hourly magnetic index is shown on the right. U indicates no data.





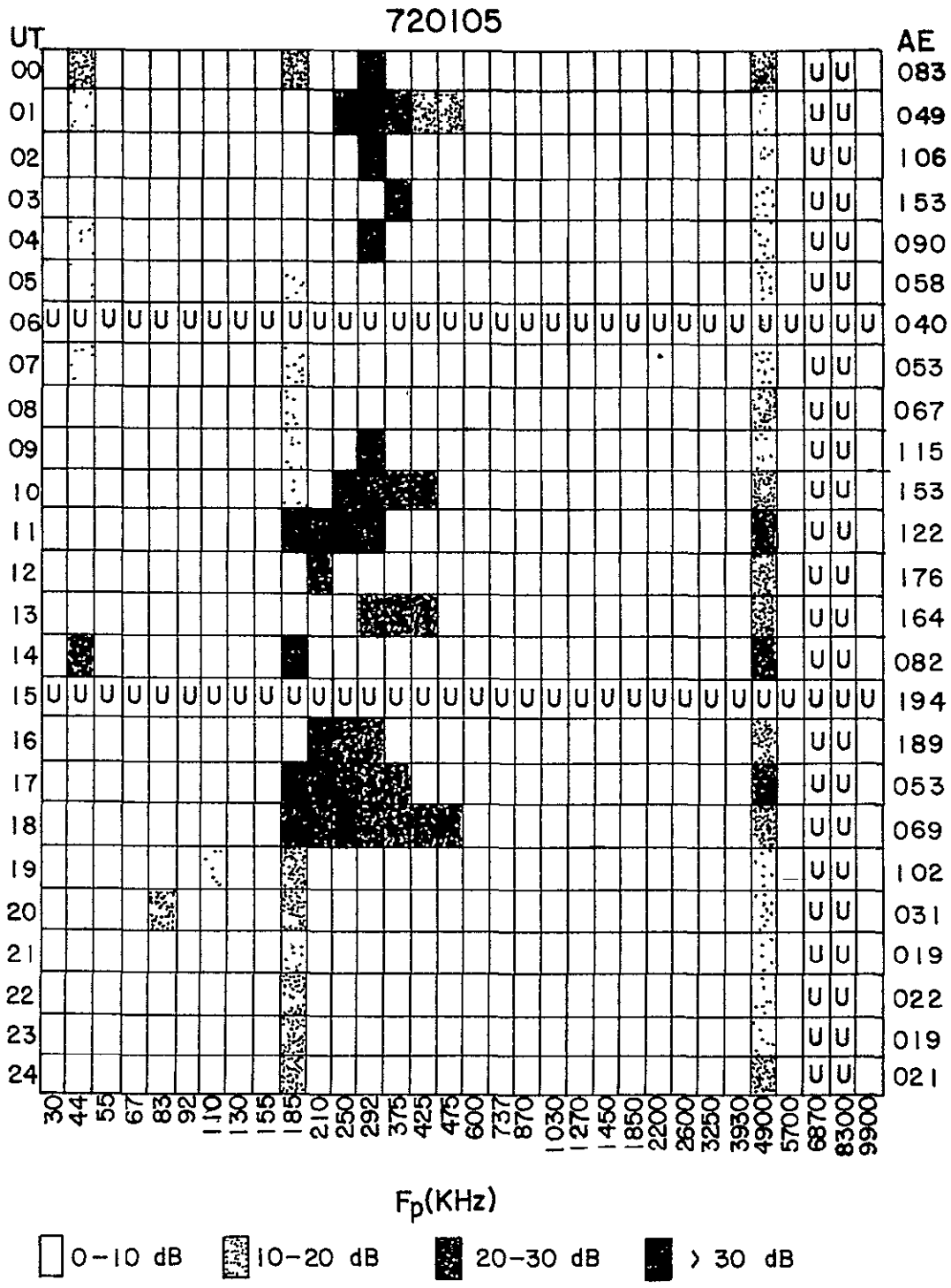


Fig. 15. IMP-6 spectral peak frequencies during a 24-hr period with no auroral substorms (Jan. 5, 1972).

quiet periods.

On October 1, 1971 (Fig. 14),  $K_p$  ranged from  $3^-$  to  $5^-$ , radial distance varied from 31.9 to 25 Re on an inbound pass, and local time for IMP-6 remained almost constant near midnight (23.8 to 0.4 LT). As with major substorm activity (Figs. 12 and 13), TKR peak occurrence during moderate activity (Fig. 14) exhibits no obvious relationship to the magnitude of AE.

On January 5, 1972 (Fig. 15),  $K_p$  ranged from 1 to  $2^+$ , IMP-6 was inbound moving from 20.8 to 14.1 Re on the evening side of Earth (18.0 to 19.5 LT). Again, TKR peaks occur even at the lowest levels (AE  $\approx$  20) of auroral magnetic activity. Part of the reason for seeing TKR enhancements  $>$  30 dB in the early and middle portions of the day in Fig. 15 is that the background curve for this day is considerably lower than those applicable to the other days in this series (Figs. 12-14). The peaks tend to cover a broader frequency range at the low compared to high AE values, but this generalization has significant exceptions which negate its applicability.

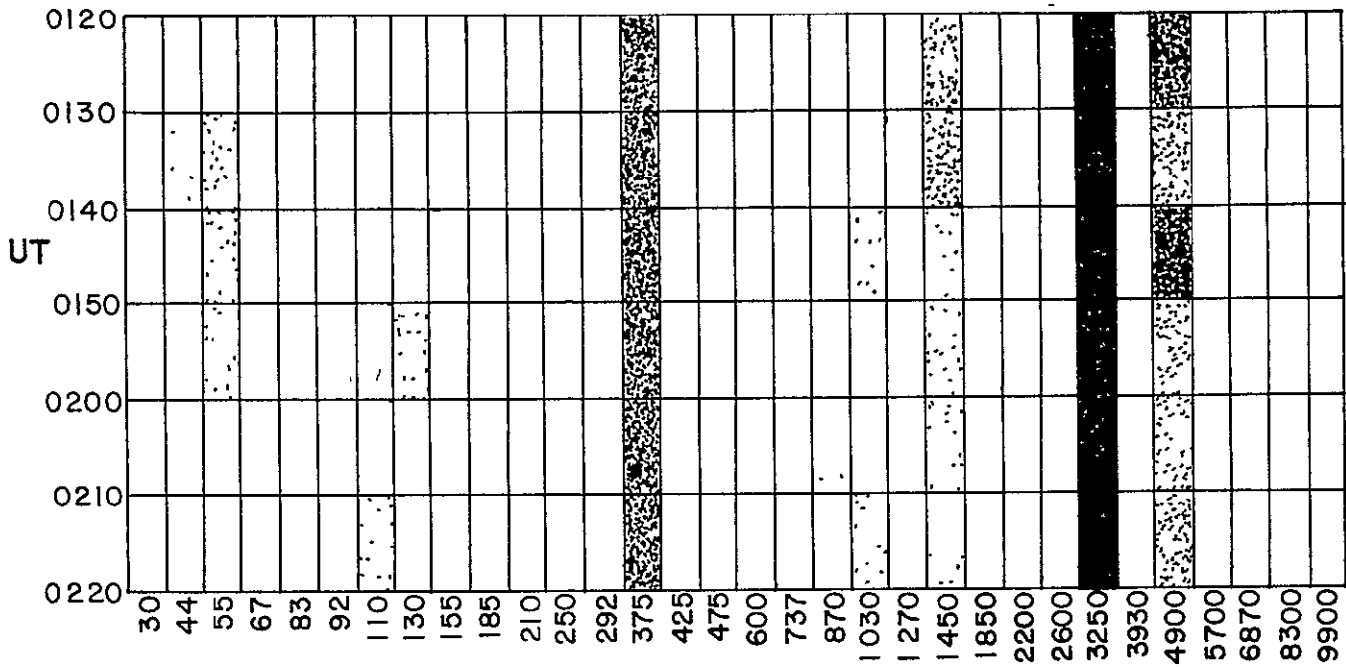
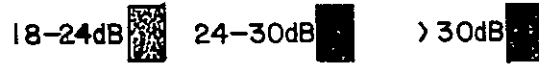
In all four summary figures (12-15), a peak is always evident with some variation in magnitude at 4900 kHz. This might stem from a calibration problem in the particular radiometer channel or from an incorrect deduction of the noise background level in this part of the spectrum. Until these possibilities are resolved, no attempt will be made to deduce any physical significance for its presence.

All of the foregoing spectra, as indicated earlier, are hourly averages. In a preliminary attempt to determine how the spectral characteristics might change in periods of less than an hour, several 10-min average spectra were generated from the data. Two sets of these, for the hours of 0120-0220 UT, August 5, 1972, and 1132-1232 UT, August 6, 1972, are illustrated in Fig. 16. The upper set corresponds to the hourly spectrum centered at 0200 UT in Fig. 12, and the lower to the spectrum centered at 1200 UT in Fig. 13. The format for Fig. 16 differs in that six levels of peak magnitude are given instead of four. Also, the background curves used to discern the peaks were derived solely from the 10-min average spectra, and they are different from the whole-day background

IMP-6 SPECTRAL PEAKS



720805, 0120-0220



720806, 1132-1232

$F_p$  (KHz)

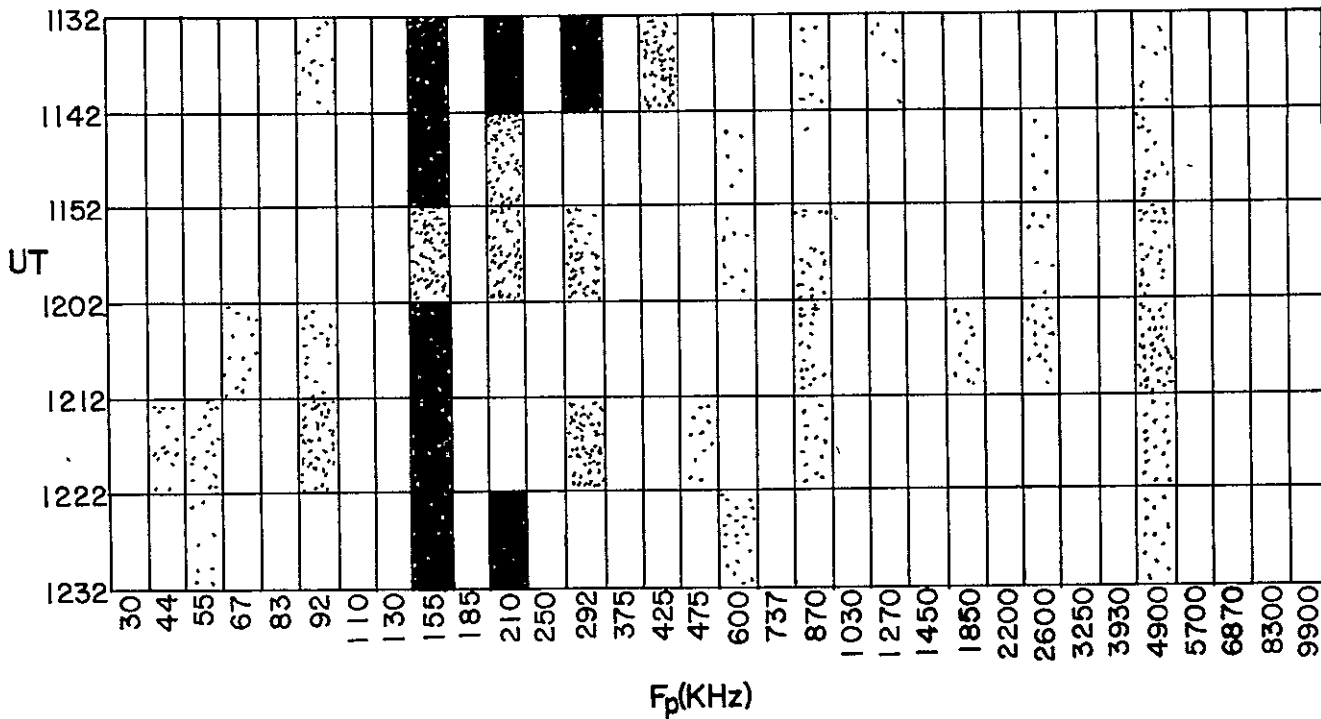


Fig. 16. IMP-6 ten-minute average spectral peaks for two 1-hr periods on Aug. 5, 1972 (top) and Aug. 6, 1972 (bottom).

curves used for August 5 and 6 in Figs. 12 and 13. For these reasons a direct comparison of the 10-min spectra (or their summation) with their corresponding hourly spectrum must be made carefully.

In the 0120-0220 spectra of Fig. 16, peaks persist for the whole hour at 375, 1450, 3250 and 4900 kHz, and these are also evident at 0200 UT in Fig. 12. The shorter-lived peak at 55 kHz (0130-0200 UT) also appears in the hourly spectrum, but those appearing in only a single 10-min period (i.e., at 92, 110, and 870 kHz) are washed out in the hourly spectrum. The peak appearing at 1030 kHz in two 10-min spectra are not seen in the hourly average, but the one at 44 kHz (0130-0140 UT) does persist in the 1-hr. spectrum.

In the 1132-1232 UT spectra of Fig. 16, 3 strong peaks occur at 155, 210, and 292 kHz, each separated by one radiometer channel. In the hourly spectrum centered at 12 UT (Fig. 13), these peaks at 155 and 210 kHz overlap and produce a single peak at 185 kHz, and the 292 kHz peak remains separate. The 4900 kHz peak in all six 10-min spectra carry over into the 1-hr spectrum, but the remaining rather numerous shorter-lived peaks are washed out in the hourly average.

The main point of Fig. 16 is that the strong spectral peaks seen in many 1-hr average spectra appear because the noise is intense for the whole hour. Enhancements of shorter duration do occur, sometimes strong enough to affect the hourly average, but often not. This indicates that hourly-averaged spectra can be utilized to investigate the physical processes which produce the noise.

From the study of the above selected spectra (Figs. 2-16) and others not illustrated here, some general features of the broad spectral characteristics of magnetospheric radio noise have emerged. They are summarized here, and in the next section some statistics of TKR peaks are discussed.

In the lower end of the spectra ( $f \lesssim 100$  kHz) the noise magnitude has a general tendency to decrease with increasing frequency as illustrated in Fig. 1 and Fig. 11 as a quasi-continuous background, but the shape is often modified. At times the TKR radiation extends below 100 kHz and adds to the background which results in a flattening of the spectrum (c.f., Fig.

10), or even a positive slope (c.f., Fig. 9). At other times an apparent enhancement or peak appears below 100 kHz, as in Figs. 2 or 3, which tends to obscure the quasi-continuous (q.c.) background. This occasional peak may arise from a process similar to that generating the TKR peaks near 300 kHz, or it may be a cutoff effect. That is, the q.c. background may have risen to a high value, but the lower frequency cutoff which is usually below the bottom frequency of the observed spectrum (25 kHz) has also increased to perhaps 40-50 kHz; the overall result of this combination would be the appearance of a peak at a frequency slightly higher than this lower cutoff.

In the higher end of the spectra (2-10 MHz) there appear to be two main contributors to a background level, upon which is superimposed enhancements that are apparently related to magnetic disturbances. Between 1 and approximately 4 MHz, cosmic noise which peaks at about 3 MHz (see Fig. 1) is usually prominent in the total spectrum but the magnitude is sometimes greater than that attributable to cosmic noise alone. From about 4 MHz up to the observed top frequency at 10 MHz, the noise magnitude nearly always increases. This positive slope is indicative of the incursion of terrestrial radio noise and interference penetrating from below the ionosphere to the satellite - that is, the "ground breakthrough" noise. Superimposed on these two background components is noise due probably to magnetospheric processes (e.g., particle precipitation) during magnetic disturbances; a preferred frequency for the peak of this noise seems to be near 3250 kHz.

The middle portion of the spectra (100-1000 kHz) is where the TKR radiation is always found. This noise, first discovered by Dunckel, et al (1970), and independently by Stone (1973), James (1973), and Gurnett (1974), peaks near 200-300 kHz. It is one of the most striking features of magnetospheric noise spectra, and contrary to the findings of Gurnett (1974) it exists not only during geomagnetic storms and substorms, but also at times of very low activity as we have shown in Fig. 15.

This TKR radiation has been detected by IMP-6 at radial distances from 5 to 30 Re, by RAE-2 at 60 Re, and by ISIS-1 (James, 1973) as close as 1.3 Re. It has been seen by IMP-6 on all sides of the earth (that is,

at all local times), although the intensity does seem to be greatest in the evening and midnight sectors, less in the post-midnight to early morning sector, and least on the dayside. It persists at all levels of geomagnetic activity with a slight tendency toward highest intensity during major substorm activity.

These characteristics and the statistical properties of TKR radiation are examined in more detail in the next section.

### 3. STATISTICS OF TERRESTRIAL KILOMETRIC RADIATION

#### 3.1 Parameters Used

To statistically investigate changes in the characteristics of magnetospheric radio noise spectra, several key parameters are utilized. The spectrum in Fig. 3, for example, illustrates the definition of these parameters.

Peak Frequency ( $f_p$ ) - the frequency at which the noise brightness exhibits a local maximum. In Fig. 3, multiple  $f_p$ 's occur at 44, 375, 1450, 3250, and 4900 kHz.

Peak Brightness ( $B_p$ ) - the noise intensity ( $Wm^{-2} Hz^{-1}$ ) at  $f_p$ .

Upper Cutoff Frequency ( $f_u$ ) - the frequency at which an enhancement centered at  $f_p$  returns to the background level on the high-frequency side of the peak. In Fig. 3, these occur at 82, 600, 1850, 3900, and 5700 kHz.

Lower Cutoff Frequency ( $f_l$ ) - same as  $f_u$  except it is on the low-frequency side of a peak. In Fig. 3, these are 30, 210, 1250, 2600, and 3900 kHz.

Peak Bandwidth (PBW) - the difference between  $f_u$  and  $f_l$  in kHz.

These definitions were used in an initial manual analysis of approximately 700 hourly spectra, to ascertain their variations as a function of local time (LMT), radial distance (R) and magnetic activity ( $K_p$ ). The 700 spectra were generated by a computer routine which searched the IMP-6 data base and extracted periods with high noise levels. The routine, designated the "Angle Plot Program", was developed by Washington Data Processing, Inc.

#### 3.2 Preliminary Analysis

The results indicate that the value of the peak frequency has no obvious relationship with R, LMT or  $K_p$ . Scatter plots of  $f_p$  against these three variables show that a high (or low) peak frequency can occur at any radial distance, local time or level of magnetic activity. Also, no pattern relating  $B_p$  or PBW to these variables could be found.

Therefore, a purely statistical determination of the distribution of fp was made. The data base utilized for this (~ 700 points) was derived from spectra taken at all local times, months (or seasons), radial distances and degrees of magnetic activity. The result is shown in Fig. 17, where the number of occurrences of a given fp is expressed as a fraction of the total number of points. The peak occurs most often (18% of the time) at a frequency of about 280 kHz, and the distribution about this mode is approximately log-normal. The small secondary peak at 3250 kHz may be due to the fact that the wavelength of this frequency is equivalent to the antenna half-wavelength (M. Kaiser, private communication).

Integration of the curve in Fig. 17 reveals that about 80% of the TKR peak frequencies lie between 125 kHz and 600 kHz, 10% fall below 125 kHz and 10% fall above 600 kHz. The fluctuation in position of the peak frequency is probably related to the source generation mechanism rather than propagation factors, as will be discussed in subsequent sections of this report.

The distributions of upper and lower cutoff frequencies as defined above were derived in a similar manner, with the results shown in Fig. 18. There is an overlap between 100 and 500 kHz because both the lower and upper cutoffs shift up or down the frequency scale more or less in concert with the shift of the peak frequency itself. In any event, the lower cutoff is found most often at about 100 kHz, and the upper at 380 kHz.

These results indicate that the mid-frequency portion of the typical composite spectrum reported by Stone (1973; see Fig. 1) needs only slight modification, in that it appears that the fall off in intensity is sharper above the peak than below it. As will be seen in the next graph (Fig. 19), the peak brightness as indicated by Stone should be increased by a factor of about 100, at least on the basis of the IMP-6 spectra analyzed here.

The final relationship derived from the manually-extracted parameters of the 700 spectra concerns the variation in peak brightness as a function of peak frequency (Fig. 19). It turns out that the sharply defined upper limit on this scatter plot is fixed by the saturation level of the IMP-6 radiometers, which increases monotonically with channel fre-

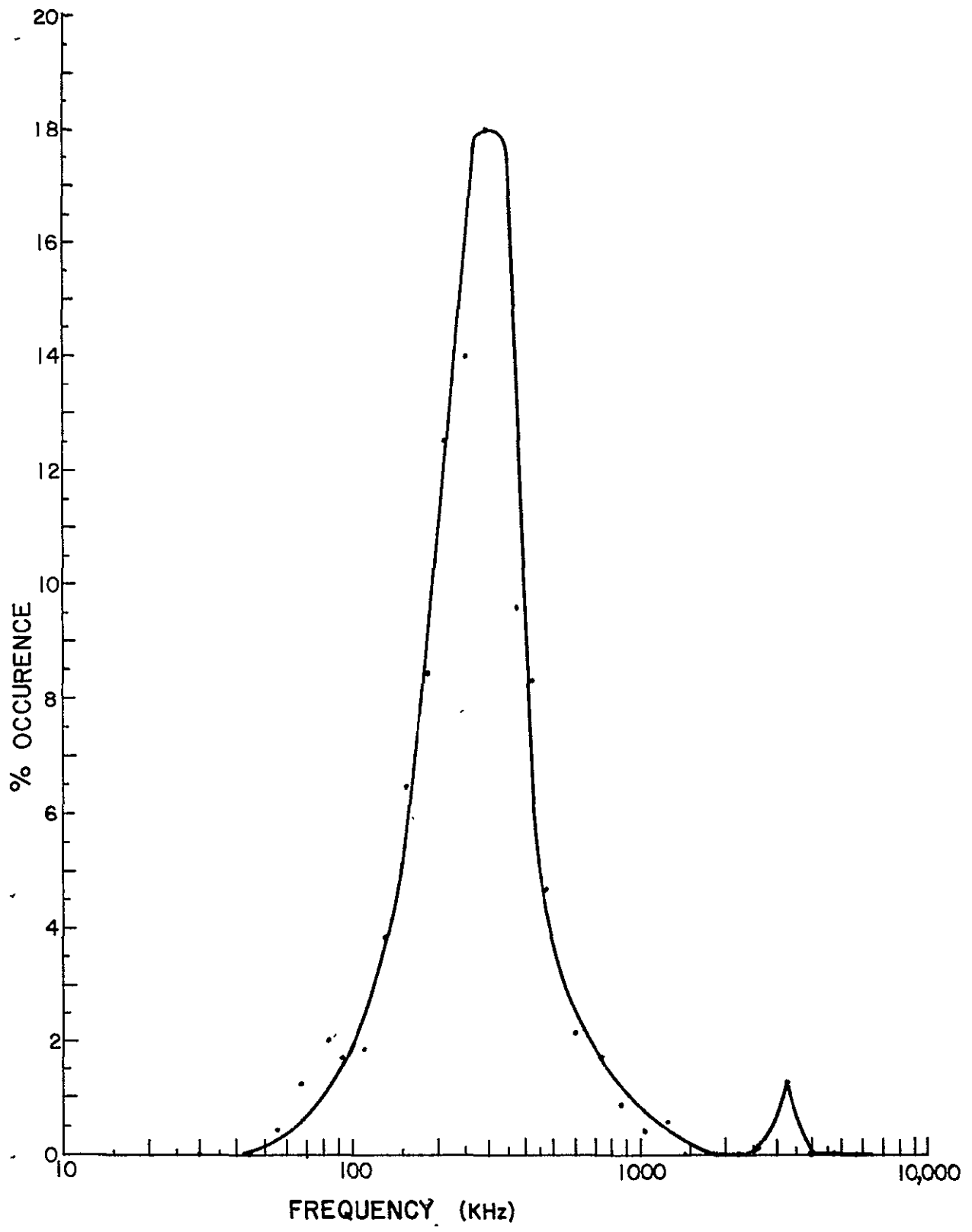


Fig. 17. Statistical distribution of TKR peak frequencies based on ~ 700 data points representing all local times, seasons, IMP-6 radial distances, and magnetic activity levels.

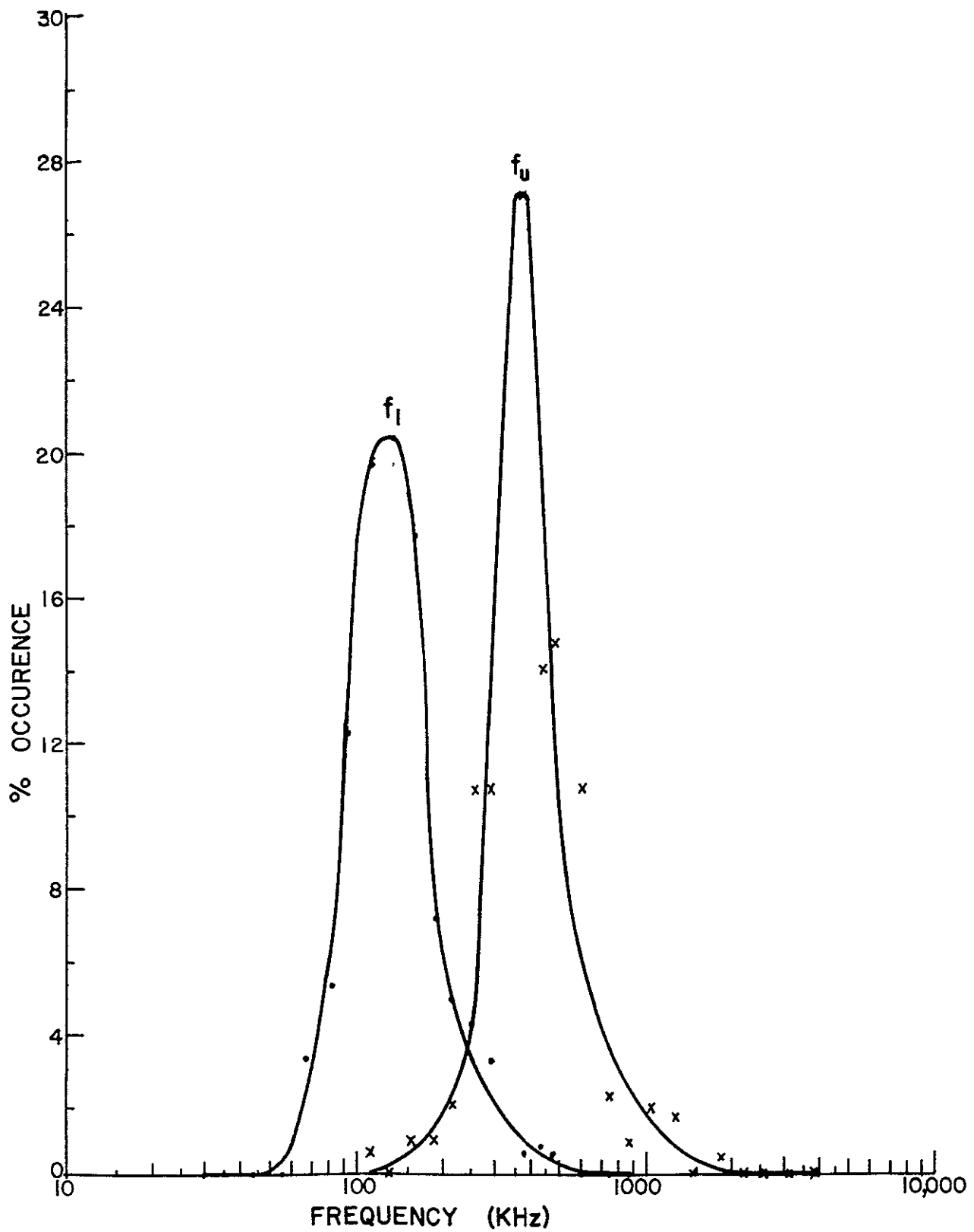


Fig. 18. Upper ( $f_U$ ) and lower ( $f_1$ ) cutoff-frequency statistical distribution of TKR enhancements based on  $\sim$  700 IMP-6 data points.

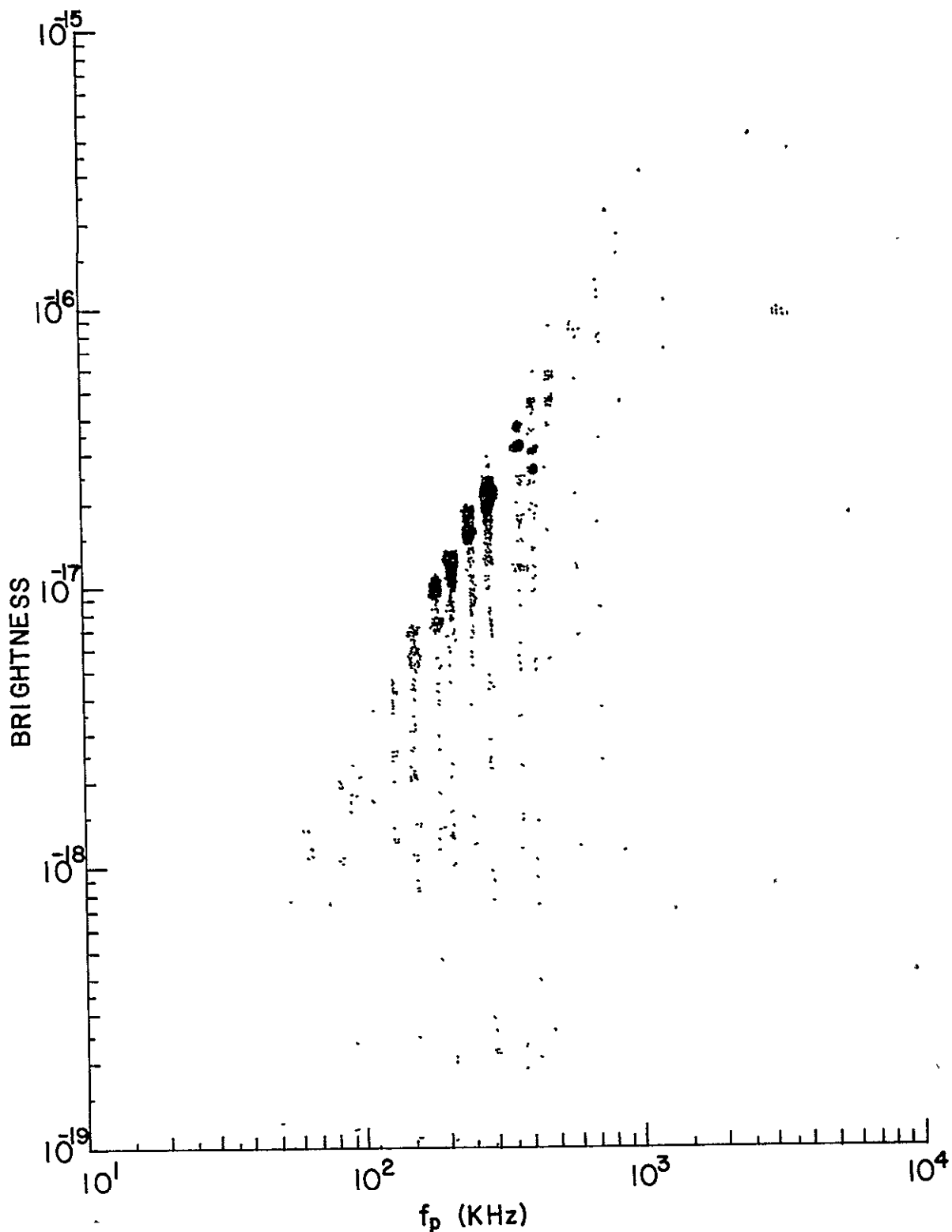


Fig. 19. Peak brightness as a function of peak frequency derived from  $\sim$  700 IMP-6 data points. All local times, seasons, radial distances and magnetic activity levels.

quency (M. Kaiser, private communication). The important point of this figure is thus the concentration of points near saturation, with relatively few at lower brightness magnitudes, regardless of frequency.

### 3.3 Computer Analysis

On the basis of these manually derived, preliminary statistics, it was decided to employ modifications of the Angle Plot Program for computer analysis of the entire IMP-6 data base. To do this, the parameters listed in section 3.1 were slightly modified. A curve-fitting routine developed by J.D. Chang of Washington Data Processing, Inc. finds the peak frequency and associated peak brightness; the upper and lower cutoff frequencies are defined at the first point above and below the peak where the brightness has decreased by a factor of two (3 dB), and the bandwidth is the difference between these two frequencies. An enhancement of at least 3 dB is required for a peak to be called out.

To improve the statistics, local mean time was grouped into six 4-hr time blocks centered on local midnight (2200-0200 LMT), local noon (1000-1400 LMT), and so on. The frequency range of interest was restricted to 100-1000 kHz. For each time block, the following plots were made:

- a. peak brightness vs. peak frequency
- b. peak brightness vs. bandwidth of peak
- c. peak brightness vs. LMT
- d. peak frequency vs. bandwidth
- e. peak frequency vs. LMT
- f. bandwidth vs. LMT

In addition, plots of peak brightness vs. peak frequency were made using all local times, radial distances, and months, for magnetic conditions defined by

$$\begin{aligned} 0 &\leq K_p \leq 2^- \\ 2 &\leq K_p \leq 5^- \\ &K_p \geq 5 \end{aligned}$$

The results of this analysis reveal several interesting features which must be taken into account when considering noise source generation mechanisms.

### 3.3.1 Peak Brightness vs. Peak Frequency

Examples of peak brightness as a function of peak frequency are given in Figs. 20 and 21 for the evening (18-22 LMT) and morning (06-10 LMT) time blocks, respectively. These two periods have the greatest and least number of peaks, respectively, of all the six 4-hr time blocks. The most striking feature is the bimodal distribution of points in both figures. The appearance of the other four 4-hr time blocks (not shown) is similar in this respect.

The main cluster of points (Fig. 20) is near the saturation level as found before (Fig. 19), but a second major clustering is near a brightness level of  $10^{-19} \text{ Wm}^{-2} \text{ Hz}^{-1}$ . Relatively few points fall between these two maxima, and very few points fall below  $10^{-19}$  in the evening time sector. The midnight (22-02 LMT) and predawn (02-06 LMT) sectors have distributions similar to Fig. 20, except in the latter sector there are fewer peaks at saturation and a gradual thickening of the population below the  $10^{-19}$  level.

Going into the morning side (06-10 LMT) there are fewer peaks near saturation and more below  $10^{-19}$  as is evident in Fig. 21. The noon sector (10-14 LMT) has a distribution quite similar to that of Fig. 21. The afternoon sector (14-18 LMT) has a bimodal distribution which is like Fig. 20, but there are relatively more peaks with brightnesses less than  $10^{-19}$ .

The grouping near  $10^{-19} \text{ Wm}^{-2} \text{ Hz}^{-1}$  shows only a slight decrease in brightness with increasing frequency. It occurs in all time blocks and makes its presence felt in other parameters investigated, as will become evident shortly. To see if it, along with the second grouping near saturation change appreciably with magnetic activity, the data base (3000 points total) was analyzed as a function of Kp. The results, for the Kp intervals specified above, are illustrated in Figs. 22, 23 and 24.

At the lowest level of magnetic activity (Fig. 22) the bimodal

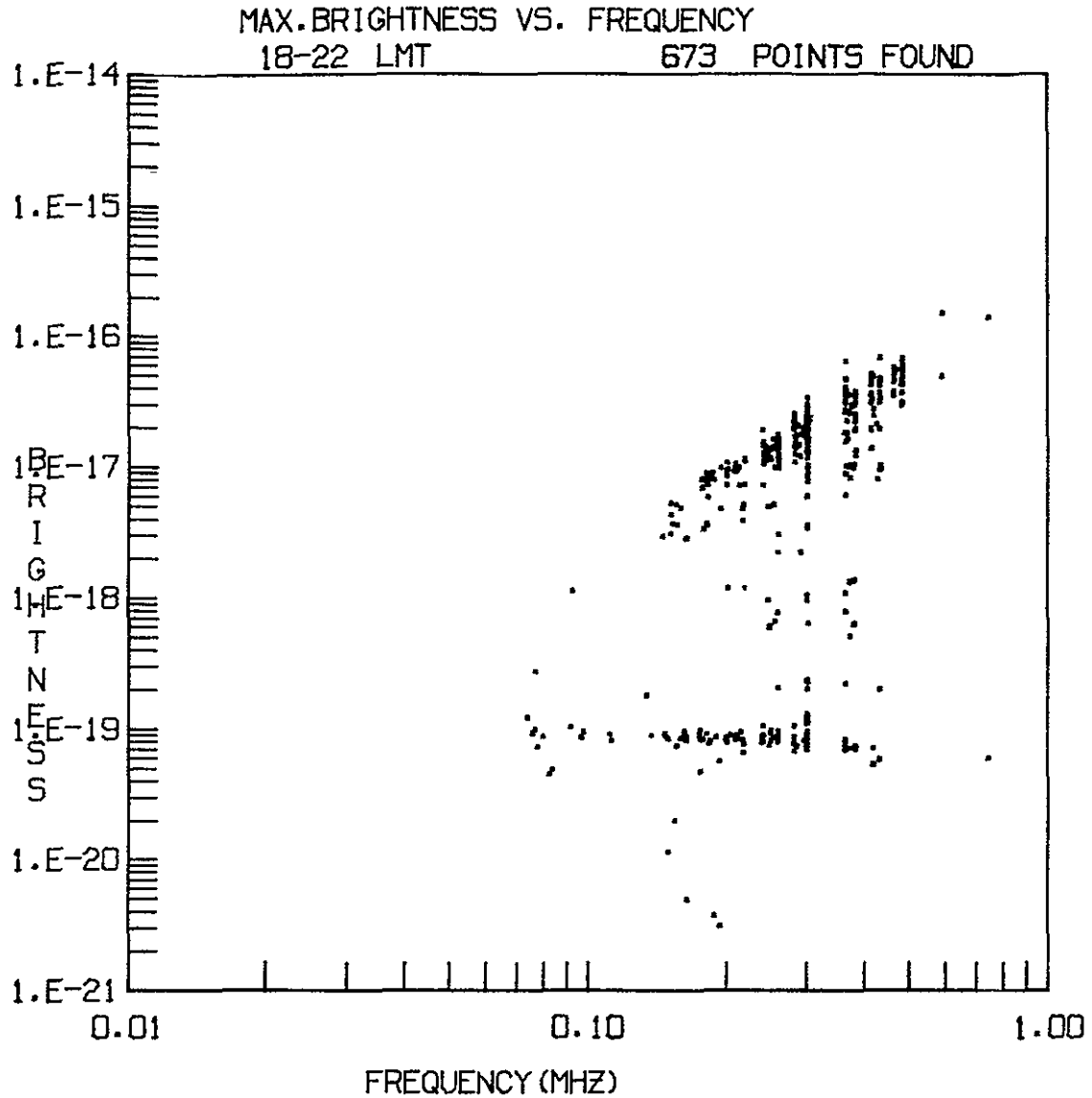


Fig. 20. Peak brightness as a function of peak frequency for the 18-22 LMT time block derived from IMP-6 data by "Angle Plot Program" computer routine. Includes all radial distances and magnetic activity levels.

distribution is strongly evident, indicating that large peaks occur even during quiet times, and the flat cluster at  $10^{-19}$  is still evident. There are a significant number of peaks below  $10^{-19}$ , negating any idea that this level is due to instrumentation threshold effects. A similar situation

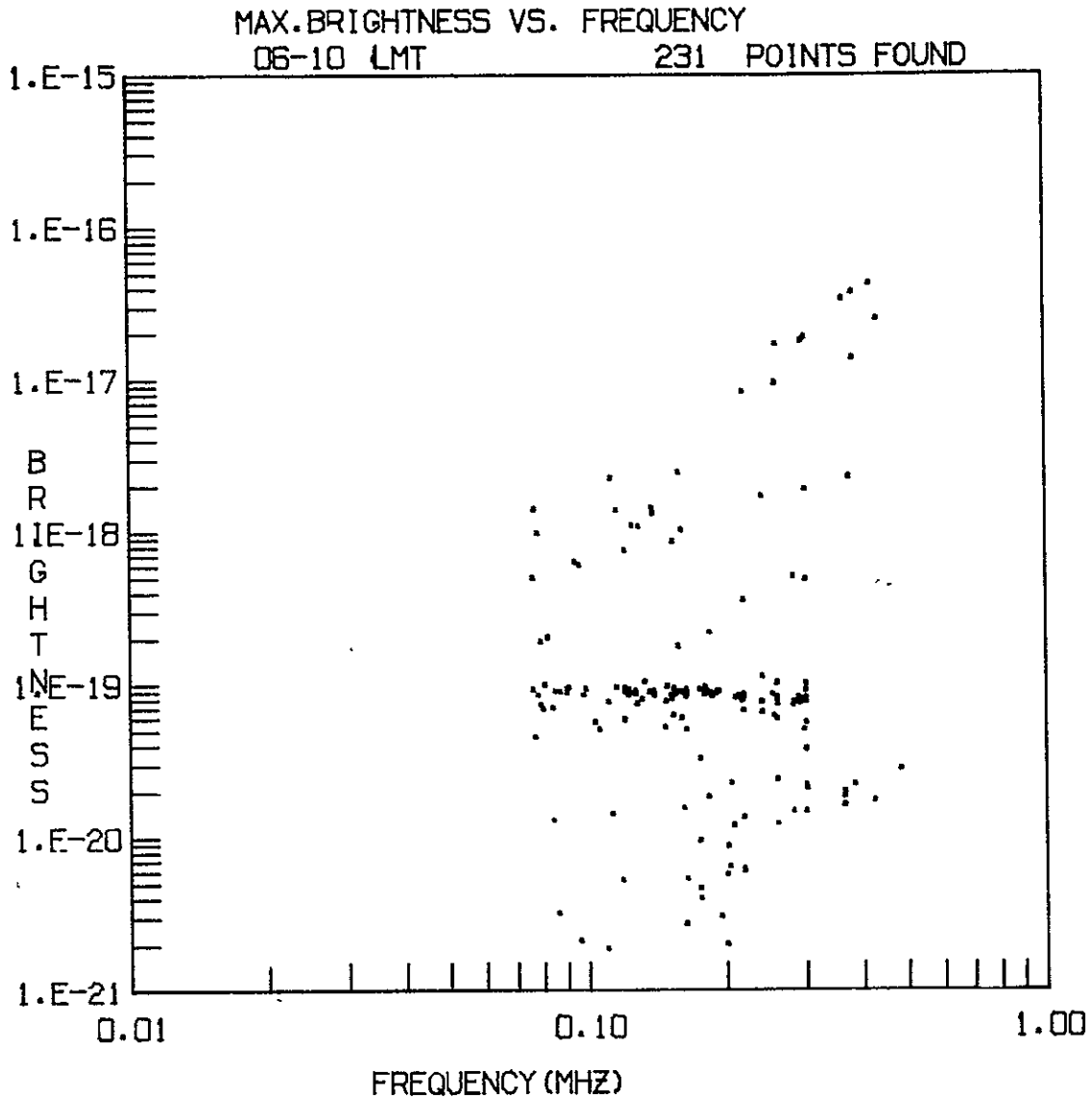


Fig. 21. Same as Fig. 20 but for 06-10 LMT time block.

exists for moderate levels of  $K_p$  (Fig. 23), and it is only with high  $K_p$  (Fig. 24) that the low-brightness peaks ( $< 10^{-19} \text{ Wm}^{-2} \text{ Hz}^{-1}$ ) disappear. Here (Fig. 24) it appears that there are relatively more peaks near saturation than near the low-brightness peak level.

Time has not permitted an analysis of the bimodal distribution with radial distance as the parameter. One might suspect, on the basis of comparing the spectra in Figs. 2 and 3 against Fig. 4, that the peaks

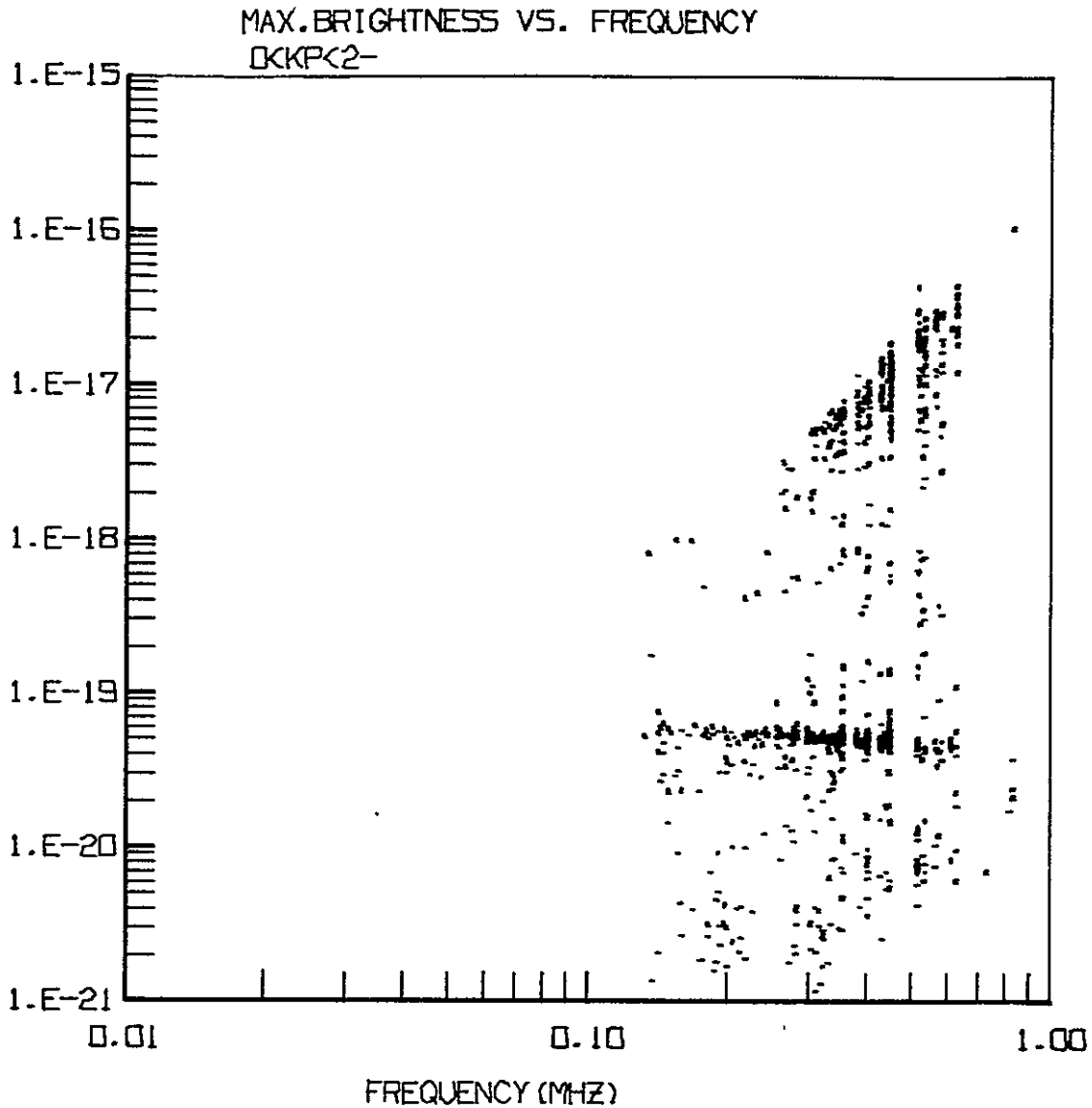


Fig. 22. Peak brightness as a function of peak frequency for quiet magnetic conditions ( $0 \leq K_p < 2^-$ ); all IMP-6 radial distances and local times included.

near  $10^{-19} \text{ Wm}^{-2} \text{ Hz}^{-1}$  might represent those occurring close in (4-6 Re), while those near saturation are seen with IMP-6 near apogee. This suspicion should be further investigated at a later date.

Apart from the possible influence of radial distance, the bimodal distribution is maintained at all levels of magnetic activity, times of

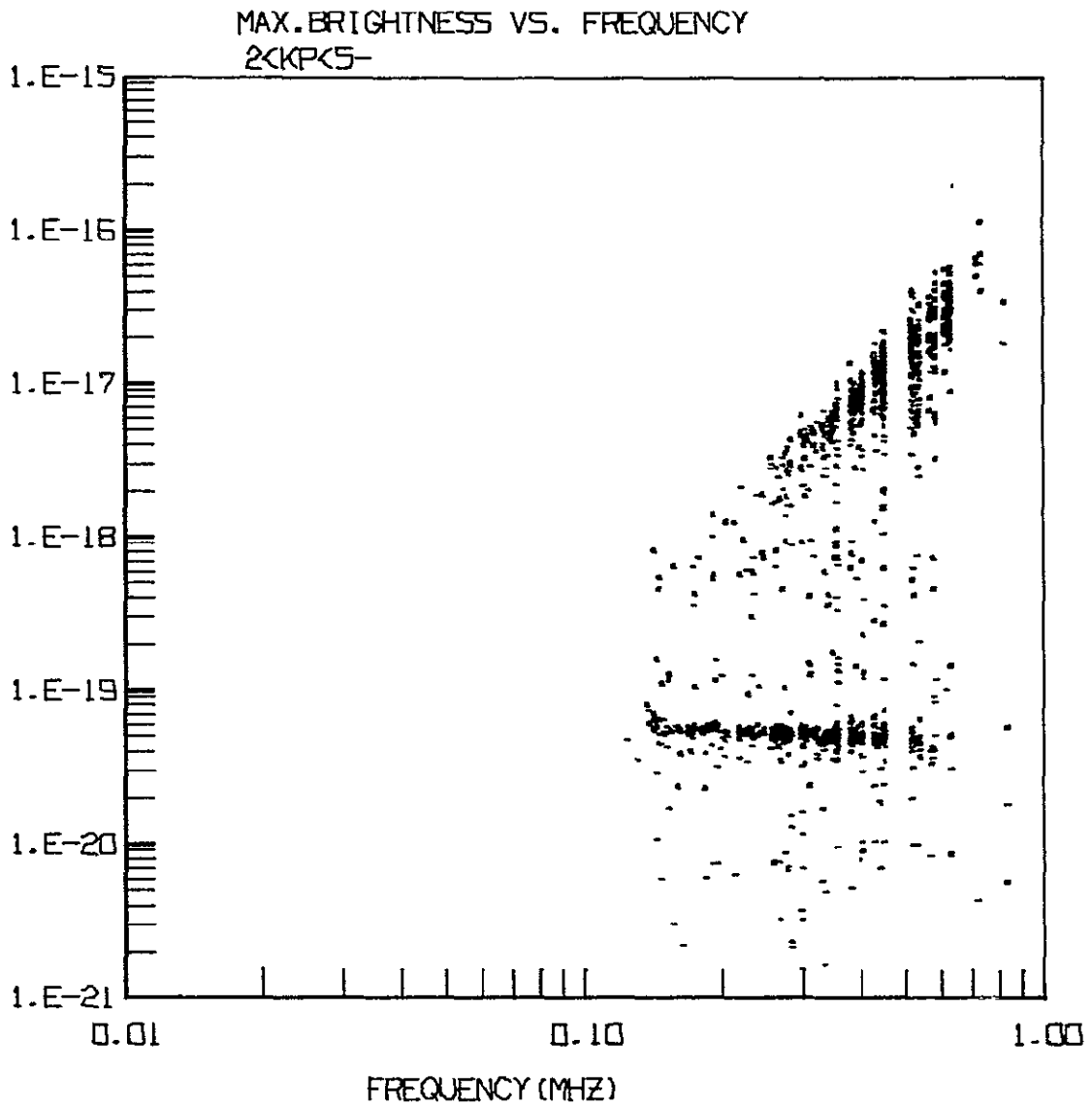


Fig. 23. Same as Fig. 22 but for  $2 \leq K_p \leq 5$ .

day, and frequencies in the TKR range. If the low-brightness cluster represents a background level which fluctuates about a mean with minor peaks ( $\sim 3$  dB), the appearance of peaks near saturation would imply that the emission source is either very strong or non-existent. That is, it is either "on" or "off" most of the time, although occasionally it is moderately active as indicated by the appearance of peaks with brightnesses

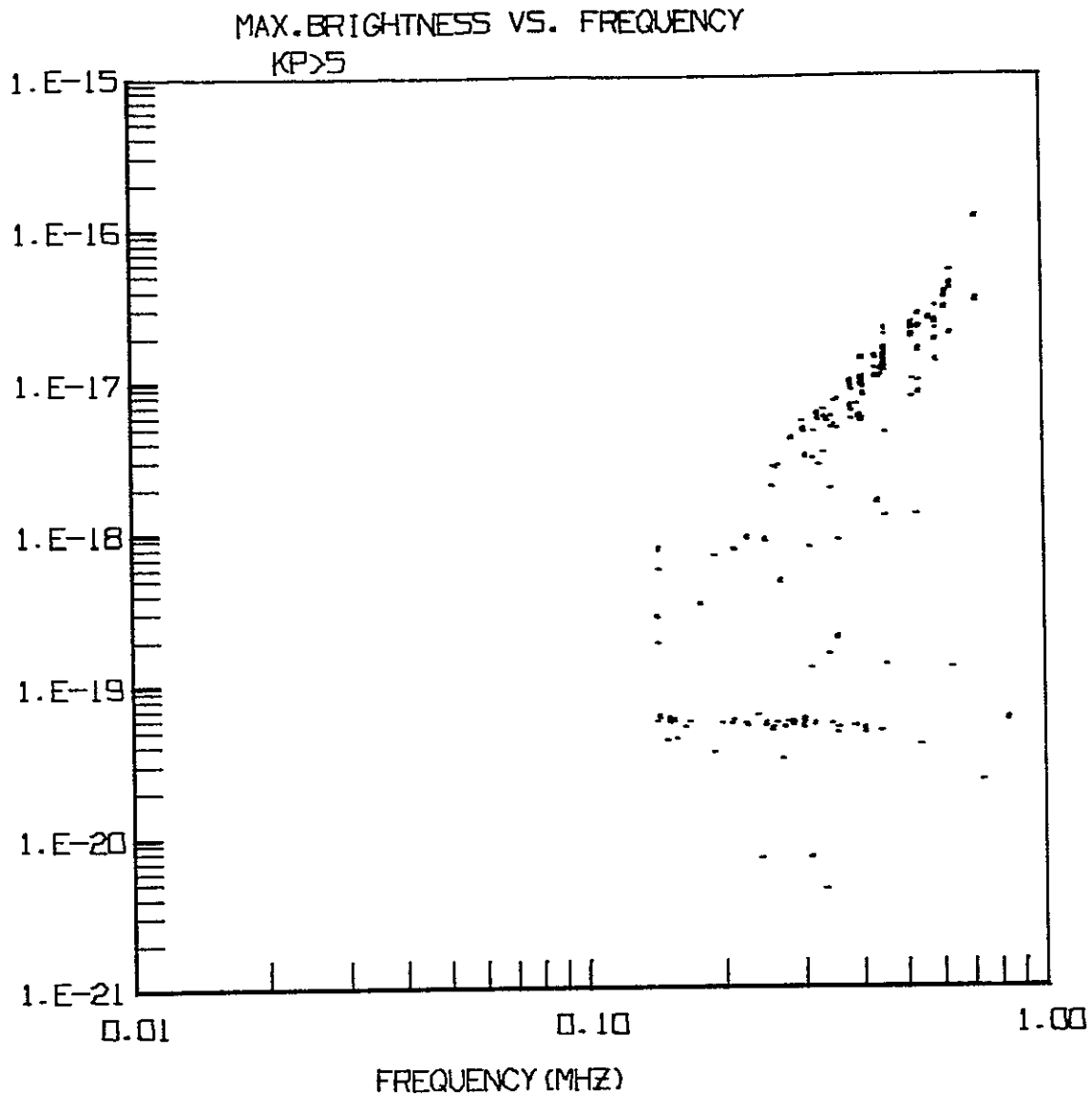


Fig. 24. Same as Fig. 22 but for  $K_p \geq 5$ .

between  $10^{-19}$  and saturation.

### 3.3.2 Diurnal Distribution of Peak Occurrence

The diurnal variations implicit in the previous section have been investigated by plotting the peak brightnesses as a function of local time. A composite of the results is given in Fig. 25. (Note the brightness scale

MAX. BRIGHTNESS VS. LOCAL MEAN TIME

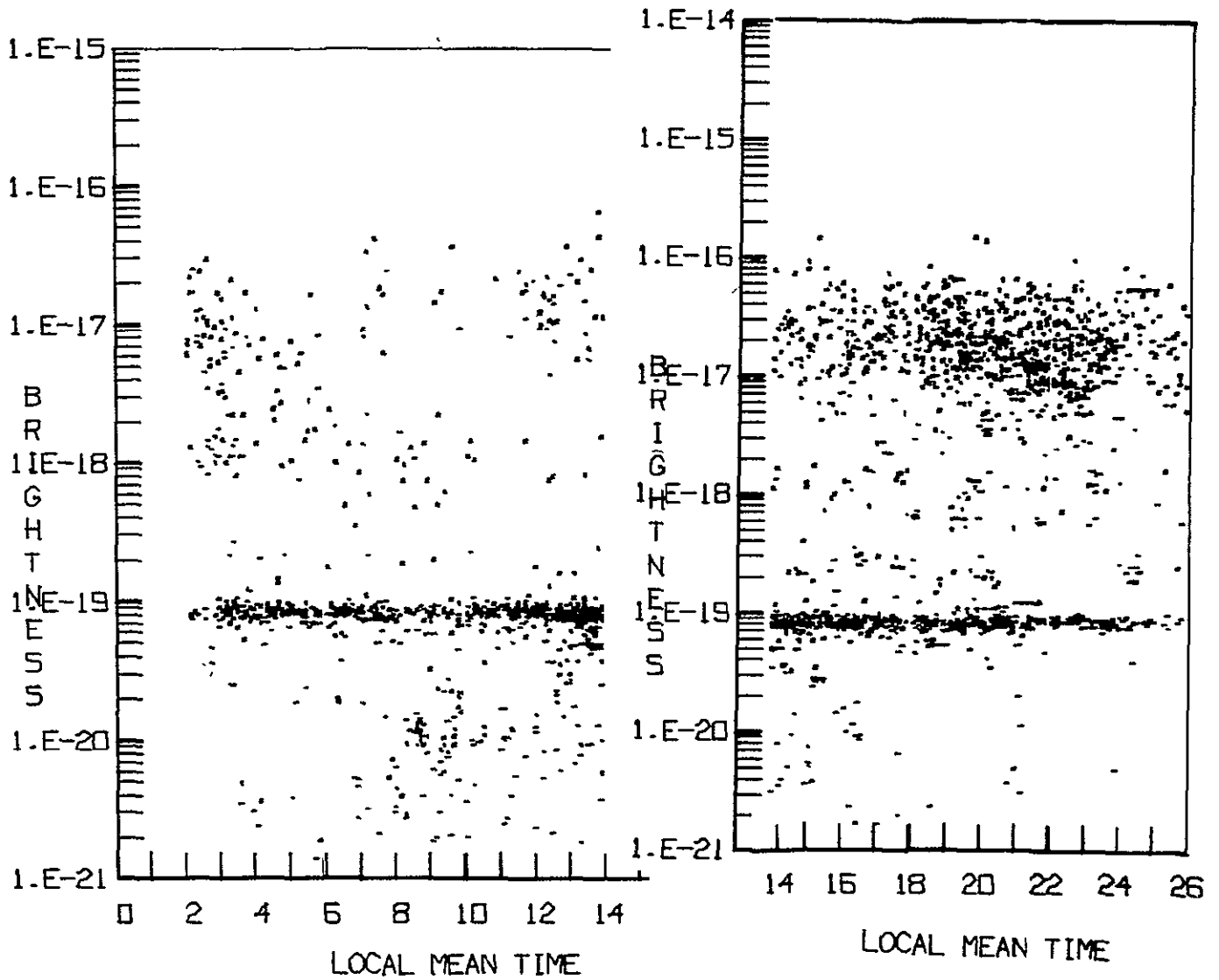


Fig. 25. Composite distribution of IMP-6 spectral peak brightnesses as a function of local time, computed in 4-hr time blocks. Note scale change at 1400 LT.

change at 14 LMT and the 22-02 LMT block positioned at 22-26 LMT.) For the whole local day, a strong component of peak brightness persists at about  $10^{-19} \text{ Wm}^{-2} \text{ Hz}^{-1}$ . A second strong component is seen between  $10^{-17}$

and  $10^{-16}$  from about 14 LMT to 24 LMT, which becomes less pronounced between midnight and 04 LMT, and is quite faint during the day time hours of 06 to 14 LMT. Again, there is a relative sparsity of peaks between these two components, and there are more low-brightness peaks during the day than the night hours.

The total number of peaks regardless of magnitude or frequency (between 100 and 1000 kHz) for each time block gives an indication of the diurnal variation as illustrated in Fig. 26. The histogram based on 3000

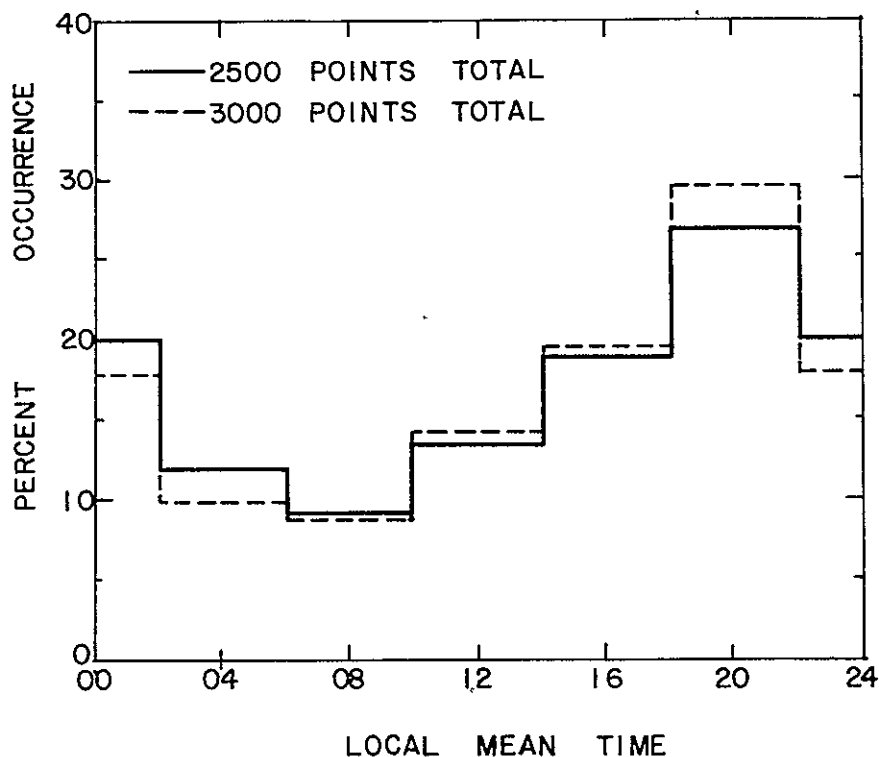


Fig. 26. Diurnal distribution of relative occurrence - frequency of TKR peaks. (Area under the histogram = 1.00).

points corresponds to the data base used in Figs. 22 through 25. The one for 2500 points is appropriate for the series of plots exemplified by Figs. 20 and 21. The 2500 points are a subset of the 3000, and both histograms are shown to indicate the degree of statistical fluctuation

imposed by two different set sizes. In this format it is clear that there is a significant diurnal change marked by a minimum in the forenoon hours and a maximum in the pre-midnight hours. This distribution is reminiscent of the diurnal variation of "splash-type" 10-keV electron precipitation events (Hartz and Brice, 1967; Hartz, 1971), wherein the maximum number of events occur in the 18-24 LT sector.

The diurnal distribution of peak frequencies is shown in Fig. 27 for the range 30 to 1000 kHz. For the whole day peaks occur between about 100 to 300 kHz; during the evening and night hours there is a tendency for a slight upward shift wherein a few peaks are seen up to nearly 750 kHz but relatively fewer are evident below about 150 kHz. The 24-hr blank between 292 and 360 kHz is due to lack of data in this frequency range. On the day side there are few occurrences above 300 kHz and rather more below 150 kHz. Thus, if there is a diurnal trend for the peak frequencies, it is toward an upward displacement on the evening and night sides, and the peaks tend to occur over a wider range of frequencies on the evening side compared to the noon and forenoon sides.

### 3.3.3 Relationships With Bandwidth

The 3-dB bandwidth of the peaks exhibits a similar diurnal pattern (Fig. 28). On the evening and night sides the width of the peak varies over a wider range of bandwidths than it does on the day side. There is a tendency for the width to be broader at night than during day for both the minimum and maximum bandwidths.

For maximum brightness versus bandwidth, there appears a bimodal distribution somewhat like those found for peak brightness as a function of peak frequency (section 3.3.1). Two of the six 4-hr time block results are illustrated in Figs. 29 and 30, for the 18-22 LMT and 06-10 LMT blocks, respectively. The peak brightness near  $10^{-19} \text{ Wm}^{-2} \text{ Hz}^{-1}$  appears to be independent of bandwidth, and it is evident in all six time blocks. The maximum cluster above  $10^{-17}$  is related to the saturation problem, and the points are more dense on the evening side (Fig. 29) compared to the morning side (Fig. 30). Fig. 29 is representative of the time block hours from 1400 to 0200 LMT, and Fig. 30 is representative of 0600-1400 LMT;

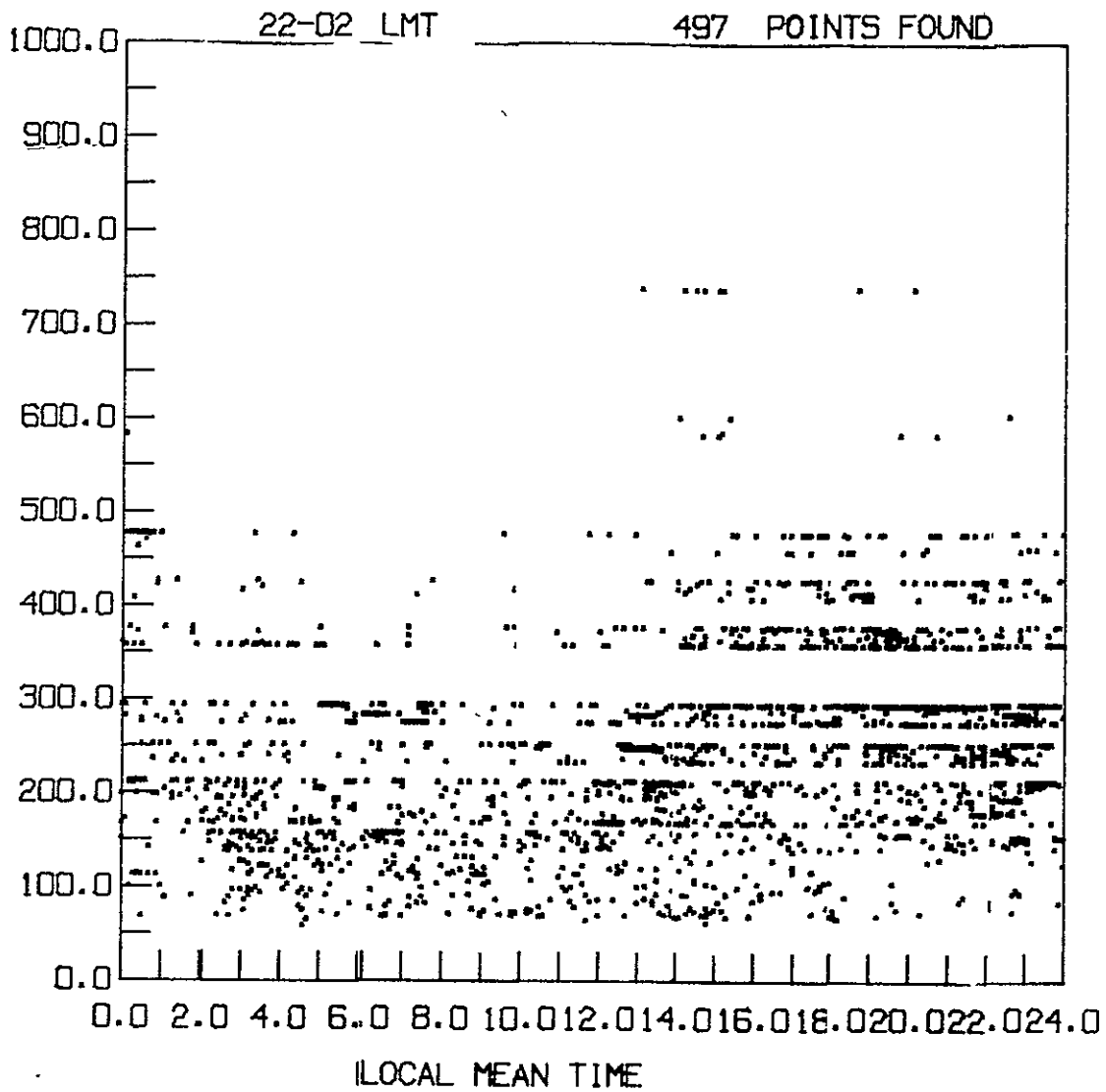


Fig. 27. Distribution of peak frequencies of TKR noise as a function of local time as derived from IMP-6 data. Ordinate is peak frequency in kHz.

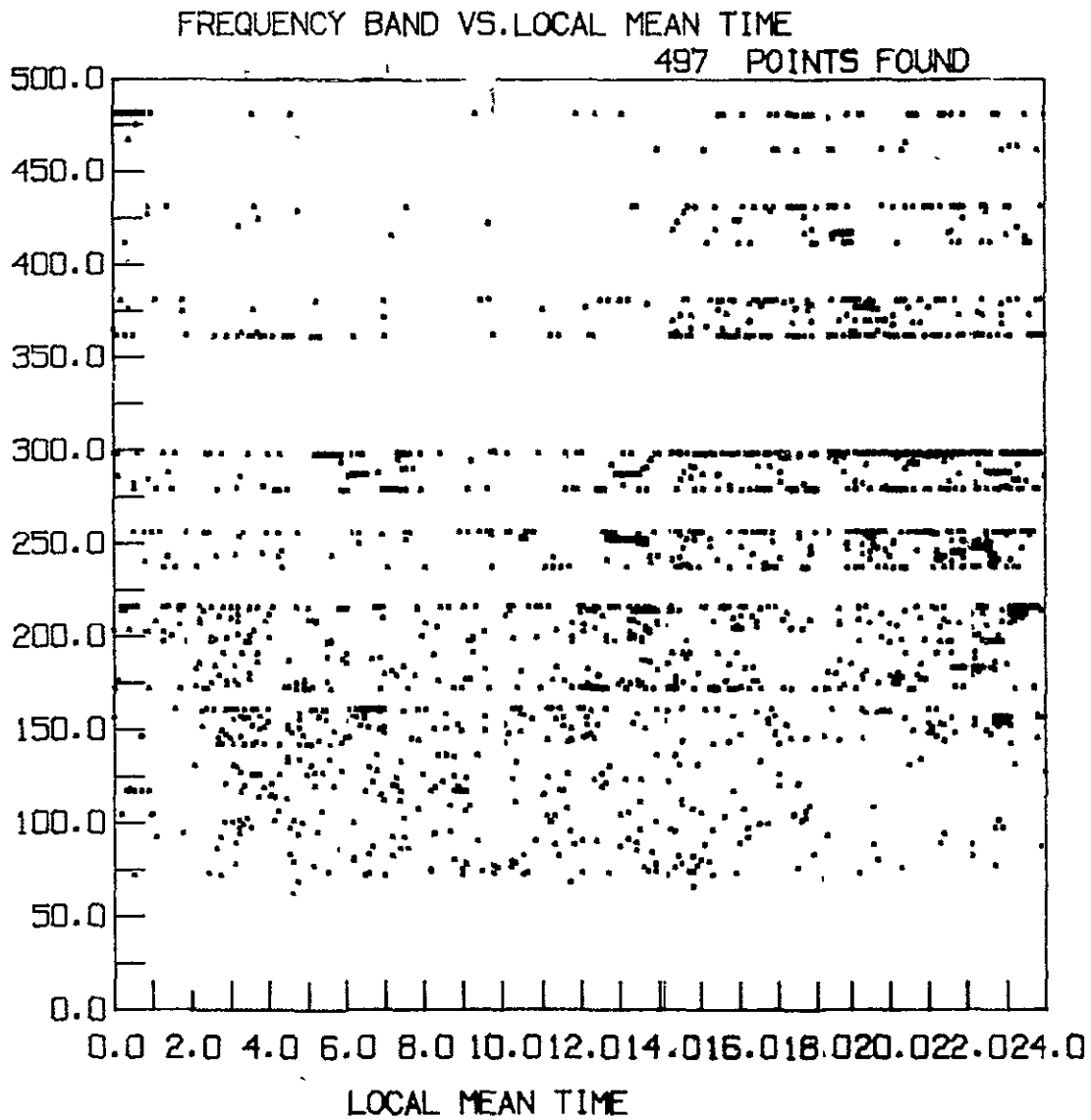


Fig. 28. Diurnal distribution of IMP-6 spectral peak bandwidths computed in 4-hr time blocks.

REPRODUCIBILITY OF THE  
ORIGINAL PAGE IS POOR

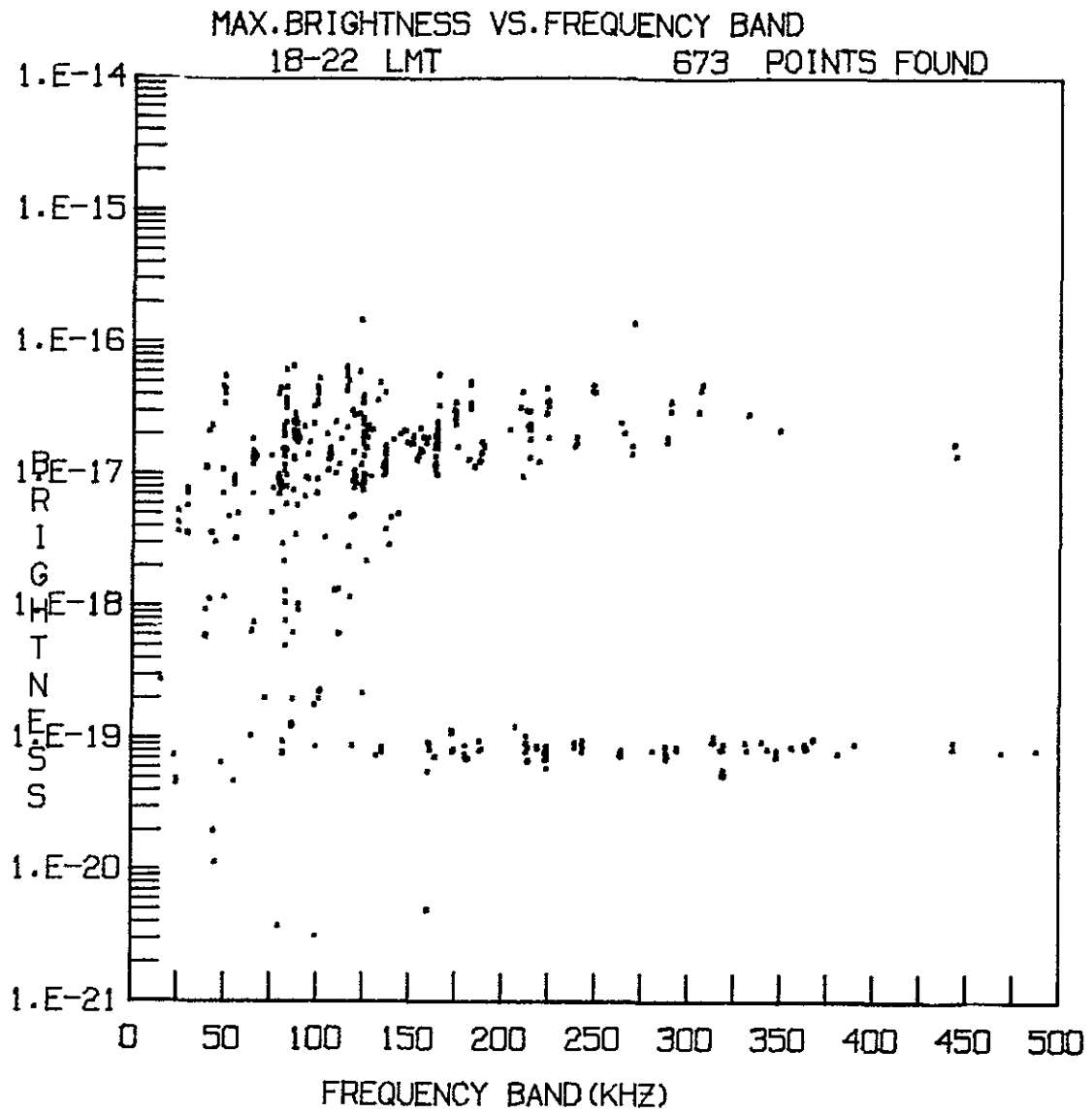


Fig. 29. Peak brightness as a function of IMP-6 spectral peak (3-dB) bandwidth for the 18-22 LMT time block.

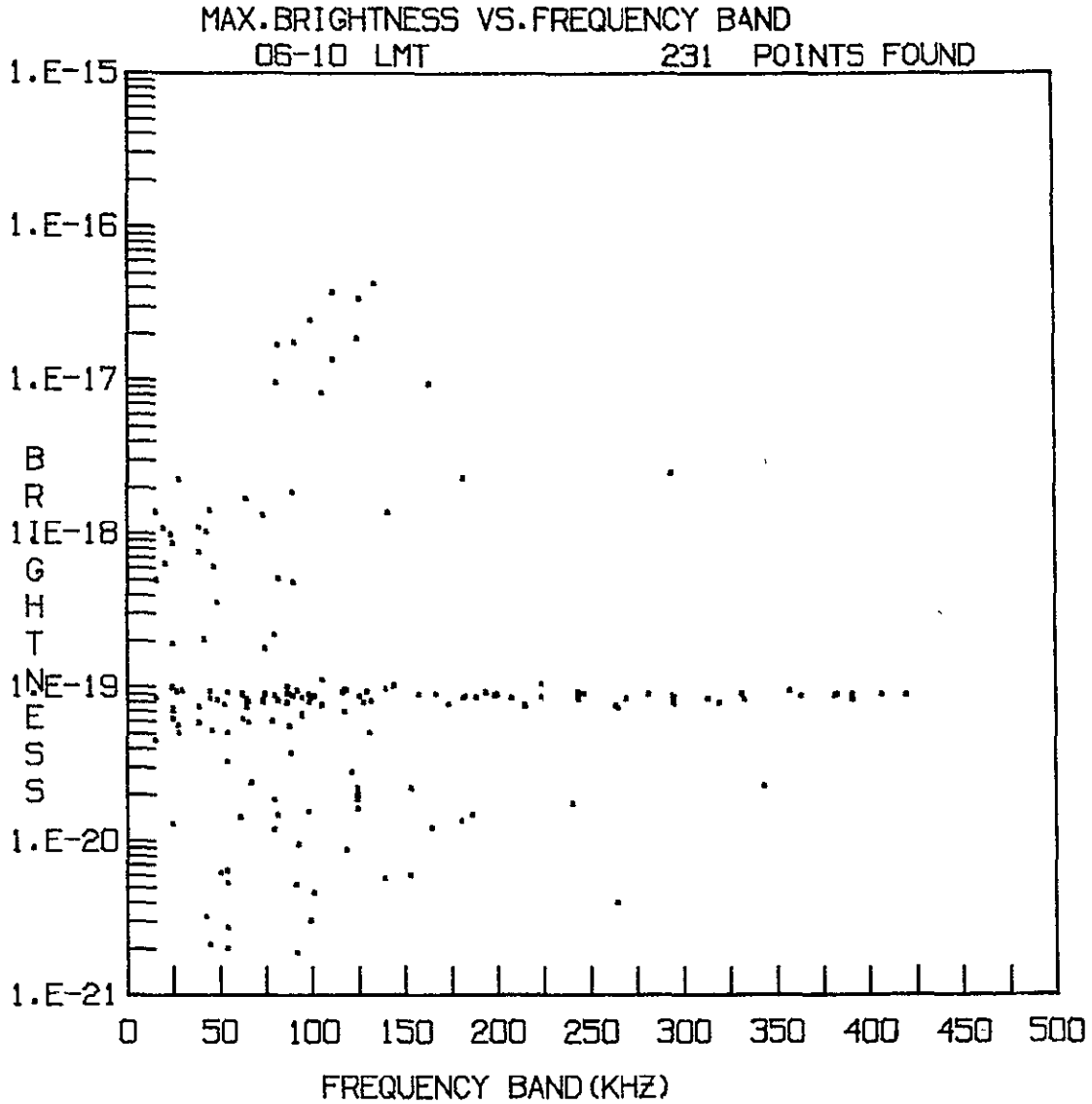


Fig. 30. Same as Fig. 29 but for 06-10 LMT time block.

the 0200-0600 LMT block has a distribution that might be described as an average of those in these two figures.

Apart from the bandwidth-independent component, there is a slight tendency for the bandwidth to increase with increasing brightness. To what extent channel saturation may obscure this relationship cannot be ascertained with the present data.

The final result of this phase of the investigation concerns the relationship between peak frequency and bandwidth of the peak. Here, too, the analysis proceeded in 4-hr time blocks, with the output expressed graphically. Two representative time blocks are illustrated in Figs. 31 and 32 for the 02-06 LT and 14-18 LT blocks, respectively. The morning time block (Fig. 31) is typical of the results for the three blocks encompassed by the hours 02-14, and the 14-18 LT result is similar to those in the 18-22 LT and 22-02 LT blocks.

The bandwidth exhibits a range of values at each peak frequency in all time blocks, but the total range decreases with increasing frequency as is evident in Figs. 31 and 32. The minimum PBW increases with increasing fp, and the maximum PBW goes the opposite way but with a smaller slope. Thus, when spectral peaks occur at the higher frequencies ( $\sim$  400 kHz) their bandwidths tend to be in the range 100-250 kHz, but peaks at the lower frequencies ( $\sim$  75 kHz) may have bandwidths from less than 50 kHz to more than 400 kHz. The minimum PBW cutoff does not appear to be due to saturation effects, but this possibility has not been completely ruled out. The shape of the envelope of the distribution of points in Figs. 31 and 32 might have interesting consequences for identifying the source generation mechanism. It may, for instance, be related to the (causative ?) precipitating particle energy spectrum in a critical way, wherein the lower the particle energy, the broader is its emission spectrum.

#### 3.3.4 Summary of Spectral Characteristics

Statistically, peak emission occurs most often (18% of the time) at a frequency of about 280 kHz, and the occurrence distribution about this value is nearly log-normal. Approximately 80% of the time the spectral peak is between 125 and 600 kHz, the other 20% being equally distributed above and below this range.

The lower cutoff frequency of the dominant TKR peak at 280 kHz is most often found at about 100 kHz, while the upper cutoff is at about 380 kHz.

The TKR peak has been observed at all hours of the day and all

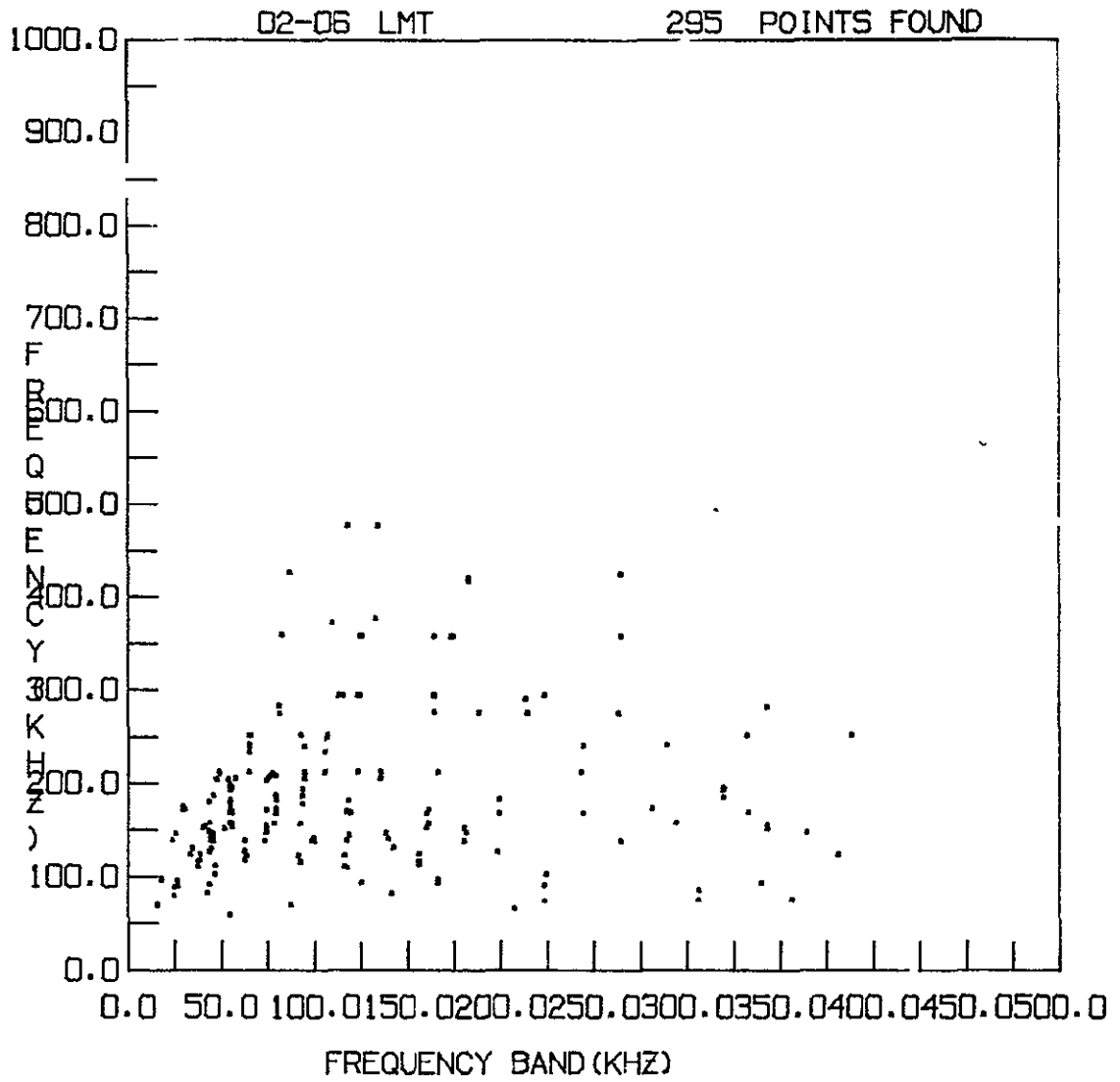


Fig. 31. Peak frequency (ordinate) as a function of 3-dB bandwidth in the 02-06 LMT time block.

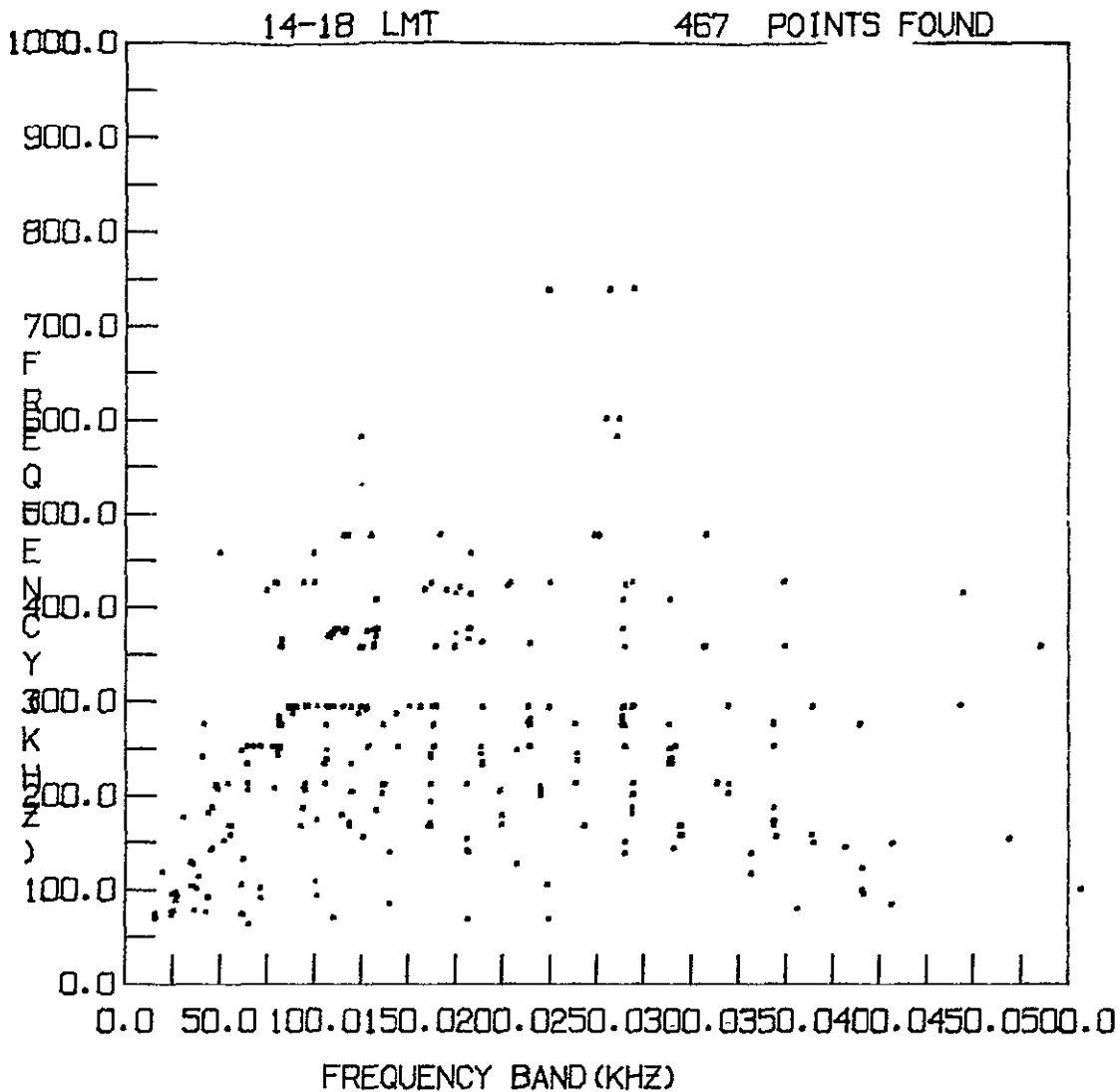


Fig. 32. Same as Fig. 31 but for 14-18 LMT time block.

levels of magnetic activity ( $K_p$  and AE) at radial distances from 1.3 Re by ISIS-1 (James, 1973) to 60 Re by RAE-2 (this report), and from 4.6 to 31 Re by IMP-6.

The relationship between peak brightness and peak frequency has a striking bimodal distribution in all hours of the day and all levels of magnetic activity. One is centered at a peak brightness of about  $10^{-19}$

$W_m^{-2} \text{ Hz}^{-1}$  regardless of peak frequency; the other is at or very near the saturation level of the IMP-6 receivers which results in an increasing brightness with increasing frequency.

A bimodal distribution is also evident in the relationship between peak brightness and bandwidth of the peak. One component is centered at  $10^{-19} W_m^{-2} \text{ Hz}^{-1}$  regardless of bandwidth; the other has a tendency toward increasing brightness with increasing bandwidth which may be partly due to channel saturation.

A preliminary investigation of large amplitude peaks corresponding to those near channel saturation revealed no obvious relationship between the value of the peak frequency and radial distance, local time or level of magnetic activity.

Taking all peaks together without regard to amplitude, radial distance of the spacecraft or level of magnetic activity, there does appear to be a diurnal variation. That is, most peaks occur in the pre-midnight hours (18-22 LT) and fewest on the morning side (06-10 LT). There is a tendency for the peak frequencies to have higher values on the evening and night sides compared to the day side, and the range of frequencies where the peaks occur tends to be somewhat larger on the evening side.

#### 4. NOISE SOURCES AND GENERATION MECHANISMS

Determination of the location of magnetospheric noise source depends upon several complicating factors. Perhaps the most important factor is identification of the appropriate generation mechanism, because the various processes are allowed only in certain regions of space. Other factors, important especially in the observational determination of source locations, are related to the noise characteristics, that is, whether the observed noise is electrostatic or electromagnetic, propagating or nonpropagating. Also, the relationship of the observing frequency to the plasma and gyro frequencies of the magnetospheric medium plays an important role.

In this section attention is confined essentially to propagating, electromagnetic noise in the frequency range of approximately 100 to 1000 kHz, in an attempt to establish the source regions and generation mechanism of the TKR radiation discussed in section 3.

##### 4.1 Noise Source Regions

An early determination of the origin of magnetospheric noise in the range 100-500 kHz was made by Jorgensen (1966) with ground-based observations at Byrd Station, Antarctica. He showed that the observable zone of noise "approximates the auroral precipitation zone". This noise was observed mainly in the evening hours until shortly after midnight, with a maximum shortly before local magnetic midnight at an invariant latitude (INL) near  $70^{\circ}$ . The normal low latitude boundary was consistent with the equatorward boundary of the auroral oval at about  $65^{\circ}$  invariant latitude. The local time dependence of the present IMP-6 results (Fig. 26) is consistent with Jorgensen's ground-based findings.

In situ measurements by Alouette 2 of 200 kHz noise presumed to be propagating in the whistler-mode by Barrington, et al (1971) exhibited a somewhat similar invariant latitude/local time distribution (Fig. 33). The observations for Fig. 33 were taken over altitudes from 640 to 3500 km, with approximately the same number of crossings at all local times. The most intense noise was observed from about 22 LT to 04 LT between  $55^{\circ}$  and

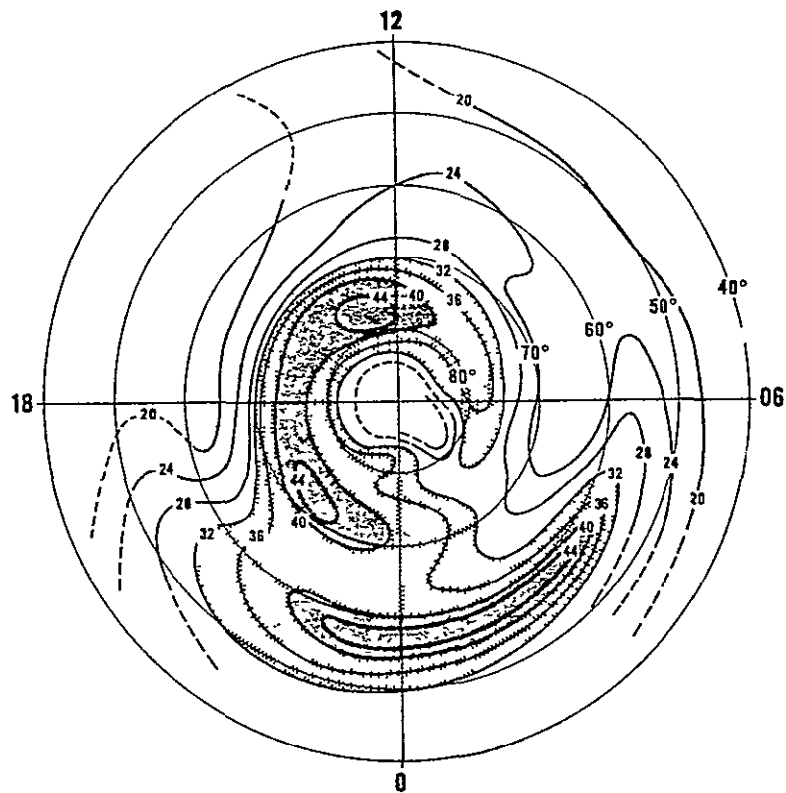


Fig. 33. Distribution of 200 kHz whistler-mode noise observed by Alouette 2, plotted in invariant/local mean time coordinates. Contours are dB above receiver threshold (Barrington, et al, 1971).

$60^{\circ}$  INL on the night side, with a second intense region centered at about 21 LT near  $70^{\circ}$  INL. A fairly intense region persists from shortly before noon to near midnight between  $70^{\circ}$  and  $80^{\circ}$ . Minimum noise was observed on the dawn side.

With OGO-6, Laaspere, et al (1971) observed 200-kHz noise at all hours of the day at altitudes between 400 and 1100 km, in invariant latitudes bounded by  $70^{\circ}$ - $80^{\circ}$  on the day side and  $65^{\circ}$ - $75^{\circ}$  on the midnight side.

The 200-kHz noise observed by these three groups (Jorgensen, 1966; Barrington, et al, 1971; Laaspere, et al, 1971) is presumed to have been propagating in the whistler mode because at the low altitudes of the space-

craft measurements the observing frequency is less than the local plasma frequency and the gyrofrequency. The ground-based observations of Jorgensen (1966) must have been of whistler-mode noise because only in this mode could it have penetrated through the ionosphere to the ground.

It is possible, however, that at least some of the noise observed by Barrington and by Laaspere could have been electrostatic. James (1973) deduced that 100-500 kHz noise detected by Alouette 2 in the dayside auroral oval (the polar cusp) was electrostatic. Maximum noise was observed as the satellite passed directly through a field-aligned sheet of precipitating electrons.

Whether the noise was electrostatic or electromagnetic propagating in the whistler mode, both James (1973) and Hartz (1971) who used the Barrington, et al (1971) data, came to the conclusion that the noise is generated not far above the satellite. The region of observed noise in the TKR range approximates the pattern of auroral particle precipitation given by Paulikas (1971), as reproduced in Fig. 34.

These early results indicate that TKR radiation is generated within a narrow range of invariant latitudes, or equivalently on a narrow band of McIlwain L shells near the boundary of open and closed field lines. The noise occurs most often in the premidnight hours where splash-type precipitation maximizes, but is also seen on the dayside where cusp particles precipitate (Fig. 34). Minimum noise occurs on the morning side where the combination of soft, cusp-particle and splash-particle precipitation appears to be a minimum.

None of these results, however, provides an indication of the height (or radial distance) at which the noise is generated. To find this parameter, direction finding techniques have been used by several investigators.

The first application of this technique was made by Fainberg, et al (1972) and Stone (1973), who utilized the spinning dipole antenna on the IMP-6 spacecraft to determine the null direction of noise at a number of points along the IMP-6 orbit. The intersection of these direction lines (Fig. 35) for 110 kHz nulls indicates that the noise was emanating from a region on the forenoon side bounded approximately by radial distances

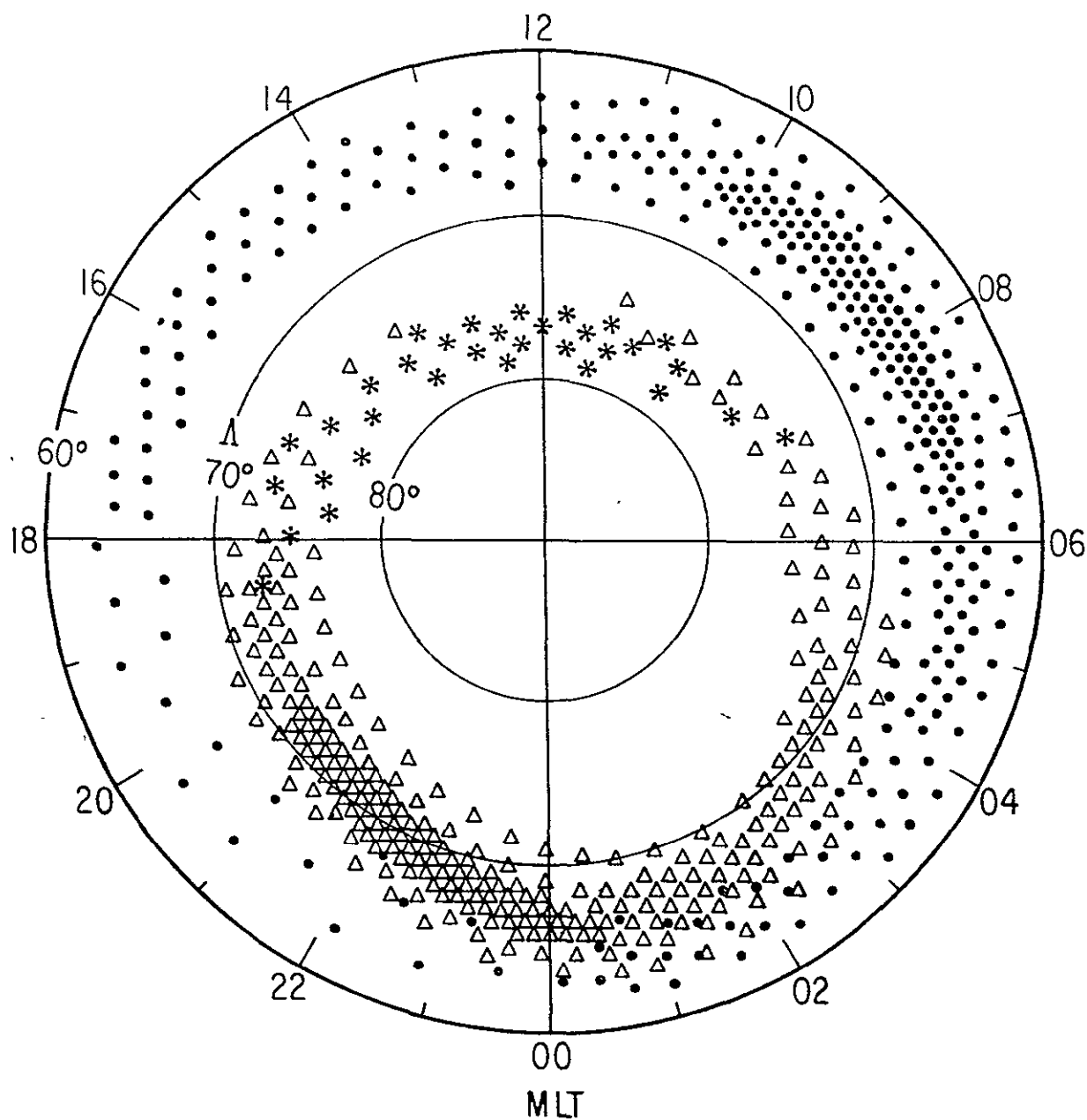


Fig. 34. Idealized representation of auroral particle precipitation, plotted in coordinates of invariant latitude and magnetic local time. Splash-type precipitation (electron energy  $E \sim 10$  keV) is indicated by triangles, drizzle precipitation ( $E \sim 40$  keV) by dots, and soft electron ( $E \lesssim 500$  eV) precipitation into the dayside polar cusp by stars (Paulikas, 1971).

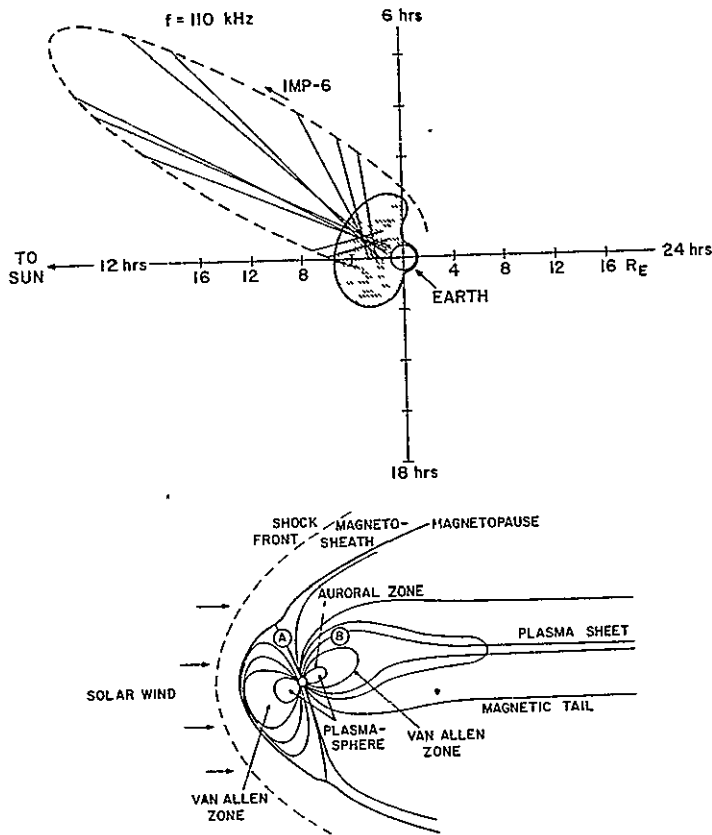


Fig. 35. Direction finding measurements on IMP-6 show daytime source region for 110 kHz noise to be in vicinity of polar cusp (position A in lower panel) in the forenoon sector. Higher frequency noise near 250 kHz detected in magnetotail near position B (after Stone, 1973).

of 2 to 5 Re. This places the source region in or near the polar cusp where low-energy ( $< 1$  keV) electron precipitation takes place on a continuous basis (Heikkila and Winningham, 1971). Other preliminary results with 250 kHz null directions located a strong source region on the night side along field lines within the auroral oval.

Additional application of this method by Kaiser and Stone (1975) using IMP-6 130-kHz nulls revealed two main source regions, one on the forenoon side and the second near midnight (Fig. 36 B). The spectral shape of the TKR for the two regions is indicated in Fig. 36 A, where it

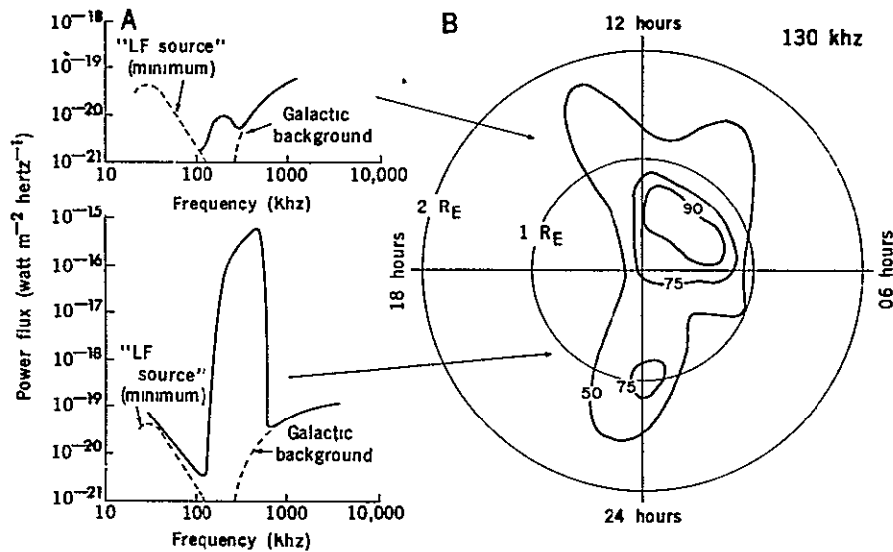


Fig. 36. (A) Representative TKR spectra showing a relatively low intensity peak on the dayside (upper panel) and a high intensity peak on the night side (lower panel). (B) Contours of relative occurrence probability of TKR noise projected onto the ecliptic plane, showing maximum occurrence of intense noise in late evening magnetic local time and of low-intensity peaks on forenoon side. (After Kaiser and Stone, 1975).

can be seen that the night side source is much more intense than that on the dayside. The occurrence-percentage contours in Fig. 36 B are projected onto the ecliptic plane; how far above or below the plane the source is located cannot be determined unambiguously by this method.

Analysis of one year of the lunar-orbiting Radio Astronomy Explorer-2 (RAE-2) 130 kHz data (Kaiser and Stone, 1975) has found the most intense source to be located on the evening side, visible from about 16 LT to 04 LT. Lower intensity noise was observed in all hours from 04 LT to 16 LT.

To gain a measure of the radial distance of the source on the evening side, Kaiser and Alexander (1975) utilized the effect of occultations of Earth by the lunar surface on RAE-2 data. By noting the times of appearance and disappearance of intense noise on 250 kHz, they were able to fix the position of the source as seen from lunar orbit on the

evening side. An example of their findings is illustrated in Fig. 37. Three determinations were made at different universal times and different levels of magnetic activity as indicated by the AE index. The first time, two source regions (both labeled 1 in the Figure) were identified, one at 17 Re in the tail, the second much closer in so that in the projection it appears on Earth's surface. The second and third revealed sources at about 2 and 3 Re, respectively. The distribution of 112 determinations at 250 kHz for the July-Dec. 1973 period is shown in Fig. 38. The average of all projected distances is 3.4 Re; about 1/3 of the sources are beyond 3.5 Re and 10% are further than 7.0 Re. As noted in Fig. 38, the electron gyrofrequency ( $f_H$ ) equal to 250 kHz and its first harmonic lie Earthward of these distances, which has important ramifications for the theories discussed in the next section.

Other direction-finding measurements by Kurth, et al (1975) and Gurnett (1974) have been concentrated on the nightside intense noise region. Kurth, et al (1975), using Hawkeye-1 and IMP-8 data, found the average source location for 178 kHz to be at about 22 LT at a radial distance of about 1.75 Re in the equatorial plane. Gurnett (1974) deduced that the radiation must emanate from regions located in the evening and night auroral zone at radial distances less than 3.0 Re.

The work by Stone and associates, and the present results, indicate that at least two major source regions must exist, one on the forenoon side which emits relatively lower intensity noise in the TKR range, and the other in the auroral oval which emits intense sporadic TKR noise especially on the evening side. The latter source is in agreement with the findings of Gurnett and associates, whose equipment sensitivity precluded investigation of low-intensity radiation.

#### 4.2 Generation Mechanisms

Several proposals have been advanced to explain the generation process for magnetospheric noise, all of which depend upon the existence of precipitating particles in one way or another. The earliest seems to have been incoherent Cerenkov radiation (Ellis, 1958), but this process was shown to be inadequate to explain the observed intensities by several

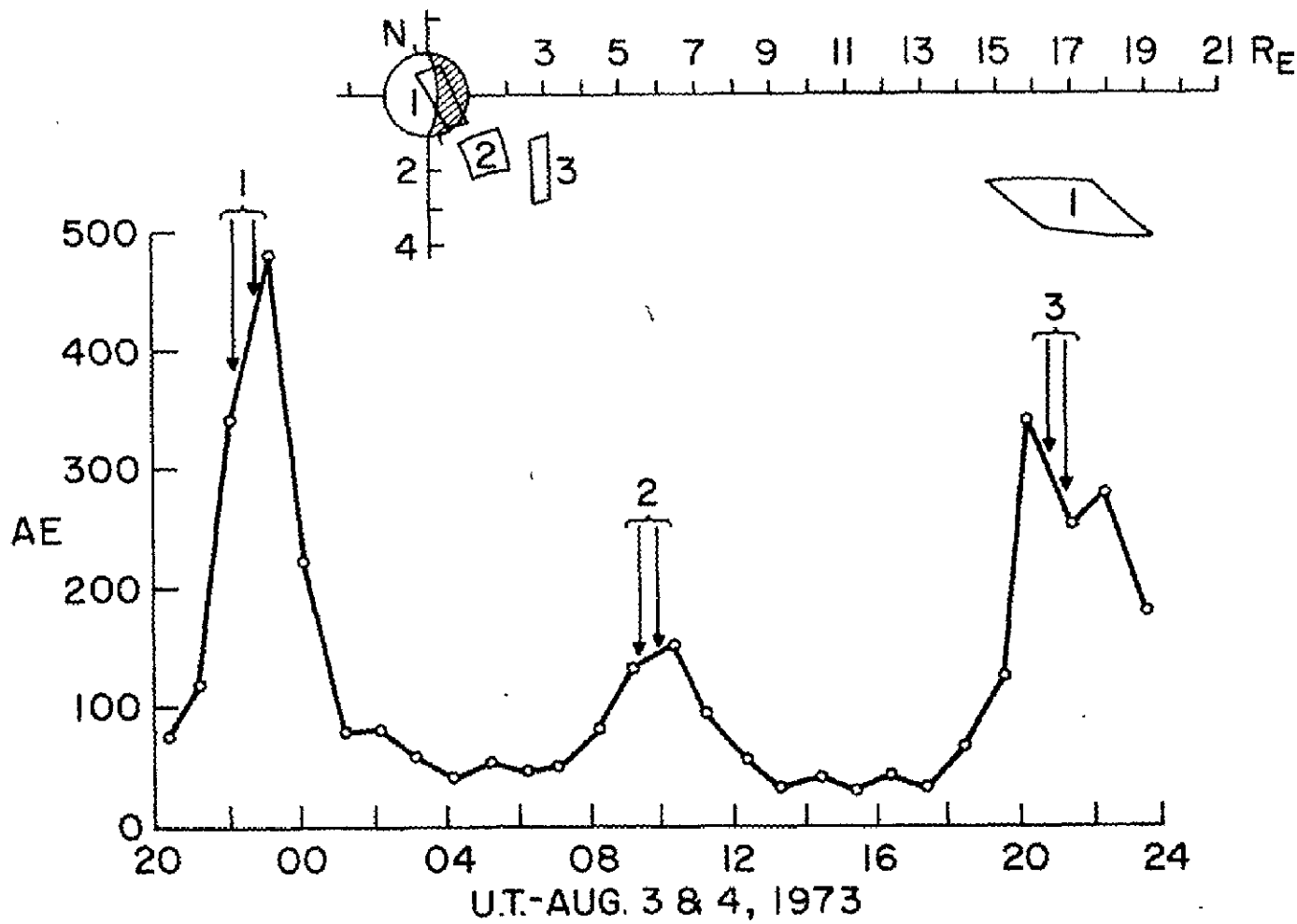


Fig. 37. Direction-finding measurements of IRR source regions by RAE-2 occultation techniques. Determination of source locations (note the double source), 2 and 3 made at indicated times when AE index was high, low, and moderate, respectively. (After Kaiser and Alexander, 1975).

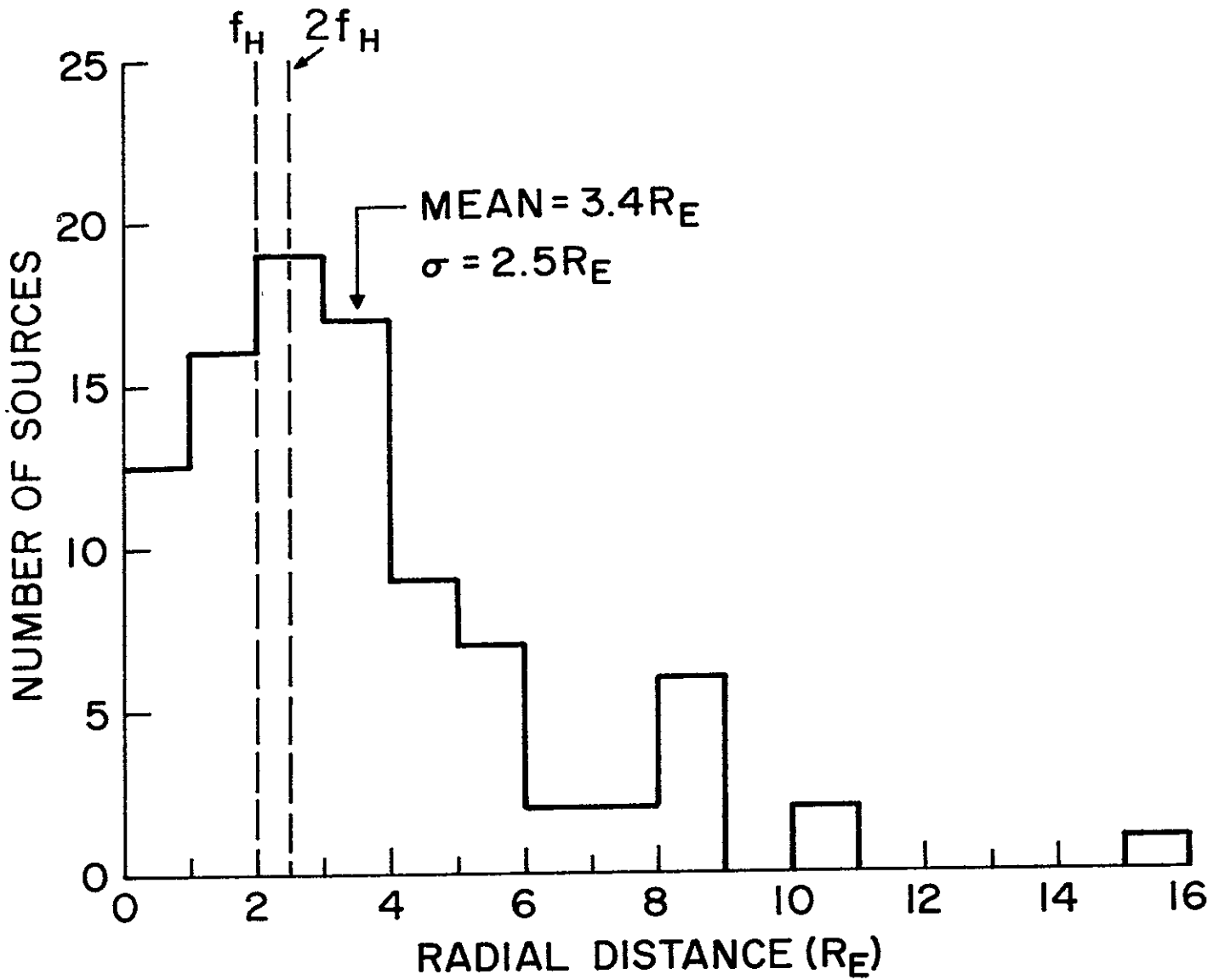


Fig. 38. Distribution of radial distances to TKR sources determined by RAE-2 occultations (after Kaiser and Alexander, 1975).

orders of magnitude (c.f., Taylor and Shawhan, 1974). The conclusion arising from this finding was that a coherent process is required to organize the electrons to increase the radiated power from them.

The discovery of VLF electrostatic noise occurring on frequencies related to the local gyrofrequency (Kennel, et al, 1970) led Fredericks

(1971), and Fredericks and Scarf (1973) to propose a nonresonant instability theory wherein modes at frequencies  $f = (n + \frac{1}{2})f_H$  are excited. The concept was applicable to radiation on 1 to 22 kHz observed in local times from at least 19 LT through midnight to 07 LT and possibly to 12 LT. Emissions were recorded on L shells out to at least 13 in the southern hemisphere at  $50^\circ$  INL, in the northern hemisphere out to  $L = 10$  at  $40^\circ$  INL, and over the equator ( $0^\circ$  INL) out to  $L = 6$ .

Scarf (1973) suggested that such a purely electrostatic plasma instability occurring at  $3 f_H/2$  may organize the phase of energetic electrons in the Jovian magnetosphere, and Gurnett (1974) applied it to the terrestrial case for TKR.

Swift and Kan (1975) consider the stimulation of VLF emission to be near the plasma frequency ( $f_N$ ), while Benson (1975) suggests emission in regions where the upper hybrid resonance frequency is less than twice the gyrofrequency. That is,  $f_T < 2 f_H$ , where  $f_T^2 = f_N^2 + f_H^2$ . James, et al (1973) have found intense 2-4 MHz radiation at low altitudes ( $\sim 1400$  km) where  $f_T = 2 f_H$ . Common to all these theories is the necessity for a warm electron beam to be streaming through a cold plasma. Only the Gurnett (1974) and Benson (1975) theories apply directly to the TKR case.

Assuming the  $3 f_H/2$  mechanism to be operative, Gurnett (1974) uses propagation cutoff arguments to establish a bandwidth of approximately 50 kHz to 1.2 MHz for TKR. Based on the same argument, the radiation can only be generated (and escape) in the nightside auroral region at radial distances of about 1.5 to 3.0 Re. Although this mechanism may explain the quasi-continuous background radiation on frequencies within this bandwidth, it is inadequate for the intense TKR in two respects. As we have seen in sections 2 and 3, the intense radiation peaking at about 280 kHz has a bandpass with a lower bound of approximately 100 kHz (not 50) and an upper bound of about 380 kHz (not 1200). The second deficiency is that Gurnett's mechanism precludes generation of TKR beyond about 3 Re, and as shown by Kaiser and Alexander (1975), TKR sources have been detected in the tail region out to at least 17 Re.

Benson's (1975) theory is somewhat more elegant in that it allows for generation of electrostatic noise with subsequent conversion to elec-

tromagnetic noise upon reflection at the surface where  $f \sim 2 f_H$ . His electron density model is essentially the same as Gurnett's (1974), and the region where the requirement  $f_T < 2 f_H$  holds is between radial distances of about 1.2 Re to 5 Re. This theory suffers the same two deficiencies as Gurnett's. For either theory to apply, the source mechanism at any given time would have to be restricted to an extremely narrow radial distance range near 2 Re in order to explain the sharply banded TKR peak. In Gurnett's case, it is difficult to envision an electron density distribution which would establish the sharp upper and lower cut-offs that are actually observed. Also, application of the  $f = (n + \frac{1}{2})f_H$  criterion to the multiple peaks in Figs. 14 and 15 of this report reveals no obvious pattern.

What is required is a mechanism which will allow generation of noise at frequencies greater than  $f_H$  or  $f_T$  at distances beyond 5 Re and also allow for the observed spectral shape of the TKR noise.

#### 4.3 Magnetospheric Lightning

An explanation for the noise generation might be found in an analogy to a terrestrial lightning flash. One may liken a lightning channel carrying a transient current to a radio antenna which emits an electromagnetic signal. The characteristics of this signal are determined mainly by the time variations of the current strength, channel length, and velocity of the current in the channel. In the resulting noise spectrum from a lightning discharge, the frequency of the peak amplitude is proportional to the channel length; the longer the channel the lower the peak frequency. From a typical lightning flash having a channel length of about 3 km, the spectrum peaks at 7 or 8 kHz.

A total lightning discharge consists not of one huge current surge, or spark lasting a few microseconds, but rather of several (generally 3 or more) strokes from the charged thundercloud either to the ground or another cloud and back again. In addition to the main and subsidiary strokes, small streamers with much shorter channel lengths can branch out from the main channel, and the whole discharge persists typically for about 500 msec. Different parts of the discharge are responsible for the

noise emission in different parts of the radio spectrum. The VLF peak at 7-8 kHz is generally generated by the return strokes along the main channel, and the semi-continuous noise in the high frequency (HF) band is suspected to stem from the streamers and short coronal discharges.

The existence of field-aligned currents in the upper ionosphere and magnetosphere (Armstrong and Zmuda, 1970; Chay, et al, 1971; Zmuda and Armstrong, 1974) and field-aligned electron bursts (Hoffman and Evans, 1968) suggests that a process qualitatively similar to terrestrial lightning discharges may be operative in the magnetosphere. The field-aligned burst may be analagous to the main lightning channel, which generates noise in the VLF and ELF bands.

Small streamers generating higher frequency noise may develop in the following way: When the precipitating column making up the main channel reaches a certain intensity it becomes unstable and splits into an electrostatic double layer (c.f., Thorne, 1975). Between the two layers there is a thin dark zone approximately 100 debye lengths ( $\lambda_D$ ) wide, over which the potential drops by an amount equivalent to  $\sim 10 kT_e/e$ , where  $k$  is Boltzmann's constant,  $T_e$  is the electron temperature and  $e$  is its charge.

Using electron temperatures of 4,000  $^{\circ}$ K for 2 Re and 50,000  $^{\circ}$ K for 6 Re (Evans, 1966), the potential drop across the dark zone is 3.45 V and 43.1 V, respectively. Further, one may compute the appropriate debye length from (Oberman, 1974):

$$\lambda_D = \left[ 4\pi n e^2 \left( 1 + \frac{Z}{\theta} \right) \right]^{-\frac{1}{2}} \quad (1)$$

where  $n$  is the average number density of particles,  $Z$  is the atomic number (= 1 assuming H to be the dominate species at the heights under consideration), and  $\theta = kT$  ( $k = 1.38 \times 10^{-16}$  erg/deg for Boltzmann's constant;  $T$  = temperature of the gas in  $^{\circ}$ K). For 2 Re,  $T = 4000$   $^{\circ}$ K (Evans, 1966) and  $n = 3(10^2)$  electrons  $\text{cm}^{-3}$  (Benson, 1975), and for 6 Re,  $T = 50,000$   $^{\circ}$ K (Evans, 1966), and  $n$  is estimated to be 100 electrons  $\text{cm}^{-3}$ . With these values, the width of the dark zone is approximately 25 m at 2 Re and 155 m at 6 Re. Combining these widths with the above-computed potential drops

the electrostatic field at 2 Re would be 0.14 V/m and at 6 Re it would be 0.28 V/m. Compared to the high-latitude dayside measurements of Maynard and Johnstone (1974) these field strengths are not unduly high.

Thus, in the high-latitude radial distance range of 2-6 Re, small streamers with lengths of the order 25-150 m could develop along the main "magnetospheric lightning" channel, and generate noise at frequencies in the TKR range. It appears that at high latitudes where the magnetic field direction (and main magnetospheric lightning channel) is essentially vertical, the side streamers would be oriented more or less horizontally, and the consequent TKR noise would propagate perpendicular to the streamer current or nearly along the magnetic field direction.

Since field-aligned splash precipitation - that is, the development of main magnetospheric lightning channels - maximizes in the late evening (Fig. 34) one could expect the occurrence of side streamers presumed to be responsible for the TKR component would also be maximum at that time. As can be seen in Fig. 26, this is the time of maximum occurrence of TKR, which tends to support the magnetospheric lightning concept.

Assuming that the time-dependent form of the side-streamer current can be described with a gaussian function

$$I(t) = A \exp\left[-\frac{1}{2}\left(t/t_1\right)^2\right] \quad (2)$$

where A is peak current and  $t_1$  is where it has decayed to its  $1/\sigma$  value, its Fourier transform into the frequency domain is also a gaussian;

$$I(\omega) = B \exp\left[-\frac{1}{2}\left(f/f_1\right)^2\right] \quad (3)$$

Here,  $\omega = 2\pi f$

$$A = B/t_1 \sqrt{2\pi} \quad (4)$$

$$\text{and } t_1 = 1/2\pi f_1 \quad (5)$$

It can be shown (Jones, 1970) that the relationship between the current pulse in the frequency domain and its associated radiated noise spectrum,  $R(\omega)$ , is

$$R(\omega) = \omega I(\omega) \quad (6)$$

Thus,

$$R(f) = 2\pi f B \exp\left[-\frac{1}{2}\left(\frac{f_o - f}{f_1}\right)^2\right] \quad (7)$$

where  $f_o$  is the peak frequency of the noise spectrum.

In this form (eq. 7) it is evident that the noise spectral shape will be skewed to the right due to the inclusion of the monotonically increasing frequency term multiplying the gaussian function. As noted in section 3, however, the experimentally observed spectral shape tends to be skewed to the left. Consideration of the most-often occurring statistical spectrum which peaks at 280 kHz with upper and lower cutoffs at 380 kHz and 100 kHz, respectively, leads to the suspicion that a single gaussian current pulse is insufficient to explain the observations.

Assuming as a first approach, that two current pulses will be sufficient, one may rewrite eq. 7 as:

$$R(f) = 2\pi f \left[ B_1 \exp\left(-\frac{1}{2}\left(\frac{f_{o1} - f}{f_1}\right)^2\right) + B_2 \exp\left(-\frac{1}{2}\left(\frac{f_{o2} - f}{f_2}\right)^2\right) \right] \quad (8)$$

where  $B_n$  is the amplitude of the pulse peaking at  $f_{on}$  with a  $1/\sigma$  value of  $f_n$  ( $n = 1, 2$ ).

In Figs. 39 and 40, theoretical spectra derived from eq. 8 are compared with the normalized spectra of Figs. 9 and 3, respectively. For Fig. 39,  $f_{o2} = 290$  kHz;  $f_2 = 45$  kHz;  $B_2 = 2B_1$ ;  $f_{o1} = 185$  kHz;  $f_1 = 18.33$  kHz. From eq. 5 it is evident that the total duration ( $\approx 6t_n$ ) of the current pulse  $B_2$  is 21.2  $\mu$ sec, while that for pulse  $B_1$  is 52.1  $\mu$ sec. Although the agreement in Fig. 39 is not perfect, it is quite good, and suggests that the spectrum is adequately produced by two transient gaus-

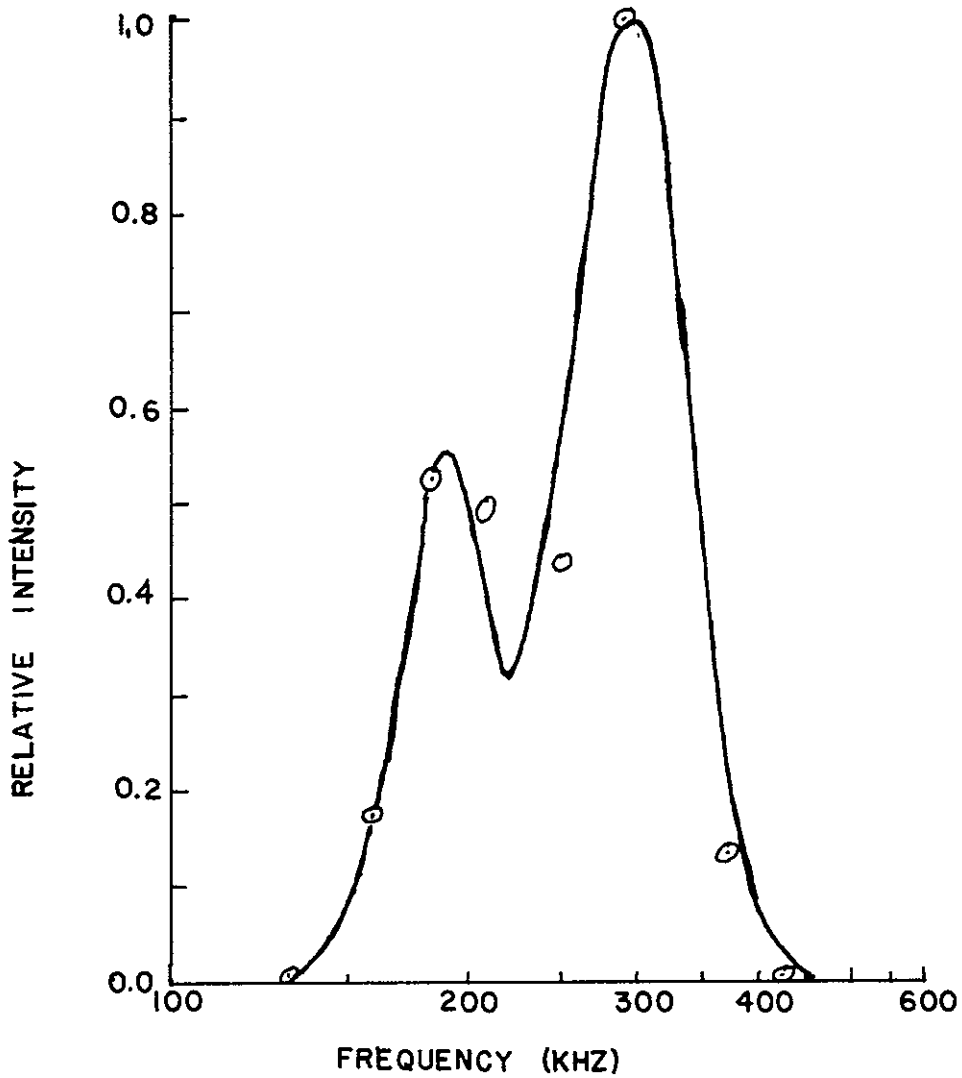


Fig. 39. Normalized IMP-6 TKR spectrum from Fig. 9 compared to theoretical spectrum generated by magnetospheric lightning with two streamer channels. The current pulse producing the noise peak at 300 kHz has a total duration of 21.2  $\mu$ sec travelling over a channel length of approximately 104 m. Its relative intensity is twice that of the 52.1  $\mu$ sec pulse producing the lower intensity peak at 190 kHz. The channel length of the longer pulse is 158 m.

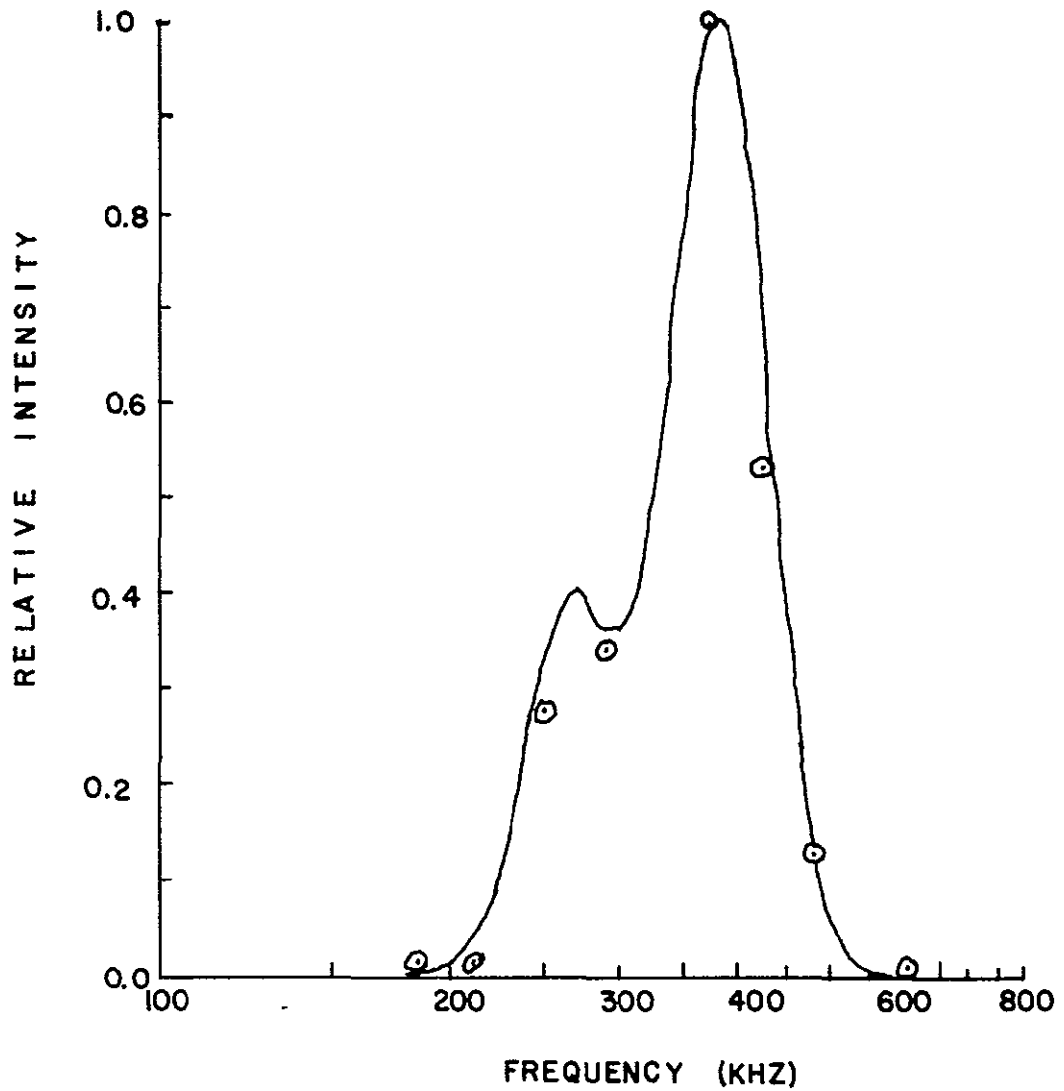


Fig. 40. Normalized TKR spectrum from Fig. 3 compared to theoretical spectrum generated by magnetospheric lightning with two streamer channels. The relative current intensity for the 380 kHz noise peak is 3 x that for the 270 kHz peak. For these two channels, respectively, the pulse durations are 19.2  $\mu$ sec and 38.2  $\mu$ sec, and the channel lengths are 80 m and 115 m. .

sian current pulses, one is  $\frac{1}{2}$  as intense and  $2\frac{1}{2}$  times longer in duration than the other. The reality of the computed valley at 220 kHz cannot be ascertained because of the lack of an experimental channel near that frequency.

For the theoretical spectrum in Fig. 40,  $f_{o2} = 375$  kHz;  $f_2 = 50$  kHz;  $B_2 = 3B_1$ ;  $f_{o1} = 260$  kHz;  $f_1 = 25$  kHz. The total current pulse widths in this case are 19.2 and 38.2  $\mu$ sec for  $B_2$  and  $B_1$ , respectively. Again, the agreement between the observed and computed spectra is quite remarkable.

It should be noted that the selection of values for the lightning channel parameters  $f_{on}$  and  $f_n$  was guided by the characteristics of the experimental spectra. Other parameters, such as current intensity and channel length, can in principle also be deduced from the spectral characteristics. For example, in a terrestrial lightning flash the peak radiation occurs at about 8 kHz and the channel length is 3 to 4 km; the length of the channel is about one-tenth of the peak radiation wavelength. By analogy, it appears that magnetospheric lightning channel lengths generating TKR noise would range from about 50 m (for 600 kHz peaks) to 240 m (125 kHz peaks) with a mode of 107 m (for 280 kHz).

Further work beyond the resources of the present effort is required to ascertain additional characteristics of magnetospheric lightning, such as current strength, velocity of current advance along the channel, orientation of the streamer channel, initiation of the stroke, and so on.

To summarize the present results, it appears that the spectral shape of observed TKR noise can be approximated by assuming that the noise is generated by lightning-like current surges in the magnetosphere. The channel lengths are typically the order of 50 to 250 m, most often near 100 m. If the current surge has a gaussian time distribution, the pulse is typically a few to a few tens of microseconds in duration. For the particular observing periods analyzed there appear to have been at least two magnetospheric lightning channels with unequal intensities active at a given time; the larger one being 2-3 times more intense and about half as long in duration as the associated lower intensity burst. Since time-averaged noise spectra were used to make these deductions, it is uncertain

whether the two surges occur simultaneously or sequentially.

The channel lengths computed here are comparable to, perhaps a bit longer than, the separation distances of electrostatic double layers at radial distances of 2 to 6  $R_e$ , which suggests that the potential difference between the layers may initiate the magnetospheric lightning streamer.

To carry the lightning analogy a bit further than warranted by the present analysis, it is interesting to speculate that aurora may be the magnetospheric counterpart of the visual component of terrestrial lightning, while magnetohydrodynamic or pressure waves are the counterpart to thunder.

As a final comment, it should be mentioned that the radio frequency of TKR noise depends upon the magnetospheric lightning streamer length according to the present theory, and therefore should be relatively insensitive to radial distance of the source location. Thus, noise can be generated by this mechanism at distances larger than those permitted by the theories of Benson (1975) and Gurnett (1974) for example.

## 5. SUMMARY AND CONCLUSIONS

Investigation and analysis of radio noise spectra from the IMP-6 and RAE-2 satellites has been conducted to determine spectral characteristics and possible noise generation mechanisms.

Gross characteristics of spectra from 30 kHz to 10 MHz can be categorized by frequency bands of approximately 30 to 100 kHz; 100 to 1000 kHz; and 4 to 10 MHz.

Below about 100 kHz the background noise magnitude has a general tendency to decrease with increasing frequency, but enhancements (peaks) are sometimes superimposed on this background which flatten or even reverse the slope. Above about 4 MHz the noise level nearly always increases with increasing frequency, possibly due to terrestrial radio noise and interference propagating through the ionosphere from Earth's surface to the spacecraft.

The middle portion of the spectrum (100-1000 kHz), referred to as terrestrial kilometric radiation or TKR noise, is marked by peak enhancements rising a factor of 100 or more above the background level. The peaks are observed on all sides of the Earth (i.e., at all local times), and at radial distances from 1.3 Re to 60 Re. They occur at all levels of magnetic activity, with a slight tendency for increasing peak intensity during strong geomagnetic disturbances.

The TKR peaks tend to have the highest intensity in the evening and midnight sectors, less in the postmidnight to early morning sector, and least on the dayside. The number of peak occurrences also follows this diurnal trend.

The radio frequency of the TKR peak is observed most often (18% of the time) at about 280 kHz, and 80% of the peaks fall between 125 kHz and 600 kHz. The lower cutoff frequency where the TKR peak falls to the background level is found most often at about 100 kHz, and the upper cutoff at about 380 kHz.

Previous theories proffered to explain the generation of TKR noise are inadequate in several respects:

- (1) the mechanism is operative in the region where  $f_N < f =$

( $f_T < 2f_H$ ), which means that the source location is confined to radial distances of about 2 to 5 Re and the emission frequency decreases with increasing radial distance of the source. Recent direction-finding measurements reported by Kaiser and Alexander (1975) show that the TKR source region can be located at radial distances greater than 5 Re out to at least 17 Re. The observing frequency (250 kHz) utilized by Kaiser and Alexander was such that the Gurnett (1974) and Benson (1975) theories would predict a source location at 2-2.5 Re. Further, the present results show no obvious relationship between peak frequency and radial distance, so the observed peak frequency does not necessarily follow the predicted decrease with increasing source distance.

(2) In these theories, propagation effects are invoked to predict a TKR band extending from about 50 kHz to 1.2 MHz, but the present results show that at a given time the typical TKR enhancement is limited to a band extending from about 100 to 400 kHz. Furthermore, no explicit method to derive the peak frequency of a TKR enhancement is contained in the theories.

(3) The previous theories are applicable to the nightside auroral zone, but TKR noise is observed also on the dayside in the vicinity of the polar cusp.

(4) Magnetic storms or auroral substorms are an implicit requirement for the Gurnett theory to work, but it has been shown in this report that TKR peaks occur even in the absence of geomagnetic disturbances.

To meet the above observationally established spectral characteristics, a new theory based on the concept of "magnetospheric lightning" was developed. This concept, analagous to the generation of atmospheric radio noise by thunderstorm lightning, satisfactorily reproduces the TKR peak frequencies as well as the upper and lower cutoff frequencies. It is suggested that transient magnetospheric current surges of a few to a few tens of microseconds in duration travelling over distances of the order of 100 m will generate the appropriate noise spectrum. The lightning-like streamers can take place at radial distances in excess of 5 Re and can occur on both day and night sides in regions where an appropriate electric

field can accelerate electrons. The duration of the current in a magnetospheric lightning channel dictates the radiation bandwidth for a given observation, and the current channel length establishes the peak frequency of the radiation.

Additional work is recommended to establish additional characteristics of the magnetospheric lightning, such as its current strength, velocity of current advance along the channel, orientation of the channel, initiation of the stroke and associated streamers, and so on.

## 6. REFERENCES

- Armstrong, J.C., and A.J. Zmuda, Field-aligned current at 1100 km in the auroral region measured by satellite, *J. Geophys. Res.*, 75, 7122, 1970.
- Barrington, R.E., T.R. Hartz and R.W. Harvey, Diurnal distribution of ELF, VLF, and LF noise at high latitudes as observed by Alouett 2, *J. Geophys. Res.*, 76, 5278, 1971.
- Bauer, S.J., and R.G. Stone, Satellite observations of radio noise in the magnetosphere, *Nature*, 218, 1145, 1968.
- Benson, R.F., Source mechanism for terrestrial kilometric radiation, *Geophys. Res. Letters*, 2, 52, 1975.
- Choy, L.W., R.L. Arnoldy, W. Potter, P. Kintner, and L.J. Cahill, Field-aligned particle currents near an auroral arc, *J. Geophys. Res.*, 76, 8279, 1971.
- Dunckel, N., B. Ficklin, L. Rorden, and R.A. Helliwell, Low-frequency noise observed in the distant magnetosphere with OGO-1, *J. Geophys. Res.*, 75, 1854, 1970.
- Ellis, G.R.A., Low-frequency radio emission from aurorae, *J. Atmos. Terr. Phys.*, 10, 303, 1957.
- Evans, J.V., Concluding remarks on ionospheric F-region temperatures, *Electron Density Profiles in Ionosphere and Exosphere*, (J. Frihagen, ed.), John Wiley and Sons, New York, p. 616, 1966.
- Fainberg, J., L.G. Evans, and R.G. Stone, *Science*, 178, 743, 1972.
- Frankel, M.S., LF radio noise from the Earth's magnetosphere, *Radio Sci.*, 8, 991, 1973.
- Fredericks, R.W., Plasma instability at  $(n + \frac{1}{2})f_c$  and its relationship to some satellite observations, *J. Geophys. Res.*, 76 (22), 5344, 1971.
- Fredericks, R.W., and F.L. Scarf, Recent studies of magnetospheric electric field emissions above the electron gyrofrequency, *J. Geophys. Res.*, 78, 310, 1973.
- Gurnett, D.A., The earth as a radio source-terrestrial kilometric radiation, *J. Geophys. Res.*, 79, 4227, 1974.

- Gurnett, D.A., and L.A. Frank, VLF hiss and related plasma observations in the polar magnetosphere, *J. Geophys. Res.*, 77, 172, 1972.
- Hartz, T.R., Particle precipitation patterns, in The Radiating Atmosphere, (B.M. McCormac, ed.), D. Reidel, Dordrecht, Netherlands, 225, 1971.
- Hartz, T.R., and N. Brice, The general pattern of auroral particle precipitation, *Planet. Space Sci.*, 15, 301, 1967.
- Heikkila, W.J., and J.D. Winningham, Penetration of magnetosheath plasma to low altitudes through the dayside magnetospheric cusps, *J. Geophys. Res.*, 76, 883, 1971.
- Herman, J.R., The Radio Noise Environment of the Magnetosphere, Final Rpt. on Contract NAS5-24007-Mod4, 1974.
- Hoffman, R.A., and D.S. Evans, Field-aligned electron bursts at high latitudes observed by OGO-4, *J. Geophys. Res.*, 73, 6201, 1968.
- Hoffman, R.A., and T. Laaspere, Comparison of very-low-frequency auroral hiss with precipitating low-energy electrons by the use of simultaneous data from two OGO-4 experiments, *J. Geophys. Res.*, 77, 640, 1972.
- James, H.G., Whistler-mode hiss at low and medium frequencies in the day-side-cusp ionosphere, *J. Geophys. Res.*, 78, 4578, 1973.
- James, H.G., E.L. Hagg, and D.L.P. Strange, Narrowband radio noise in the topside ionosphere, AGARD Conf. Proc. No. 138, Technical Editing and Reproduction Ltd., London, p. 24-1, May, 1974.
- Jones, D.L., The spectrum and structure of atmospherics, Progress in Radio Science 1966-1969, Vol. 1, (G.M. Brown, N.D. Clarence and M.J. Rycroft, eds.), URSI, Brussels, Belgium, p. 401, 1970.
- Jørgensen, T., Morphology of VLF Hiss Zones and their Correlation with Particle Precipitation Events, *J. Geophys. Res.*, 71, 1367, 1966.
- Kaiser, M.L., and J.K. Alexander, New source location measurements of terrestrial kilometric radiation, paper presented at USNC/URSI Meeting, Boulder, Colorado, October, 1975.
- Kaiser, M.L., and R.G. Stone, Earth as an intense planetary radio source: Similarities to Jupiter and Saturn, *Science*, 189, 285, 1975.
- Kennel, C.F., F.L. Scarf, R.W. Fredericks, H.J. McGehee, and F.V. Coroniti, VLF electric field observations in the magnetosphere, *J. Geophys. Res.*, 75, 6136, 1970.

- Kurth, W.S., M.M. Baumbach, and D.A. Gurnett, Direction-finding measurements of auroral kilometric radiation, *J. Geophys. Res.*, 80, 2764, 1975.
- Laaspere, T., W.C. Johnson, and L.C. Semperebon, Observations of auroral hiss, LHR noise, and other phenomena in the frequency range 20 Hz to 540 kHz on OGO-6, *J. Geophys. Res.*, 76, 4477, 1971.
- Maynard, N.C., and A.D. Johnstone, High-latitude dayside electric field and particle measurements, *J. Geophys. Res.*, 79, 3111, 1974.
- Oberman, C., Plasmas, in *Encyclopedia of Physics*, 2nd Edition, (R.M. Besancon, ed.), Van Nostrand Reinhold Co., New York, p. 717, 1974.
- Paulikas, G.A., The patterns and sources of high-latitude particle precipitation, *Rev. Geophys. Space Phys.*, 9, 659, 1971.
- Scarf, F.L., A new model for the high-frequency decametric radiation from Jupiter, Rep. 24876-6001-RU-00, 8 pp., TRW Systems Group, Redondo Beach, Calif., 1973.
- Stone, R.G., Radio physics of the outer solar system, *Space Sci. Rev.*, 14, 534, 1973.
- Swift, D.W., and J.R. Kan, A theory of hiss and implications on the origin of auroral electrons, *J. Geophys. Res.*, 80, 985, 1975.
- Taylor, W.W.L., and S.D. Shawhan, A test of incoherent cerenkov radiation for VLF hiss and other magnetospheric emissions, *J. Geophys. Res.*, 79, 105, 1974.
- Thorne, R.M., Wave-particle interactions in the magnetosphere and ionosphere, *Rev. Geophys. Space Phys.*, 13, 291, 1975.
- Zmuda, A.J., and J.C. Armstrong, The diurnal flow pattern of field-aligned currents, *J. Geophys. Res.*, 79, 4611, 1974.